Alma Mater Studiorum – Università di Bologna

DOTTORATO DI RICERCA IN

Scienze Biomediche e Neuromotorie

Ciclo XXXIII

Settore Concorsuale: 06/D3 - MALATTIE DEL SANGUE, ONCOLOGIA E REUMATOLOGIA

Settore Scientifico Disciplinare: MED/15 - MALATTIE DEL SANGUE

THE BITTER TASTE RECEPTORS: A NEW MECHANISM OF COMMUNICATION BETWEEN LEUKEMIC CELLS AND THE MICROENVIRONMENT

Presentata da: Dott.ssa Valentina Pensato

Coordinatore Dottorato

Prof. Pietro Cortelli

Supervisore

Dott.ssa Lucia Catani

Co-Supervisori

Dott.ssa Matilde Y. Follo

Dott. Antonio Curti

Dott.ssa Valentina Salvestrini

Esame finale anno 2021

Abstract

Acute Myeloid Leukemia (AML) is a clonal disease sprouting from a rare population of leukemic stem cells. Increasing interest is gaining the ability of leukemia cells to detect changes in the microenvironment. Bitter taste receptors (TAS2Rs or T2Rs) are typical G-protein coupled receptors normally located in the oral cavity. Recent studies showed that T2Rs are widely expressed in various tissues where they are involved in the regulation of physiological processes, thus suggesting a wider function in "sensing microenvironment". In the present thesis, we further investigated T2R role by analyzing AML cell lines, AML primary cells, and normal hematopoietic stem cells (HSCs). T2R activation on AML cell lines, and AML primary cells with high doses of agonist (Denatonium, DEN) induced a reduction of cell viability associated to apoptosis induction, while non-toxic doses reduced cell migration, and AML sample clonogenic capacity. In addition, DEN-treatment altered mitochondrial bioenergetic capacity; T2R activation prompted AML cells to a quiescent phenotype and made them more prone to oxidative and metabolic stress. Moreover, we tested the therapeutical potential of T2R agonist with and without chemotherapic agent. Interestingly, we observed that DEN had a synergistic effect with Cytarabine (Ara-C), reducing leukemia cell viability. The combination allowed to reach a high toxicity using lower doses of chemotherapeutic agent. Furthermore, this result was in line with the down-regulation of Ara-C-related multi-drug resistance protein (ABCC4) expression. Also, we analyzed T2R expression and function on normal HSCs. HSCs expressed several T2R subtypes, and the T2R activation with DEN did not affect their viability and did not induce cell death for apoptosis, but was involved in the differentiation of HSCs into the myeloid lineage. Indeed, the DEN exposure enhanced the engraftment in transplanted mice.

In conclusion, our results indicated that the T2R receptor system was expressed and functional in both leukemic cells and HSCs. These results needed to be further deepened to highlight the off-target effect of T2R activation, to discover novel pathways modulating leukemic cells, and to develop new classes of therapeutic molecules.

Index

INTRODUCTION

RESULTS I

RESULTS II

Introduction

1. THE HEMATOPOIETIC SYSTEM

1.1. The hematopoiesis

Blood is a connective tissue responsible for the homeostasis control of the body. This function is assured by a series of mature cells, each with a specific function. Since most terminally mature cells are not capable proliferating, but rather are destined to be destroyed by either programmed cell death or necrosis, they must be replenished daily by a complex differentiation process defined as hematopoiesis (Fig.1).

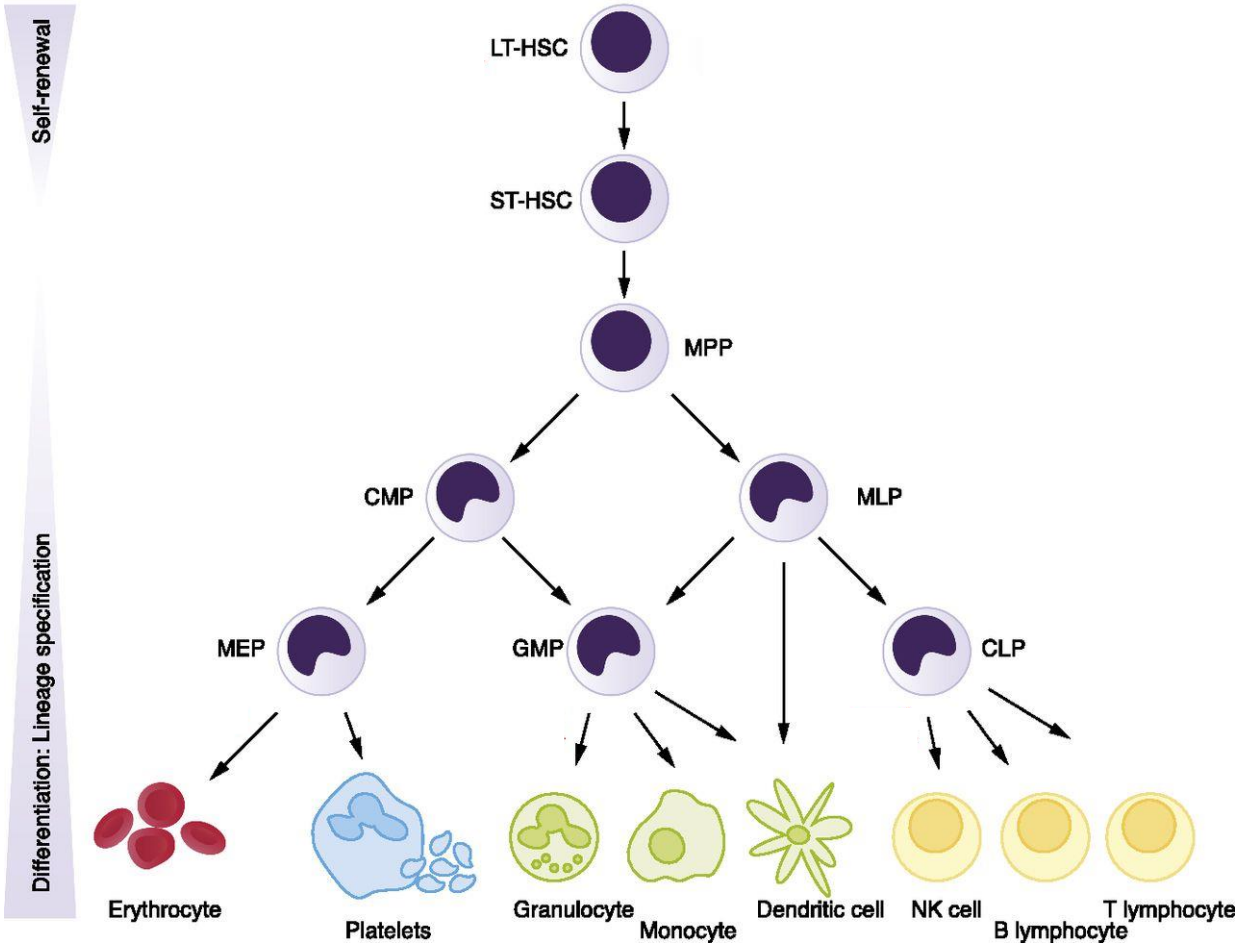

Figure 1. Differentiation hierarchy of hematopoietic stem cells (modified: [1]).

In adults this process takes place in the bone marrow (BM), starting from a highly specialized cell defined the Hematopoietic Stem Cell (HSC). Adult humans are estimated to require ~10^{11}-10^{12} new blood cells each day [2], although hematological stresses such as bleeding or infections can dramatically alter these requirements. Due to their function have been defined two kinds of HSCs: The *long-term hematopoietic stem cells* (LT-HSCs), which proliferate for a lifetime, and the *short-term hematopoietic stem cells* (ST-HSCs), which proliferate for a limited time, possibly a few months. The LT-HSCs are self-renewal and are capable to generate daughter HSCs by cell division. While the ST-HSC has a multipotent differentiation potential, they can differentiate into lymphoid and myeloid precursor cell. This happens through a hierarchical pathway with increasingly restricted lineage potential [3-5]. The precursor cells are called common lymphoid progenitor cells (CLPs) and common myeloid progenitor cells (CMPs), and are the progenitors of the two major lineages of blood cells. Lymphoid precursors differentiate into T cells, B cells, and natural killer cells [6]. Myeloid precursors differentiate into monocytes, macrophages, neutrophils, eosinophils, basophils, megakaryocytes, and erythrocytes [7]. The mechanisms and pathways that lead to their differentiation are still being investigated. Due to the ease of obtaining mouse BM, the hematopoietic research area utilises mouse models to further and deepen this process. The findings in mouse models are often extended to human hematopoiesis [8], because both rely on the HSCs at the top of the hierarchy to generate all blood and immune cell types. These hierarchical pathways of differentiation are shared by some progenitors [8, 9]. Also, both mouse and human hematopoiesis occur within the BM microenvironment. However, it is important to remember that HSC properties and behavior in such a

different environment could differ massively from those under conditions in the human niches [10].

Although the functional diversity of the hematopoietic progenitors has been established, the mechanisms by which this variability is generated in the hematopoietic system remain unclear. The heterogeneity of the stem cell compartment is considered to be the result of the integration of intrinsic and extrinsic signals. Extrinsic factors are primarily environmental stimuli (such as humoral factors, chemokines, adhesion molecules, and growth factors), produced by the medullary stroma to generate the milieu. In this perspective, the localization of HSCs in "niches" of different cytokine composition would be a mechanism of generating heterogeneity in the HSC population. In addition to these extrinsic factors, there are also mechanisms intrinsic to the stem cell itself, capable of generating variability through randomly generated gene programs at each cell division. For example, each cell can, at any time, decide between different destinies: self-renewal, differentiation, apoptosis, or migration [11].

1.2. The hematopoietic stem cells

The “stem cell” concept was first proposed by Till and McCulloch in the 20th century, following their pioneering studies of the blood system regeneration *in vivo*. They transplanted limited number of syngeneic donor BM cells, and ten days after observed cellular colonies that formed in the spleens of the mice. The subsequent analyses of these colonies revealed that a small sub-population of the donor BM cells possessed two remarkable properties, the ability to generate multiple types of myeloid erythroid cells, and the ability to self-replicate [12, 13]. These findings introduced the two defining criteria of stem cells: the multi-potency and the self-renewal. The HSCs are the only

cells within the hematopoietic system that possess the potential for both capacities. Hence, HSCs have become an attractive source for HSC transplantation and regenerative medicine [14, 15].

The field of stem cell research has greatly expanded since the initial studies of Till and McCulloch, thanks to new methods and *in vivo* models of study, which have increased knowledge of the HSC and the mechanisms involving them. It is well-known that HSCs are very rare, and it is calculated that in humans they represent no more than the 0.005-0.01% of all the cells in the BM.

The using of hematopoietic clonogenic assays within a liquid or semisolid media (colony-forming unit, CFU) and long term culture-initiating cell (LTC-IC), have made the study of HSC function possible, while the development of flow cytometry combined with immune-magnetic isolation technique, and sorting strategies, have provided high-purity isolation and identification of HSCs and progenitors using various cell surface markers. The first cell-surface marker used to enrich human HSCs (hHSCs) was CD34, a ligand for L-selectin that is expressed by only 0.5-5% of all blood cells in human fetal liver, cord blood (CB) and adult BM [4]. The other common surface markers used for identifying hHSCs and progenitors, *in vitro* and *in vivo*, are CD38, CD90, CD45RA, CD10, IL3Ra and Lin^-, where the Lin markers include T, B, NK, and myeloerythroid specific markers (Fig.2) [16, 17].

Another approach for the study of HSCs is the *in vivo* experiments. For instance, it is possible to study the human hematopoiesis evaluating the xenotransplantation models, utilizing immune-deficient mice [16]. Only functionally multipotent HSCs are able to reconstitute the entire hematopoietic system within these irradiated recipients and support long-term recipient survival [4, 5]. Transplantation assays are often combined

with limiting dilution analyses, which make it possible to estimate the frequency of functional HSCs within the original cell population [18]. Genetic markers are commonly used to track the donor cells within recipients by making discrimination of donor-derived cells from any residual recipient cells possible [19].

However, it is important to remember that these are only models, and that the correlation between the human and mouse BM microenvironment is not well known.

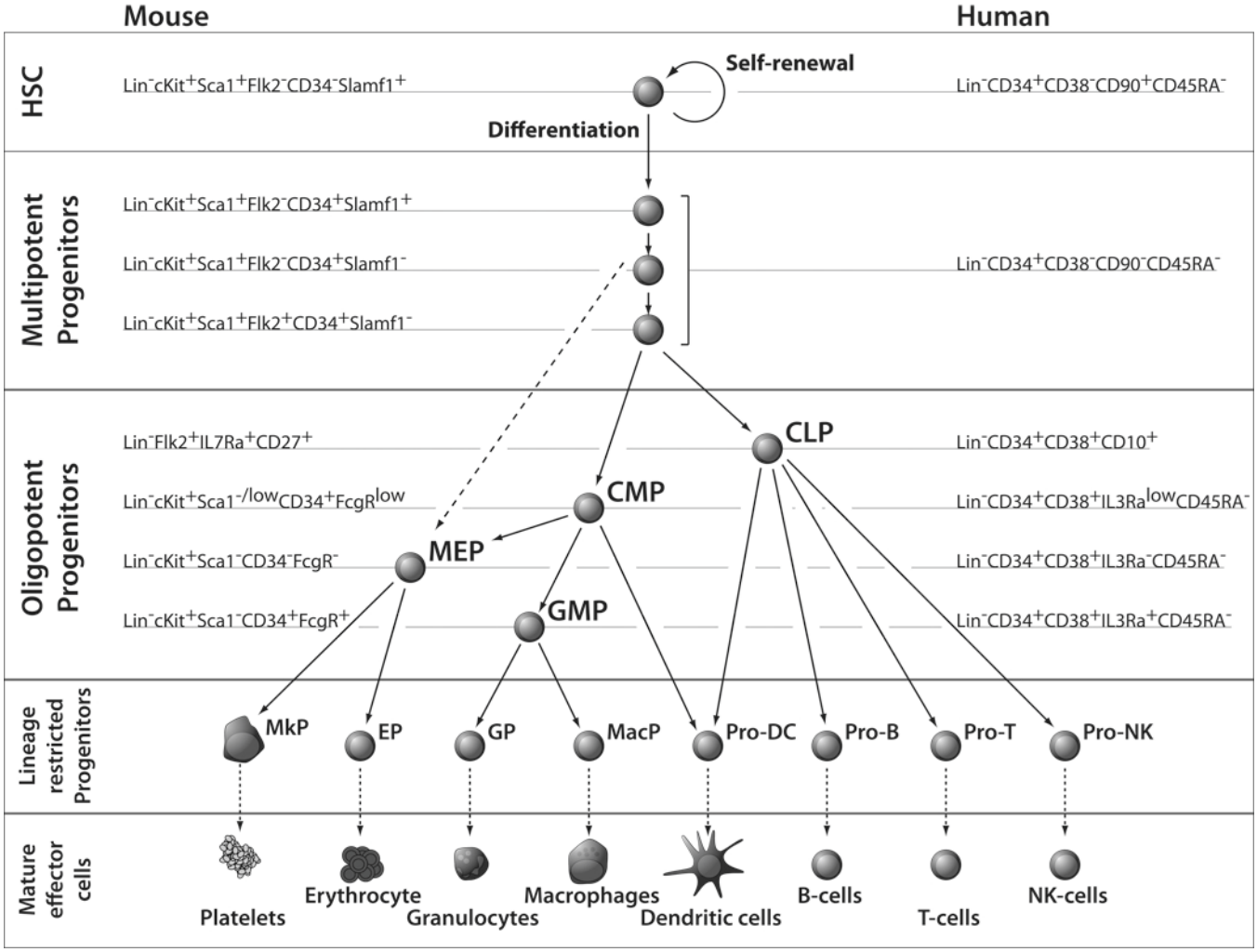

Figure 2. Antigenic profiling of murine and human hematopoietic cell compartments [4].

1.3. The stem cell niche

The hematopoietic microenvironment is the place of origin of cell proliferation, differentiation, and development. Fibroblasts, macrophages, osteoblasts, endothelial cells, and T cells are present and active in producing growth factors [20]. In this milieu, the self-renewal capacity of HSC, which is important in maintaining their pool size, is regulated by key genes and proteins such as transcription factors, epigenetic modifiers, and cell cycle regulators, as well as extrinsic factors from this microenvironment (Fig.3) [21, 22]. The niche is the specialized place in which stem cell fate, and proliferation rate is regulated, and where cells are protected from exhaustion and cell death [23, 24]. By using advanced imaging techniques and genetic tools in murine models, it was possible to shed light on the stem cell niche.

According to the anatomical location, at least two different hematopoietic microenvironments exist in the BM: the endosteal niche and the perivascular niche [25, 26]. The endosteal niche is localized in the outer edge of the BM and includes mesenchymal stem cells (MSCs), osteoblasts, fibroblasts, macrophages, and adipocytes [27, 28]. The perivascular (arteriolar and sinusoidal) niche is adjacent to the BM vasculature and mainly composed of vascular endothelial cells (ECs) and MSCs [25, 29, 30]. Through BM imaging and computational modeling is has been revealed that quiescent HSCs are associated specifically with small arterioles, that are ensheathed exclusively by rare $NG2^+$ pericytes. Conditional depletion of $NG2^+$ cells induces HSC cycling and reduces functional long-term repopulating HSCs in BM. These observations indicate that arteriolar niches are indispensable to maintain HSC quiescence. [31, 32]. Other results demonstrate that myeloid- and lymphoid-biased HSCs are located in, and regulated by, separate BM niches occupied by megakaryocytes and arterioles,

respectively [33], while the HSC expansion is restricted in the BM cavities where bone remodeling occurs. These findings suggest the unknown heterogeneity in the HSC niche [34].

MSCs are the most important component of HSC niche, in fact, it has been shown that they can facilitate HSC engraftment in both animal transplantation models and clinical studies [35]. MSCs are also one of the major sources of niche regulatory factors [30], and produce chemokines and cytokines that help HSC maintenance, such as CXCL12, stem cell factor (SCF), angiopoietin-1 (Ang-1), interleukin-7 (IL-7), and vascular cell adhesion molecule 1 (VCAM-1). In addition, osteoblasts can also produce other molecules that are important for HSCs, such as osteopontin (OPN), thrombopoietin (TPO), annexin-2, and angiopoietin-1 [30, 36]. HSCs are intimately associated with ECs throughout their lifecycle from embryonic development to adult aging. ECs are specialized cells lining the interior surface of blood vessels [37]. Rather than acting as an inert barrier, ECs play role in the maintenance, self-renewal, and differentiation of HSCs. Studies revealed that specific deletion of *Scf*, *Cxcl12,* or *Jag1* gene in ECs impairs HSC maintenance at a steady-state, confirming ECs a source of extracellular factors in niche [30, 32].

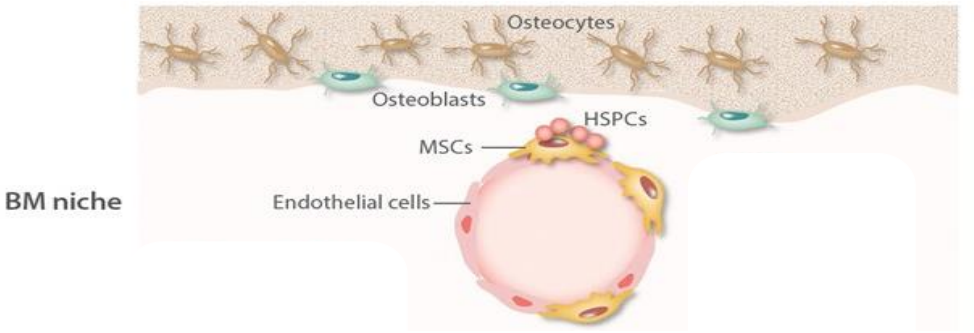

Figure 3. Schematic representation of BM niche (modified: [35]).

A better understanding of HSCs interaction with their niche will help to overcome the great need for HSCs in clinical applications.

2. THE ACUTE MYELOID LEUKEMIA

2.1. Acute myeloid leukemia

Acute Myeloid Leukemia (AML) is a clonal disease that develops from a rare population of leukemic stem cells (LSCs). The neoplastic transformation alters the mechanism that regulates the proliferation and differentiation of the stem cells, preventing the physiological maturation process [38]. This results in the accumulation of blasts first in the BM, and then in the peripheral blood (PB) and other organs and tissues. These immature cells are totally or partially unable to give birth to mature cells but retain some morphological and immunophenotypic characteristics of the normal compartment. For this reason, the AML patients have a greater susceptibility to infections (caused by leukocytosis), asthenia, wheezing and heart disease mainly due to a decrease in hemoglobin levels and there are also hemorrhagic manifestations (attributable to thrombocytopenia) [39]. Moreover, the release of cytokines from the same leukemic cells, lymphocytes, and monocyte/macrophages lead to general symptoms such as fever, pain, weight loss, and sweat. It is also possible to find cases of hepatomegaly, splenomegaly, lymph node enlargement, skin lesions, and other lesions due to the infiltration of blasts into non-hematopoietic organs and tissues [40].

AML occurs at all ages but is more common in older adults, who have an average age of 60 to 65 years. The frequency and distribution of AML in different geographic areas and in different populations changes substantially due to genetic and environmental factors [41]. The exposure to ionizing radiation, cytotoxic drugs, and substances (e.g. benzene)

appear to play a decisive role in the development of AML disease. The remission rates, in which there is the disappearance of leukemic cells and the normalization of hematopoietic compartment, and survival depend on several factors including patient age, cytogenetics, presence of molecular alterations, changes within the leukemic clone and previous bone marrow disorders [42].

Based on biological, clinical, and prognostic features, the AML type can be classified into three major categories:

1. Primary or *de novo* AML, which appears in subjects for whom there is not demonstrable a significant exposure to leukemogenic agents;
2. Secondary AML, which follows exposure to leukemogenic agents, including chemotherapy and/or radiation for other neoplasms;
3. Secondary AML, arising from a pre-existing myelodysplastic syndrome (MDS) or myeloproliferative disease.

The method used for the AML classification is based on the morphology of the leukemic population, and is called FAB (French-American-British) system. This classification identifies different AML subtypes relying on the blast differentiation and on the maturation capacity of the neoplastic clones (Table 1).

FAB	CYTOTIPE	FREQUENCY (%)	MORPHOLOGY	CYTOCHEMISTRY	SURFACE ANTIGENS
M1	MYELOBLASTIC without maturation	18	Blast cells (type I and II) > 90%	Peroxidase or Sudan B (> 3% positive blast cells)	**CD13, CD33,MPO, (CD14)**
M2	MYELOBLASTIC with maturation	35	Blast cells (type I and II) < 90%	Peroxidase or Sudan B (> 20% positive blast cells)	**CD13, CD33, MPO**
M3	PROMYELOCITIC MICROGRANULAR	9 1	Hypergranular blast cells, with Auerrods Hypergranular blast cells, with multilobulated nucleous	Peroxidase or Sudan B	**CD13, CD33, MPO** **CD13, CD33, MPO**
M4	MYELOMONOCYTIC	20	Blast cells (type I and II) and other mature granulocytic cells < 80%	Peroxidase or Sudan B Nasde NaF partially resistant, Anae	**CD13, CD33, CD14**
M5	MONOBLASTIC	13	Monoblast cells > 80%	Nasde NaF-sensitive, Anae	**CD14, CD13, CD33**
M6	ERYTHROBLASTIC	3	Erythroblast cells > 50% and blast cells (type I and II) > 30% of non-erythroid cells	Pas (erythroblast cells) Peroxidase or Sudan B	**CD235a**
M7	MEGAKARYOBLASTIC	1	Blast cells (type I and lymphoid type) > 30%, severe myelofibrosis	Platelets peroxidase	**CD41**

Table 1. FAB classification of Acute Myeloid Leukemia.

The World Health Organization (WHO) amended the FAB classification in 2008, considering the genetic abnormalities widely present in AML and highlighted by cytogenetic observations. Since then, there have been numerous advances in the identification of unique biomarkers associated with some myeloid neoplasms and acute leukemia, largely derived from gene expression analysis and next-generation sequencing. For this reason, in 2016 a monograph was published that represents the revision of the prior classification rather than an entirely new classification and attempts to incorporate new clinical, prognostic, morphologic, immunophenotypic, and genetic data that have emerged since the last edition (Fig.4) [43].

Acute myeloid leukemia (AML) and related neoplasms

AML with recurrent genetic abnormalities
AML with t(8;21)(q22;q22.1);*RUNX1-RUNX1T1*
AML with inv(16)(p13.1q22) or t(16;16)(p13.1;q22);*CBFB-MYH11*
APL with *PML-RARA*
AML with t(9;11)(p21.3;q23.3);*MLLT3-KMT2A*
AML with t(6;9)(p23;q34.1);*DEK-NUP214*
AML with inv(3)(q21.3q26.2) or t(3;3)(q21.3;q26.2); *GATA2, MECOM*
AML (megakaryoblastic) with t(1;22)(p13.3;q13.3);*RBM15-MKL1*
Provisional entity: AML with BCR-ABL1
AML with mutated *NPM1*
AML with biallelic mutations of *CEBPA*
Provisional entity: AML with mutated RUNX1
AML with myelodysplasia-related changes
Therapy-related myeloid neoplasms
AML, NOS
AML with minimal differentiation
AML without maturation
AML with maturation
Acute myelomonocytic leukemia
Acute monoblastic/monocytic leukemia
Pure erythroid leukemia
Acute megakaryoblastic leukemia
Acute basophilic leukemia
Acute panmyelosis with myelofibrosis
Myeloid sarcoma
Myeloid proliferations related to Down syndrome
Transient abnormal myelopoiesis (TAM)
Myeloid leukemia associated with Down syndrome

Figure 4. WHO classification of Acute Myeloid Leukemia [43].

AML therapy is defined based on the patient's age, cytogenetic or molecular risk category, and comorbidities (the fitness condition). Patients younger than 60 years receive a treatment program based on the administration of cytotoxic agents. The aim is to reduce the leukemic cell population and allow the residual HSCs to recreate a normal hematopoietic microenvironment. The classic induction therapy is defined as "3+7" and consists of anthracycline in combination with cytarabine (Ara-C) (administrates for three days and in continuous infusion for 7 days, respectively). The

complete remission is the most important goal to be reached, and in this phase, patients can be subjected to the administration of chemotherapeutic drugs to maintain the obtained result (1 or 2 times). At the end of this therapeutic phase, patients can receive the HSC transplantation or stop the therapy having developed relevant toxicities or adverse events that contraindicate transplantation.

The high toxicity of currently available drugs and the resistance to the conventional chemotherapy approaches in younger patients highlights the need to identify new therapeutic strategies. Thus, the most promising molecules are represented by:

- *FLT3* inhibitors, in patients with *TP53* gene mutation;
- *MDM2* inhibitors, in patients without any *TP53* gene mutations, to reactive the pro-apoptotic function of the oncosuppressor *TP53*;
- Demethylating agents (5-azacitidine), in patients with AML characterized by a number of blast cells not exceeding 30% of the total cellularity.

The relapse after the first remission and the refractory are the main unfavorable prognostic factors in AML patients. Therefore, these patients should undergo an experimental program based on the administration of innovative compounds, with different mechanisms of action.

Many patients will die rapidly due to AML. Few patients may reach a second remission with experimental drugs and undergo a second transplant from a different donor.

Elderly patients over 60 are not candidates for intensive chemotherapy, due to the comorbidities and high-risk features of AML, that suggest not using the standard agents. For them, the use of two demethylating agents, decitabine and 5-azacitidine, is approved. These drugs lead the complete remission of one-third of entire elderly AML patients.

Currently, alongside the identification of disease-specific alleles harbored by AML clones, the contribution that cell-extrinsic factors have in AML development by influencing AML cell genomic landscape and therapy-resistance is gaining increasing interest [44, 45]. Further in-depth analysis of these mechanisms will be a help to identify new therapeutic strategies.

2.2. The leukemic niche

The AML derives and is maintained by a pool of LSCs, which can self-renew, like the HSCs. LSCs are resistant to conventional chemotherapeutic drugs and are considered responsible for disease relapse following periods of apparent complete remission. In addition, LSCs have properties similar to the normal HSCs. Thus, the identification of LSC molecular markers is an important goal in this research field.

In the last few years, research has started to focus on the contribution that cell-extrinsic factors have in leukemia generation and persistence. It is conventionally thought that BM cell subsets deliver signals by direct cell-to-cell contact or secreted factors. For example, nucleotides and their specific receptors are emerging as novel and important modulators of inflammation and immunity, and are players in host-tumor interaction [46]. Thus, leukemia cell ability to sense the changes in the microenvironment is important for different cell functions, including the responsiveness to the antineoplastic agents.

In this context, LSCs depend on the interaction of the CXCL12-CXCR4 axis for mobilization and homing processes [47], and on the integrin VLA-4 and VLA-5 for adhesion to the medullary stroma. Moreover, the retention within the niche depends on the presence of membrane-associated proteins that can be cleaved by

metalloproteinases (MMPs). MMPs and the tissue inhibitor of metalloproteinases (TIMPs) play an essential role in AML cell progression and invasion [48]. The MMP expression level is often increased in AML niche, and this could lead to the release of different factors that allow the expansion and self-renewal of LSCs outside the microenvironment [49, 50]. Indeed, it has become evident that BM niches fuel the growth of leukemia cells and contribute to the therapy resistance and metastatic potential of leukemia cells by shielding LSCs [51].

On the other hand, the receptors also play important role in detect the endogenous or exogenous molecules. For example, it is reported that the purinergic receptors trigger the anti-proliferative, and pro-apoptotic functions in LSCs [52].

In this scenario, it is necessary describe briefly the key components of BM niche that are involved in LSC growth and regulation (Fig.5):

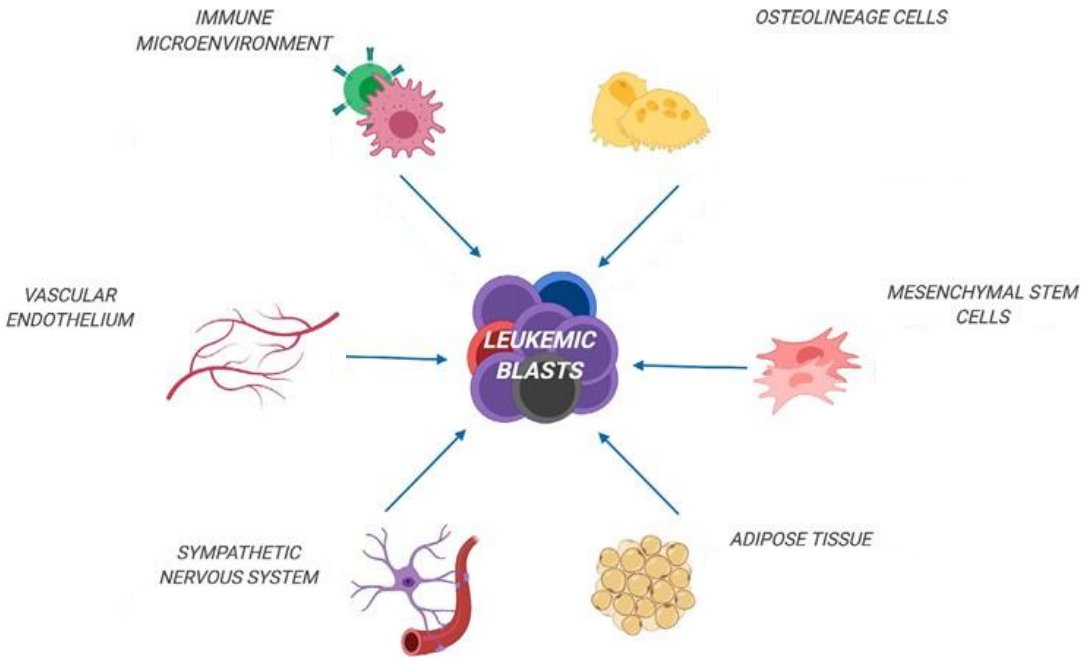

Figure 5. Interactions between leukemic blasts and the niche (modified: [53]).

1. The MSC function, which in normal activity provides signals through the secretion of SCF and CXCL12 in BM niche, is dramatically perturbed by AML cells leading to a block in normal osteogenesis [54] and subsequent reduction in osteoblast formation [55-57]. AML-derived MSCs modulate the expression of surface molecules decreasing the interaction with HSCs, and increasing the levels of $CD271^+$ cells, known for favor leukemia cell expansion through up-regulation of CXCL12 [53]. It is reported that MDS patients-derived MSCs are able to instruct the stroma to overproduce N-cadherin, insulin-like growth factor-binding protein 2 (IGFBP2), vascular endothelial growth factor A (VEGF-A), and leukemia inhibitory factor (LIF), which promoted MDS expansion [58].
2. The function of leukemia-associated immune cells is not well known. Studies showed that AML cells can create an immunosuppressive microenvironment, where both innate and adaptive immune responses are profoundly deregulated. It has been shown that AML cells reduce T and natural killer (NK) cell function and cytotoxicity altering the surface expression of relevant activating receptors, inducing the expansion of immunosuppressive regulatory T cells (Treg) [45]. These findings highlight the pivotal role of leukemic blasts in creating a defective anti-leukemia immune response in a tolerogenic microenvironment. Moreover, several studies showed a clear correlation between the expression of T cell immunosuppressive enzyme Indoleamine 2,3-dioxygenase (IDO) in AML with the reduction of T cell infiltration and a poor prognosis [59, 60]. Another mechanism by which leukemic cells evade immune-mediated control is through the regulation of immunological checkpoints, such as programmed death-1 (PD-1) and cytotoxic T-lymphocyte antigen 4 (CTLA-4) [45].

3. The vascular endothelium plays an important role in regulating the development and functions of other BM cell types, but its disruption represents a pivotal step in the progression of leukemia within the BM milieu. Primary AML-BM biopsies display increased blood vessel formation when compared with healthy BM [61]. Moreover, xenograft studies showed that leukemic BM colonization induces angiogenesis, an increase in nitric oxide (NO) production, vascular permeability, and hypoxia [62, 63], which is closely associated with AML chemoresistance [64]. The interaction through the CXCL12-CXCR4 axis, as well as transmembrane glycoprotein CD44, are recognized as a critical extrinsic signaling event promoting leukemic cell survival [53].
4. Recent studies have shown the involvement of osteoblasts in the regulation of leukemia development. It has been observed that healthy osteoblasts transmit signals that affect the fate of AML cells; on the other hand, their ablation accelerates the leukemia progression in several mice models of AML [65]. A single activation of ß- catenin signaling in osteoblasts is enough to lead to the development of MDS, eventually progressing to AML in mice [53].
5. Another way for leukemic cells to alter the BM niche is the induction of sympathetic nervous system damage. In healthy conditions the MSCs are associated with the sympathetic nervous system to regulate the milieu multiple functions [66, 67], whereas in disease the leukemic cells induce sympathetic neuropathy, leading to an aberrant expansion of $Nestin^{+}$ MSCs while restricting the number of mature osteoblasts through ß2-adrenergic signaling. The result is the decreased expression of CXCL12, SCF, Ang-1, and VCAM1 [57].

6. In steady-state conditions, the MSCs give rise to adipocytes believed to negatively regulate the HSCs function [68]. Following injury, the stromal cell compartment is enriched with adipocyte-biased stroma progenitors, followed by the accumulation of adipocytes within BM [69]. It emerged that adipocytes act promoting tumor cell survival. Obese leukemia patients display inferior chemotherapy responsiveness when compared with non-obese patients in AML adult patients [70]. Moreover, fatty acid oxidation represents an important energy source for leukemic blasts. AML cells enhance the production of free fatty acids from BM adipocytes, via the up-regulation of Fatty Acid-Binding Protein 4 (FABP4), that fueling AML blast survival [71].

3. THE BITTER TASTE RECEPTORS

3.1. The taste receptors

The possibility that we can distinguish between the main tastes (sour, salty, sweet, umami and bitter) depends on the presence of taste receptors on the tongue that recognize the taste of an ingested substance and transmit it through the nervous system to the cerebral cortex, where that original signal is transformed into a sensory-taste experience. In mammals, the taste system includes taste receptor cells (TRCs) organized in taste buds. Three types, fungiform, foliate, and valleys, are found in the tongue. The apical portions of the TRCs are exposed in the oral cavity and interact with the stimuli of taste, which are chemicals usually soluble in water. Sour and salty taste sensations are detected by ionic channels, while the sensation of sweet, umami, and bitter taste are detected by specific G protein-coupled receptors (GPCRs).

The type 1 taste receptors (TAS1Rs or T1Rs), encoded by the *TAS1R* gene located on chromosome 1, are activated by sweet and umami molecules. These receptors are functional only as heterodimers, with TAS1R3 serving as an obligate partner for both the umami receptor (TAS1R1+TAS1R3) and the sweet receptor (TAS1R2+TAS1R3). These receptors are classical "C" type receptors, with large N-terminal ligand binding domains that exhibit venus flytrap ligand-binding module similar to other C type GPCRs, such as the metabotropic glutamate, the $GABA_B$, and the calcium-sensing receptors (Fig.6). Heterologous expression of the sweet receptor TAS1R2/TAS1R3 shows that it responds to sugars, synthetic sweeteners, D-amino acids, and some sweet-tasting proteins [72-76].

These receptors will not be considered in this study.

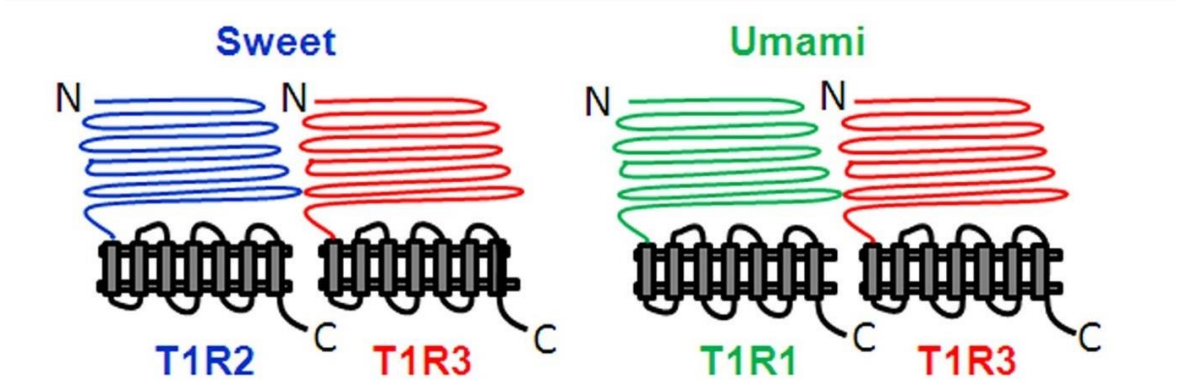

Figure 6. Diagrammatic representation of sweet and umami GPCRs [77].

In this study, we will focus on bitter taste receptors (TAS2Rs or T2Rs), a classical "A" type receptors that are similar in structure to the opsins and the olfactory receptors [78, 79]. In humans, TAS2Rs comprise 25 distinct members of the GPCR family [80], encoded by the *TAS2R* genes located on chromosomes 5, 7, and 12. These receptors have been

considered to function as monomers [79], but recent data suggest that they can also form functional oligomers [81]. They have short N-terminal domains, with ligand binding in the extracellular loops and transmembrane domains [77] (Fig.7).

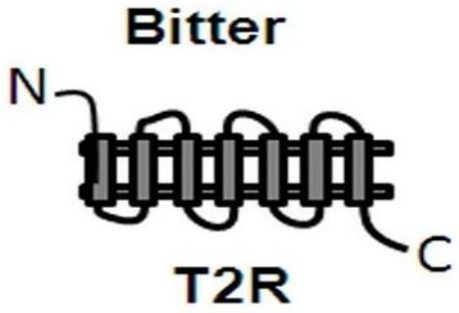

Figure 7. Diagrammatic representation of bitter GPCRs [77].

Upon receptor activation by a wide range of chemical molecules, the G protein gustducin dissociates its α and βγ subunits. The latter activates phospholipase C isoform β2 (PLCβ2), which in turn produces downstream inositol 1,4,5-trisphosphate (IP3). Activation of the IP3 receptor on the endoplasmatic reticulum releases calcium (Ca^{2+}) into the cytosolic compartment [82]. Simultaneously, there is also an activation of phosphodiesterases (PDEs) that attenuate cyclic adenosine monophosphate (cAMP) levels, decreasing protein kinase A (PKA) activity. Cytosolic Ca^{2+} activates the nonselective cation channel, transient receptor potential cation channel subfamily M member (TRPM5), causing plasma membrane depolarization, and activates voltage-gated sodium (Na^{+}) channels, required to potential the signalling propagation [77, 83, 84] (Fig.8).

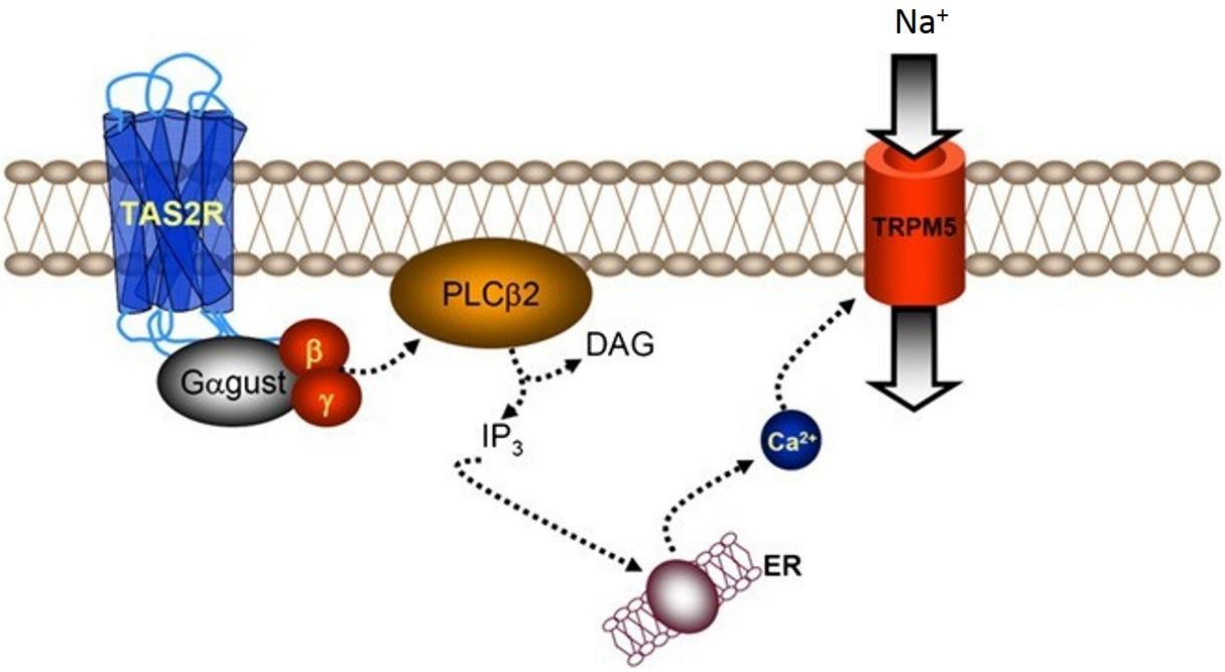

Figure 8. Signal transduction cascade of G protein-coupled taste receptors (modified: [85]).

3.2. TAS2R extraoral expression

Traditionally, the bitter taste is thought to guide the organism to avoid harmful toxins and noxious substances and thus is critical to animal and human survival. Intriguingly, several recent studies have shown that TAS2Rs are not exclusively detectable in the oral cavity, but are expressed in many extra-oral tissues, such as the respiratory and endocrine system, the gastrointestinal tract, the reproductive tissue and the brain [86-90] (Fig.9). Although the TAS2R extra-oral functions are still poorly understood, some evidence suggests that TAS2Rs may represent a receptor system, used by different cell types to sense external stimuli. The results of several studies have demonstrated that TAS2R extra-oral expression is involved in and regulates important biological processes germane to the nature of the tissue in which they reside.

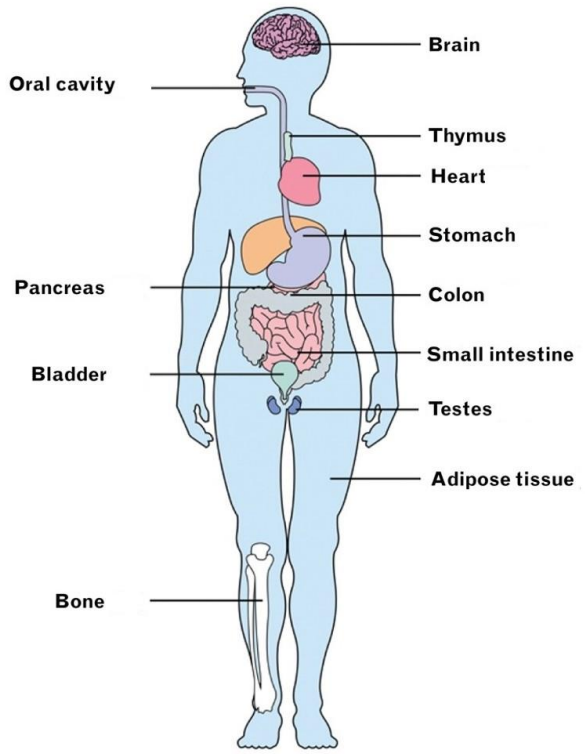

Figure 9. Oral and extra-oral tissues where taste receptors have been described as being expressed [86].

These receptors carry out different biological functions in their varied locations; for example, the expression of TAS2Rs was shown in the gastrointestinal (GI) tract, where they function in sensing luminal contents and GI hormones [91]. Successive investigations have discovered that they are involved in the detection of bacterial stimulants in upper airways, bronchodilation in lower airways, vasoconstriction in the vasculature, nutrient sensing in heart, spermatogenesis in testis, negative regulation of thyroid-stimulation hormone (TSH)-dependent functions in the thyroid, anti-inflammation and sensing quorum-sensing molecules in the immune system, and keratinocyte differentiation in the skin [89, 90, 92-98].

A paracrine role of TAS2Rs was first reported in a specialized small intestine enteroendocrine cell (EEC). Increased Ca^{2+} from the TAS2R activation leads to the

release of a peptide hormone cholecystokinin (CCK), which acts either through CCK2 receptors in the neighboring enterocytes to promote multidrug resistance protein 1 (MRP1, also known as ATP-binding cassette B1, ABCB1) to pump bitter-tasting toxins out of the cells [99] or through CCK1 receptors in sensory fibers of the vagal nerve that then transmit signals to the brain to control food intake [100]. Besides, it has been found that activation of TAS2Rs (e.g. TAS2R9) in enteroendocrine L cells stimulates the release of hormones, including glucagon-like peptide 1 (GLP-1) [101].

It has been also observed that a subset of pancreatic islet cells expresses TAS2R7, which when activated may regulate glucose homeostasis [102].

Moreover, studies report that the activation of TAS2Rs in the brain by the exogenous ligands might cause the secretion of CCK, regulating food intake, and other physiological processes [103, 104].

Accumulating evidence suggests that TAS2R-mediate physiological signaling contributes to the innate immunity in the epithelia of the organs that are connected to the external environment. Various TAS2Rs are expressed in the ciliated epithelial cells of human airways. Human ciliated airway cells express TAS2R4, TAS2R43, and TAS2R46, and their activation increase Ca^{2+} release and ciliary beat frequency, accelerating the clearance of microorganisms and their derived products [93]. Sinonasal-ciliated epithelial cells express the bitter taste receptor T2R38, localized within the motile cilia. When human ciliated epithelial cells were stimulated with the T2R38-specific bitter agonist (e.g. phenylthiocarbamide, PTC), or microbe-derived quorum-sensing molecules, such as acyl-homoserine lactones (AHLs), they exhibited low-level calcium responses that activated nitric oxide synthase-mediated production of intra-cellular nitric oxide, a potent bactericide [105]. TAS2Rs are not limited to ciliated

epithelial cells in the upper airway, but they are also expressed in solitary chemosensory cells (SCCs), a rare non-ciliated epithelial population. TAS2R activation in SCCs propagates a Ca^{2+} wave to the surrounding cells through gap junctions, causing a robust secretion of broad-spectrum antimicrobial peptides and ß-defensin [105-107]. The TAS2R-mediated defense systems in ciliated epithelial and in SCC work in concert to maintain human lower airway health [108]. Moreover, in the gut, the activation of taste receptors in tuft cells initiates the type 2 immune response against parasites [109-111]. Also, the expression of multiple TAS2Rs has been detected in subpopulations of circulating leukocytes [112].

TAS2R expression has been also described in the skin, though not ubiquitously, and it has been demonstrated that their expression varies with skin location (presumed-sun-exposed vs. non-exposed), sex, age, and where are involved in innate immunity, wound healing, and differentiation [113].

Overall, these evidences show that the taste receptors are an important system through which our organism recognizes substances and attaches a sensitive meaning.

3.3. T2R extraoral roles in pathophysiology

The impact on systemic physiology of bitter taste signaling in tissues has recently begun to emerge. The relevance of extra-oral bitter taste signaling is reflected in the finding that polymorphisms in human TAS2Rs have been linked to varied pathophysiologic processes, including resistance to bacterial infection, development of cardiovascular disease [114], and even cancer [115]. TAS2R variants have also been linked to human metabolic dysfunction. For instance, a non-function haplotype has been associated with an increased risk for type II diabetes [116].

The pathophysiological roles of TAS2Rs in the respiratory tract have been well reported, in which they act as targets for asthma management [117-119], but their roles in other systems have begun to emerge. In human colonic mucosa, the number of TAS2R38 immunoreactive cells is significantly increased in overweight and obese subjects versus lean subjects and is also correlated with body mass index values [120]. In the brain of Parkinson's disease patients, TAS2R5 and TAS2R50 are decreased, whereas TAS2R10 and TAS2R13 are augmented at both premotor and parkinsonian stages in the frontal cortex area [121]. TAS2R4, TAS2R5, TAS2R14, and TAS2R50 are down-regulated in the dorsolateral prefrontal cortex of schizophrenia patients [122]. Since the brain is further isolated by the blood-brain barrier, the changes in TAS2Rs raise the possibility that endogenous ligands for TAS2Rs exist throughout the human body [108].

In other studies was observed that TAS2Rs, especially TAS2R7, are upregulated in parathyroid adenoma samples compared with parathyroid hyperplasia samples [123]. Also, it was found that cystic fibrosis (CF) patients with TAS2R38 functional allele have a better rhinologic quality of life score compared to CF patients with non-functional genotypes [124].

It is important to investigate the potential role of TAS2Rs in pathophysiology because could contribute to the development of novel therapeutic strategies, and also because the pathological environment in disease conditions may regulate TAS2R functions. This has been reviewed elsewhere [125, 126].

3.4. T2R extraoral roles in cancer

Cancer cells, including leukemia cells, are known to adapt and turn ancestral and phylogenetically conserved functional pathways into malignant settings [127]. TAS2R expression has recently been reported in diverse tumor types, including neuroblastoma [128], pancreatic [129], prostate [130], ovarian [130] and breast cancer [131]. No clear evidence of their function has been provided, although a potential role in cancer biology has recently been suggested. It has been reported that TAS2R38 is expressed in tumor cells in patients with pancreatic cancer. Moreover, the TAS2R38-specific agonists activate mitogen-activated protein kinases. Interestingly, although there is no correlation between the frequency of TAS2R38-positive tumor cells and clinical and pathological parameters, the TAS2R38 ligands upregulate the multidrug resistance protein 1 (MDR1, or ABCB1), a major player in the chemoresistance of pancreatic cancer [132, 133].

A differential TAS2R expression in non-cancerous breast epithelial versus breast cancer cells, and the down-regulation of TAS2R4 in breast cancer cells have also been demonstrated [131], suggesting a mechanism by which the breast cancer cells may escape from apoptosis, which would otherwise be induced by bitter agonists [108]. Moreover, it has been reported that TAS2R4 and TAS2R14 are involved in the regulation of proliferation and migration of highly metastatic breast cancer cells [134]. In neuroblastoma cells, TAS2R8 and TAS2R10 play an important role in inhibiting the self-renewal potential and the invasion ability of cancer cells. In particular, the over-expression of TAS2Rs inhibits migration, invasion, and matrix metalloproteinase activity. Moreover, TAS2Rs suppress the expression levels of hypoxia-inducible factor-1α (HIF-1α), a well-known regulator of tumor metastasis, as well as its downstream

targets [128]. On the other hand, several bitter taste compounds have been found to exhibit anticancer or chemotherapy enhancing activities. The exact mechanisms are often unknown [77, 135-140].

In this context, the effect of TAS2R activation in AML cells are not reported. In clinical studies have been reported the use of Quinine, an anti-malaria drug known to be a bitter taste agonist, in combination with other chemotherapeutic drugs for the treatment of AML patients [141]. The authors demonstrated that Quinine reversed the MDR of human leukemia cells, and examined the possible use of this bitter taste compound in combination with chemotherapy drugs.

For this reason, it was important implement the knowledge of TAS2Rs in leukemia cells.

Aim of the Study

Over the past years, the contribution of cell-extrinsic factors in AML generation and maintenance has gained increasing interest. In this framework, the ability of leukemia cells to detect signals by cell-to-cell contact, secreted factors, or other changes in the microenvironment, and to react accordingly is particularly relevant. Among cell membrane receptors used by cells to sense external stimuli, T2Rs are proving particularly noteworthy. Indeed, recent studies have highlighted an extra-oral expression of T2Rs, questioning their exclusive role as sensors of bitter taste and expanding the spectrum of their functions. In particular, T2R expression has been reported in various tumor cell types, but their activity on AML cells is still unknown.

The primary aim of this study was to investigate the expression and function of T2Rs in AML cells and in their normal counterpart, $CD34^+$ cells. In particular, our study wanted to assess the effect of T2R activation in AML and $CD34^+$ cell genetic profile and functions, as well as its effect on chemotherapy response.

These results may have implications for the discovery of novel pathways modulating leukemic cells and for the development of a new class of therapeutic molecules.

Materials and Methods

1. Cell isolation and culture

The AML cells used for this study were obtained from the BM or PB of 47 untreated AML patients at diagnosis (blasts > 80%), upon signed informed consent. The patient's characteristics are summarized in Table 2. The research was approved by the Ethics Committee of Policlinico S. Orsola-Malpighi, University Hospital of Bologna (approval code: 94/2016/O/Tess).

# PT	Cell source	Molecular abnormalities	Karyotype	WBC, cells/μL	Sex	Age
1	BM	NA	complex	8.470	F	62
2	PB	FLT3-ITD+, NPM1+, TP53 wt	NA	64.250	M	70
3	BM	FLT3-TKD+, NPM1+, DNMT3A+ (R882C)	+(4)	129.000	F	60
4	BM	FLT-3, NPM1, TP53 wt	t(6;14)(q25;q32), t(1;5)(p22;q33)	1.540	M	67
5	PB	FLT3-ITD+, FLT3 TKD wt, TP53 wt; IDH1 and IDH2 wt; DNMT3A+ (R882H),	normal	68.780	M	69
6	PB/BM	NPM1wt, FLT3 wt	+(8)	NA	M	68
7	BM	FLT3 wt, IDH1and IDH2 wt, NPM1 wt	t(6;14)(q25;q32), t(1;5)(p22;q33)	2.300	M	38
8	BM/PB	FLT3 wt, NPM1+	normal	25.300	F	63
9	BM/PB	FLT3-ITD wt, FLT3-TDK wt, NPM1+	NA	1.600	M	59
10	BM	FLT3 ITD, NPM1+	normal	90.800	F	73
11	BM	FLT3-ITD wt, FLT3-TKD wt, IDH1+, IDH2 wt	normal	>30,000	M	19
12	BM	PML-RARα	(15;17)(q22;q12), -Y	8.060	M	43
13	BM/PB	FLT3-ITD+	normal	70.000	M	65
14	BM	NA	normal	NA	M	79
15	BM/PB	NA	normal	260.000	M	72
16	BM/PB	FLT-ITD+, NPM1+, WT-1	normal	46.000	M	31
17	BM/PB	FLT3-ITD wt, FLT3-TKD+ , NPM1+, IDH1 wt, IDH2 wt, TP53 wt	normal	118.780	F	61
18	PB	NA	NA	11.800	M	90
19	BM	NA	NA	33.000	F	74
20	BM	NA	na	NA	F	71
21	BM	NA	normal	NA	F	66
22	BM/PB	FLT3 ITD wt, FLT3- TKD wt, NPM1+	normal	3.700	F	59
23	PB	FLT3 wt, NPM1 wt	+(8)	11.000	M	70
24	BM/PB	NA	complex	NA	F	72
25	PB	NA	NA	195.000	M	51
26	BM	FLT3wt, NPM1wt e DNMT3A wt	+(19)	12.500	M	72

27	BM	FLT3-ITD	normal	38.000	F	61
28	BM	FLT3 wt, NPM1 wt	NA	36.000	M	70
29	PB	PML-RARα	t(15,17)	99.300	F	77
30	BM	FLT3-TKD+, NPM1 +	normal	82.200	F	76
31	BM	FLT3 wt, NPM1+, TP53 wt	normal	1.700	M	73
32	BM	FLT3-ITD+, NPM1+, TP53wt, IDH1 and IDH2wt	normal	55.360	M	65
33	BM	FLT3-TKD, NPM1+	normal	2.400	F	50
34	BM	NA	iperdip	2.440	F	74
35	BM	NA	NA	5.300	F	69
36	BM	NA	complex	238.000	M	69
37	BM	FLT3 wt, NPM1 wt	del(7)	1.400	M	61
38	BM	FLT3-ITD, NPM1+	normal	95.000	F	50
39	BM	FLT3 wt, NPM1 wt	normal	88.000	M	45
40	BM	FLT3 wt, NPM1 wt	normal	37.200	F	38
41	BM	FLT3 wt, NPM1 NA	complex	7.360	M	61
42	BM	FLT3 wt, NPM1 wt	complex	71.810	F	62
43	BM	FLT3 wt, NPM1 NA	normal	660	M	64
44	BM	FLT3-ITD, NPM1+	normal	189.500	M	63
45	BM	NA	normal	3.150	F	66
46	BM	FLT3 wt, NPM1 na	normal	4.000	M	74
47	BM	FLT3 wt, NPM1 wt	normal	3.800	F	51

Table 2. Patient characteristics [**Legend**: PB, peripheral blood; BM, bone marrow; NA, Not available].

Normal $CD34^+$ cells were isolated from CB buffy coats obtained from the Cord Blood Bank (ERCB) of Immunohematology and Transfusion Medicine, S. Orsola-Malpighi, University Hospital of Bologna.

Mononuclear cells (MNCs) from PB, BM, and CB were isolated by a density gradient centrifugation (Lympholyte, Cedelane, Burlington, Canada).

The enrichment of $CD34^+$ cells from CB-derived MNCs were obtained using an immunomagnetically separation according to the manufacturer's instruction (Miltenyi Biotec). The separation is based on the magnetically labeled CD34 antigen, a single chain transmembrane glycoprotein expresses on human progenitor. The HSCs are

present at a frequency of about 0.1-0.5% in CB but are rapidly enrich using MicroBeads directly conjugated to CD34 antibodies for labeling of CD34-expressing. At first, the MNCs were magnetically labeled with CD34 MicroBeads in Miltenyi buffer (PBS supplemented with 2mM EDTA and 0.5% bovine serum albumin, BSA) at 4 °C for 30 minutes. Then, the cell suspension was washed to remove the unloaded MicroBeads and loaded onto a MACS® Column which is placed in the magnetic field of a MACS Separator. The magnetically labeled $CD34^+$ cells were retained within the column and the unlabeled cells ran through, because were $CD34^-$. After removing the column from magnetic field, the $CD34^+$ cells retained within the column were flushed out pushing the plunger into the column. To increase the purity of CB-derived $CD34^+$ cells, the eluted fraction was enriched over a second MACS® Column.

Human myeloid leukemia cell lines, OCI-AML3, and THP-1 were purchased from DMSZ (Braunschweig, Germany). Knockout (CRISPR-Cas9 targeting TAS2R4, TAS2R10, TAS2R8, TAS2R13 or TAS2R30 genes) THP-1 cells were purchased from Synthego Inc. Primary AML cell, and AML cell line cultures were maintained in RPMI 1640 medium with L-Glutamine (Lonza), and CB-derived $CD34^+$ cells were cultured in Dulbecco's Modified Eagle Medium (DMEM) (Sigma Aldrich), both supplemented with 10% heat-inactivated fetal bovine serum (FBS, Gibco), 1% Penicillin/Streptomycin (Pen/Strep) (MP Biomedicals, Verona, Italia), 1% Hepes buffer (Corning), and maintained at 37 °C in a humidified 5% CO_2 incubator, with or without increasing doses of Denatonium Benzoate (DEN) (#D5765-1G), Quinine (#145904-10G), Chloroquine Diphosphate salt (#C6628-25G), Ara-C (#147-94-4) (Sigma Aldrich).

2. *In Silico* Gene Expression Analysis

For *in silico* analysis, all calculations were performed using R version 3.6.1. CEL files raw data were normalized using Robust Multi-Array Average (RMA) and log2 transformed. In The Cancer Genome Atlas (TCGA) (https://gdc.cancer.gov/about-data/publications/laml_2012) datasets downloaded, the Affymetrix U133 Plus 2 was used to perform RNA-expression profiling. The differential expression levels of T2Rs were assessed in 183 AML samples, also in association with clinical data, and in 12 CB-derived $CD34^+$ cells (Gene set: GSE19835) by the limma package (Bioconductor). The following T2R transcripts probes were: TAS2R1, TAS2R3, TAS2R4, TAS2R5, TAS2R7, TAS2R8, TAS2R9, TAS2R10, TAS2R13, TAS2R14, TAS2R16, TAS2R38, TAS2R39, TAS2R40, TAS2R41, TAS2R42, TAS2R43, TAS2R44, TAS2R45, TAS2R46, TAS2R48, TAS2R49, TAS2R50, TAS2R60. For all statistical analysis, we considered p-value<0.05 and Benjamini–Hochberg adjusted p-values <0.05.

3. Quantitative real-time polymerase chain reaction (qRT-PCR)

In order to quantify the expression levels of the mRNA of genes, we used the qRT-PCR. At first, cells were disrupted in an RLT Buffer solution 1% ß-mercaptoethanol (ß-ME) and cell lysates were homogenized through a syringe. Total RNA was isolated using a Rneasy Micro kit (Qiagen) according to the manufacturer's instruction and quantified by Nanodrop ND-1000 spectrophotometer (NanoDrop Technologies). To avoid genomic DNA contamination, 1µg of RNA samples were treated with DNase I (1U/µl) and incubated at 37 °C for 30 minutes in 10X reaction buffer with $MgCl_2$ (Thermo Fisher scientific). After that, it was added 50mM EDTA and incubated at 65 °C for 10 minutes, this prevented the RNA hydrolyzation that happens during heating with divalent

cations in the absence of a chelating agent. For cDNA synthesis, 1µg of denatured total RNA was reverse transcribed using an Improm II kit (Promega) and random hexamers (Promega) according to the manufacturer's instruction. qRT-PCR was performed using the ABI-PRISM 7900 Sequence Detection System (Applied Biosystems). The qRT-PCR reactions were performed using a 96-well Optical Reaction Plate. For each PCR run, 5µl of cDNA product was mixed with 2x Platinum Super mix (Thermo Fisher Scientific) in a total volume of 25µl. The thermal cycling conditions consisted of an initial stage of 50 °C for 2 minutes, 95 °C for 10 minutes, 40 cycles of melting at 95 °C for 15 seconds, and annealing and elongation at 60 °C for 1 minute. Threshold cycle (C_t) values for target genes and endogenous reference gene (Glyceraldehyde 3-phosphate dehydrogenase, GAPDH) (Table 3) were determined automatically. Relative quantification was calculated using ΔC_t comparative method [135]. Briefly, the relative level of a specific cDNA was calculated by subtracting the C_t value of the endogenous reference gene from the C_t value of the specific gene. cDNA, synthetized as described before, from a Universal RNA (Agilent genomics) was used as the reference sample. All reactions were performed in duplicate.

Gene	accession number	purchased from	Probe ID	product size bp
TAS2R4	NM_016944	IDT	Hs.PT.58.24880205.g	131
TAS2R8	NM_023918	IDT	Hs.PT.58.27572746.g	133
TAS2R10	NM_023921	IDT	Hs.PT.58.25022966.g	112
TAS2R16	NM_016945	IDT	Hs.PT.58.3030778.g	110
TAS2R30/47	NM_001097643	IDT	Hs.PT.58.40967668.g	147
TAS2R38	NM_176817	IDT	Hs.PT.58.1997269.g	122
TAS2R39	NM_176881	IDT	Hs.PT.58.25428396.g	123
TAS2R43	NM_176884	IDT	Hs.PT.58.26835465.g	137
TAS2R46	NM_176887	IDT	Hs.PT.58.26491131.g	142
GAPDH	NM_002046	IDT	Hs.PT.58.40035104	123
TAS2R13	NM_023920.2	Applied Biosystem	Hs00256781_s1	132
GNAT3	NM_001102386.2	Applied Biosystem	Hs01385397_m1	109
GNB1	NM_001282538.1	Applied Biosystem	Hs00929799_m1	64
PLC-b2	NM_001284297.1	Applied Biosystem	Hs00190117_m1	69
GAPDH	NM_001289745.1	Applied Biosystem	Hs00266705_g1	74

Table 3. RT-PCR probes used.

4. Gene expression profile (GEP)

Gene expression profiling measures mRNA levels, showing the pattern of genes expressed by a cell at the transcription level. To investigate the effect of DEN exposure on AML cells, we carried out GEP analysis on 61 AML samples (49 from a publish dataset [132] and 12 new cases) using GeneChip Human Transcriptome Array 2.0 (Thermo Fisher Scientific). The preparation of labelled single-stranded complementary DNA (ss-cDNA) was performed according to the manufacturer's recommendation. Three independent replicates of each condition were hybridized to Clariom S Arrays HT Human (Thermo Fisher Scientific) according to the manufacturer's recommendations. Data quality control and normalization (signal space transformation robust multiple-array average, sst-RMA) and Supervised analysis were carried out by Expression Console software and Transcriptome Analysis Console software, respectively (both from

Thermo Fisher Scientific). For cells, data were normalized on vehicle-treated cells before comparison. Genes in AML samples with a 1.5-fold differences and $p \leq 0.05$ were considered for enrichment analyses. Functional annotation clustering was performed using David Bioinformatics Resources 6.8 (National Institute of Allergy and Infectious Disease), and Thomson Reuter's MetaCore software suite (Clarivate Analytic).

5. Cytosolic Ca^{2+} concentration measurements

Calcium ions (Ca^{2+}) represent an important class of second messengers used by the G protein-coupled receptor (GPCR). Under basal conditions, the concentrations of cytoplasmic calcium are very low, but tend to increase following GPCR stimulation. Thus, we measured the Ca^{2+} release after DEN exposure to investigate the TAS2R activation. Cytosolic free Ca^{2+} concentrations were measured in a thermostat controlled (37 °C) and magnetically stirred Cary Eclipse Fluorescence Spectrophotometer (Agilent Technologies) with the fluorescent indicator fura-2/acetoxymethyl ester (fura-2/AM). $2x10^6$ AML cells or $5x10^5$ $CD34^+$ cells were loaded with 2µM fura-2/AM for 20 min in the presence of 1mM $CaCl_2$ and 250µM sulfinpyrazone in saline solution (125mM NaCl, 5mM KCl, 1mM $MgSO_4$, 1mM NaH_2PO_4, 20mM HEPES, 5.5mM glucose, 5mM $NaHCO_3$, and 1mM $CaCl_2$, pH 7.4), rinsed, and re-suspended at a final concentration of 10^6/ml in the same buffer. After stabilization of the signal, cells were stimulated with 10mM DEN, with or without the presence of two cell permeant chelators, BAPTA-AM and EDTA, which are selective for intracellular Ca^{2+}. Excitation ratio and emission wavelength were 340/380 and 505 nm, respectively.

6. Western blot analysis

To prove the presence of protein levels, we performed western blot analysis. Cells were washed twice with a washing buffer, composed of PBS and 1mM protease inhibitor Phenylmethanesulfonyl fluoride (PMSF) (Sigma Aldrich) at 4 °C for 5 minutes at 2000 rpm. Cells were then lysed at 4 °C for 30 minutes in Cell Lysis Buffer (Cell Signaling Technology), enriched with PMSF and protease inhibitors (Complete mini Protease Inhibitor cocktail table, Roche). The extracted proteins were quantified according to the Bradford method with Coomassie G-250 (Thermo Fisher Scientific) by using Bio-photometer (Eppendorf). 30µg of proteins were diluted with 2x Laemli sample Buffer 2% ß-ME (Bio-Rad) and denatured at 96 °C for 5 minutes. Denatured proteins were loaded in a 10-12% polyacrylamide-gel electrophoresis (Mini-PROTEAN® TGX Stain-Free Precast Gels, Bio-Rad). A marker (Precision Plus Protein™ Kaleidoscope™ Prestained Protein standards, Bio-Rad) composed of a mixture of ten multi-colored recombinant proteins was used as protein molecular weight standard. The protein separation was performed in TGS (10X Tris/Glycine/sodium dodecyl sulfate, SDS) running buffer (Bio-Rad). After the separation, the proteins were transferred from the gel to a nitrocellulose membrane through the Trans-Blot® Turbo™ Transfer System (Bio-Rad). The membrane was then incubated for 1h at room temperature with gentle shaking, in a blocking solution of TBS with 0.1% of Tween (Sigma) and 5% of dry milk or BSA. For the staining, the membrane was incubated with the following primary antibody (Ab) (Table 4), diluted in the blocking solution, at 4 °C overnight with gentle shaking. After 3 washes in TBS 0.1% Tween, the membrane was then incubated with horseradish-peroxidase (HRP)-conjugated secondary Ab (Table 4), diluted in blocking solution, at room temperature for 1h with gentle shaking. After 3 washed in TBS 0.1%

Tween, protein bands were detected at Chemidoc instrument (Bio-Rad) using ECL™ Prime and ECL Select™ Western Blotting Detection Reagent and (GE Healthcare, Amersham™), according to the manufacturer's protocol.

Antibodies	Company	Catalog No.	Clone
Goat Anti-T2R4	Santa Cruz Biotechnology	sc-169494	T-13 polyclonal
Rabbit Anti-T2R10	Santa Cruz Biotechnology	sc-169473	D-12 polyclonal
Goat Anti-T2R47	Santa Cruz Biotechnology	sc-34859	L-12 polyclonal
Mouse Anti-PLC β2	Santa Cruz Biotechnology	sc-515912	B-2 monoclonal
Goat Anti-Actin	Santa Cruz Biotechnology	sc-1616	I-19 polyclonal
Rabbit Anti-Phospho-Histone H2A.X	Cell Signaling Technology	9718	20E3 monoclonal
Rabbit Anti-CDK2	Cell Signaling Technology	2546	78B2 monoclonal
Rabbit Anti-T2R8 Antibody	Abcam	ab75109	polyclonal
Rabbit Anti-GNB1	Abcam	ab137635	polyclonal
Rabbit Anti-T2R13	ThermoFisher Scientific	PA5-39709	polyclonal
Mouse Anti-Cdc25A	ThermoFisher Scientific	MA5-13794	DCS-120 monoclonal
Mouse Anti-Cyclin A2	ThermoFisher Scientific	MA1-180	6B4D11 monoclonal
Rabbit Anti-Cyclin D1	ThermoFisher Scientific	MA5-16356	SP4 monoclonal
HRP-conjugated Donkey Anti-Goat IgG	Santa Cruz Biotechnology	sc-2033	
HRP-conjugated Donkey Anti-Mouse IgG	Santa Cruz Biotechnology	sc-2314	polyclonal
HRP-conjugated Donkey Anti-Rabbit IgG	Bethyl	A120-108P	polyclonal

Table 4. Following primary and secondary antibodies used in western blot analysis.

7. Cell cycle

To study changes in the cell cycle distribution of cells following treatment with DEN, we used the Propidium Iodide (PI)/RNase assay. PI is a fluorescent vital dye that stains DNA and RNA. PI binds to both DNA and RNA, so the latter must be removed by digestion with ribonucleases. The content of DNA as determined by flow cytometry, can reveal useful information about the cell cycle and the proteins involved in the regulation of the cell cycle. Cells in G2 and M phases of the cell cycle have double the DNA content of those in G0 and G1 phases. Cells in S phase have a DNA content lying between these extremes. PI is detected in the orange range of the spectrum using a 562-588 nm band pass filter.

The cell cycle distribution was assessed after 24-48 hours of treatment. Cells were first permeabilized with PBS-0.1% NP-40 at 4 °C for 15 minutes and then labelled with PI/RNase Staining Buffer (BD) at room temperature for 15 minutes. The DNA content was assessed by CytoFlex (Beckman Coulter) and results were analysed by Kaluza Analysis Software (Beckman Coulter).

8. Viability and proliferation assay

In order to assess the effects of the presence of DEN (w/ or w/o Ara-C), Quinine, and Chloroquine on the viability and proliferation in AML cells and CB-derived $CD34^+$ cells, we used the CellTiter 96 AQuenous proliferation assay (Promega), a colorimetric method for determining the number of viable cells. The reagent solution contains a tetrazolium compound [3-(4,5-dimethylthiazol-2-yl)-5-(3-carboxymethoxyphenyl)-2-(4-sulfophenyl)-2H-tetrazolium, inner salt; MTS] and an electron coupling reagent (phenazine ethosulfate; PES), that enhance the formation of a stable solution. The

quantity of formazan product as measured by the amount of absorbance is directly proportional to the number of living cells in the culture.

$1x10^5$ AML or $5x10^4$ $CD34^+$ cells/100µl culture medium were seeded into 96-well microplate and treated as indicated. After culturing, 20µl of CellTiter 96 AQuenous One Solution reagent was added to each well and the microplate was incubated for 3-4 hours at 37 °C. Optical density value was measured by an ELISA plate reader (Multiskan Ex, Thermo Electron Corporation) at a wavelength of 492 nm. Each variant group was performed in triplicates.

CellTiter-Glo® Luminescent Cell Viability Assay (Promega) is a homogeneous method to determine the number of viable cells in culture based on quantitation of the ATP present, and it was used in some experiments. Briefly, $5x10^4$ cells/100 µl culture medium were seeded into a 96-well microplate and treated as indicated. After culturing, according to the protocol's instruction, we added 100µl of CellTiter-Glo® Reagent to each well, mixed contents for 2 min on an orbital shaker to induce cell lysis. After 10 min incubation at room temperature, luminescence was recorded with the Sparke multiplate reader (Tecan). Each condition was analysed in triplicates.

9. ApoTox-Glo™ Triplex Assay

The ApoTox-Glo™ Triplex Assay (Promega) combines three assay chemistries to assess viability, cytotoxicity and caspase 3/7 activity within a single assay well. Briefly, CB-derived $CD34^+$ cells were plated in 96-well plate ($2x10^4$/100µl) and treated with increasing doses of DEN for 48h. At the end of culture, according to the protocol's instruction, we added 20µl of Viability/Cytotoxicity Reagent to each well. After 2h incubation at 37 °C, cell viability and cytotoxicity (wavelength 400Ex/505Em,

485Ex/520Em, respectively) were assessed by measuring fluorescence with the Sparke multiplate reader (Tecan). After the measurement of cell viability, the Caspase-Glo® 3/7 Reagent was added into each well, the plates were briefly mixed by an orbital shaker and incubated for 30 min at 37 °C. Caspase-3/7 activation was determined by measuring luminescence within the following ranges of 0.5-1 second. Each variant group was performed in triplicates.

10. Clonogenic assay

To evaluate the effect of DEN exposure on the clonogenic capacity, $1x10^5$ AML cells or $5x10^2$ $CD34^+$ cells were resuspended in 100µl IMDM supplemented with 10% FBS and cultured in 1ml of methylcellulose, supplemented with the following cytokines: 50ng/ml of SCF, 20ng/ml of GM-CSF, 20ng/ml of G-CSF, 20ng/ml of IL-3, 20ng/ml of IL-6 and 3U/ml of Epo (StemMACS HSC-CFU complete with Epo, MACS Miltenyi Biotec) according to the manufacturer's specifications. The cell/methylcellulose suspension was aliquot into 35mm petri dishes and incubated for 10 days (AML cells) or 14 days (CB-derived $CD34^+$ cells) at standard condition in the presence of increasing concentrations of DEN. The evaluation of stem and progenitor cells as colony-forming units (CFU) were scored under an inverted microscope (Zeiss). The HSC colonies were classified by the colour and morphology in colony-forming-unit granulocyte, macrophage (CFU-GM), burst-forming-unit erythrocyte (BFU-E), and colony-forming-unit erythrocyte (CFU-E). In dedicated experiments, CFU assays were preceded by a 6-day liquid culture in the presence of SCF (50ng/ml), IL-3 (50ng/ml) and GM-CSF (10ng/ml), with or without DEN.

11. Human long-term culture-initiating cell (LTC-IC) assay

In our experiments, long-term culture-initiating cell (LTC-IC) assay was performed according to the manufacturer's instruction (STEMCELL™ Technologies). The murine stromal cell line, M2-10B4, genetically engineered to produce G-CSF and IL-3, was used as feeder layer. It was irradiated at 8000cGy, resuspended in MyeloCult™ H5100 medium supplemented with 10^{-6} Hydrocortisone (STEMCELL™ Technologies) and seeded $4.5x10^5$ cells/well in a 24-well plate. After 24 hours, $5x10^3$ highly purified CB-derived $CD34^+$ cells were planted onto each well and treated as indicated. After 5 weeks, the cells were harvested and the clonogenic potential of cultured cells was assessed in CFU assays (explain above). The number of LTC-IC present in the initial test cell suspension was calculated dividing the total number CFUs detected in the culture by the average number of clonogenic progenitors per LTC-IC (harvested from LTC-IC culture and planted in the dishes) [142].

12. Flow cytometer analysis

The evaluation of protein expression was analysed using superficial or intracellular staining. All the staining, described below, was analysed by a flow cytometer (BD AccuriTM C6, BD Becton Dickinson) and FCS Express 4 Software (De Novo Software).

12.1. Cell intracellular staining

The culture cells were harvested and washed twice with PBS. After we used the Fixation/Permeabilization Solution Kit (#554714) (BD), according to the protocol's instruction. Thus, cells were fixed/permeabilized by fix/perm BD buffer at 4 °C for 20 minutes. After being washed with perm/wash buffer 1X, cells were stained with primary

Ab (Table 5) at 4 °C for 1 hour. Where necessary, cells were staining with conjugated secondary Ab (Table 5) at room temperature for 30 minutes.

Antibodies	Company	Catalog No.	Clone
Mouse PLK-1 Antibody	Thermo Fisher Scientific	MA5-17152	monoclonal
Rabbit Anti-Active Caspase-3 PE	BD	550821	monoclonal
Anti-Mouse IgG (H+L), F(ab')2 Fragment Secondary Ab Alexa Fluor® 488 Conjugate	CellSignalling	4408S	

Table 5. Following primary and secondary antibodies used in cell intracellular staining.

12.2. Cell surface staining

After culturing, the cells were harvested and washed with PBS. We stained cells with primary Ab (Table 6) at room temperature for 20 minutes. Where necessary, cells were staining with conjugated secondary Ab (Table 6) at room temperature for 20 minutes.

Antibodies	Company	Catalog No.	Clone
Mouse Anti-Human CD184 PE	BD	557145	monoclonal
Mouse Anti‑Human ABCC4 / MRP4 Antibody	LSBio	LS-C191873-100	monoclonal
F(ab')2-Goat Anti-Mouse IgG (H+L) Secondary Antibody, PE	eBioscience™	12-4010-82	polyclonal

Table 6. Following primary and secondary antibodies used in cell surface staining.

12.2.1. Stem cell compartment analysis

In order to evaluate the effect of DEN exposure on HSC compartment, we analysed the frequency of the following hematopoietic progenitors after treatment with DEN: HSC: $CD34^{+}CD38^{-}CD45RA^{-}CD90^{+}$; MPP: $CD34^{+}CD38^{-}CD45RA^{-}CD90^{-}$; MLP: $CD34^{+}CD38^{-}$

$CD45RA^+CD90^-$; CMP: $CD34^+CD38^+CD123^{low}CD45RA^-$; MEP: $CD34^+CD38^+CD123^-CD45RA^-$; GMP: $CD34^+CD38^+CD123^+CD45RA^+$.

Highly purified CB-derived $CD34^+$ cells were cultured in standard condition in presence of increasing doses of DEN. After 48 hours and 6 days, cells were harvested, washed in PBS and stained with primary Ab at 4 °C for 20 minutes (Table 7).

Antibodies	Company	Catalog No.	Clone
CD45RA PE-Cy™7	BD	337186	
Mouse Anti-Human CD34 BV421	BD	562577	monoclonal
Mouse Anti-Human CD38 APC	BD	555462	monoclonal
Mouse Anti-Human CD90 FITC	BD	555595	monoclonal
Mouse Anti-Human CD123 PE	BD	340545	

Table 7. Following primary antibodies used in cell surface staining to analyse the frequency of hematopoietic progenitors.

Labeled cells, and the different stem/progenitor cell subsets were identified (Fig.10) and acquired with a flow cytometer FACScanto II (Becton Dickinson). The results were analysed by Kaluza Analysis Software (Beckman Coulter).

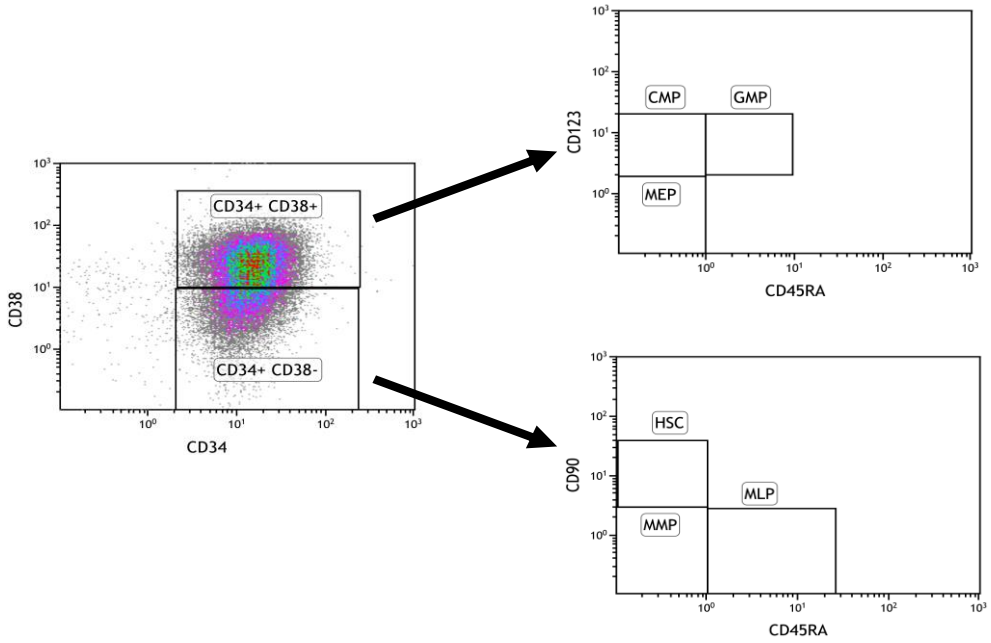

Figure 10. Gate strategy for individuation of hematopoietic stem/progenitor cells.

13. Seahorse XF Cell Mito Stress Test

To investigate the alteration in cellular bioenergetics of AML cells after DEN exposure, we used the Seahorse XF Cell Mito Stress Test, which measures key parameters of mitochondrial function by directly measuring the oxygen consumption rate (OCR) of cells.

Cell Mito Stress Test assay was performed following the standard protocol. Briefly, THP-1 and OCI-AML3 were seeded at the concentration of $5x10^5$/ml in a 24-well plate and treated with increasing doses of DEN. After 24h incubation, growth medium from each well was replaced by pre-warmed assay medium (XF base medium supplemented with 1.025mM glucose, 2mM glutamine and 1mM sodium pyruvate, pH 7.4) and counted. Cell were seeded at $5x10^4$/well for THP-1 and $1.5x10^5$/well for OCI-AML3 in Seahorse 96-well plates coated with CellTak (BD Biosciences, San Jose, CA, USA) to

facilitate attachment and the incubated in un-buffered DMEM pH 7.4 at 37 °C in a non-CO_2 incubator for 40 minutes. Oxygen consumption rate (OCR) was detected after injection of oligomycin (1µM), Carbonyl cyanide-p-(trifluoromethoxy)phenylhydrazone (FCCP) (0.5µM), and the combination of antimycin and rotenone (0.5µM) (XF Cell Mito Stress Test Kit, Seahorse Bioscience) to allow to pre-equilibrate with the assay medium before the analysis. The assays were performed by using the XFe96 analyser (Agilent Technologies) and the data were analysed by the Wave software (version 2.2.0, Seahorse Bioscience) after normalization.

14. Glucose Uptake-Glo™ Assay

The Glucose Uptake-Glo™ Assay is a non-radioactive, plate-based, homogeneous bioluminescent method for measuring glucose uptake in human cells based on the detection of 2-deoxyglucose-6-phosphate (2DG6P).

Glucose uptake was performed according to the manufacturer's instructions. Briefly, cells were seeded at $5x10^4$/well in 96-well plates and treated with increasing doses of DEN. After 24h of incubation, we added 50µl of 1mM 2DG per well and incubate 10 minutes at room temperature. After that, we added 25µl of Stop Buffer, 25µl of Neutralization Buffer, and 100µl of 2DG6P Detection Reagent. We incubated the culture microplates for 5h at room temperature, and then the luminescence was detected by a Microplate Reader.

15. Migration assay

To assess the effect of TAS2R activation on cell migration, we performed experiments by using the transwell assay. 100µl RPMI 10% FBS, containing $1x10^5$ AML cells were planted in the upper layer of a cell culture insert with permeable membrane (diameter

6.5 mm, pore size 8µm Corning Costar), while 600µl medium was added to the bottom chamber. After overnight incubation at 37 °C in 5% humidified CO_2 atmosphere, inserts (upper chambers) were removed and cells transmigrated into lower chambers were recovered and counted under an inverted microscope (Nikon) using 5X magnification. In some experiments, increasing doses of DEN were added to the upper or lower chamber alone or in presence of 150ng/ml CXCL12 (Meridian Life Science), otherwise cells were incubated for 4 hours in the presence of increasing doses of DEN, which was then washed out before migration assay.

16. Apoptosis

To evaluate cell apoptosis after DEN treatment, we used the Annexin-V FLUOS Staining kit (Roche Diagnostics, Germany). Thanks to the high affinity of Annexin-V for phosphatidylserine (PS), this test allows to mark the PS residues that are exposed on the membrane cell during the early stages of the apoptotic process. Moreover, necrotic cells show PS residues on the cell membrane, but the absence of an integral membrane help the incorporation of PI.

After the indicated treatment, cells were harvested and stained according to the manufacturer's instruction. $1x10^6$ cells were resuspended in 100µl Incubation Buffer, stained with 2µl FITC-conjugated Annexin-V and 2µl PI for 10 minutes at room temperature and analysed by a flow cytometer (BD AccuriTM C6, BD Becton Dickinson) and FCS Express 4 Software (De Novo Software). These results were compared to the apoptotic rate of untreated cells.

17. Immunofluorescence

We analysed protein expression by immunofluorescence staining. Thus, we transferred $1x10^6$ cells on a microscope slide (DIAMOND) using the Cytospin (Shandon Elliott) at 500 rpm for 10 minutes. Then, cells were fixed with 4% paraformaldehyde (PFA) for 10 minutes, washed three times with cold PBS and for other three times with PBS-0.1% Tween. Cells were permeabilized using PBS-0.25% Triton for 5 minutes. Before the staining with primary Ab (Table 8), cells were incubated with the blocking solution (PBS supplemented with 0.1% Tween and 1% BSA) for 30 minutes at room temperature. After that, the staining with primary Ab was performed for 30 minutes at room temperature in the dark, and the same condition was applicate for the staining of conjugated secondary Ab (Table 8). Stained cells were examined under fluorescence Axiovert microscope with CCD camera (Zeiss).

Antibodies	Company	Catalog No.	Clone
Rabbit Anti-Caspase-3	Invitrogen	700182	recombinant monoclonal
Goat Anti-T2R4	Santa Cruz Biotechnology	sc-169494	T-13 polyclonal
Mouse Anti-PLC β2	Santa Cruz Biotechnology	sc-515912	B-2 monoclonal
Rabbit Anti-GNB1	Abcam	ab137635	polyclonal
Swine Anti-Rabbit Secondary Antibody	Dako	F0205	polyclonal
Rabbit Anti-Goat Secondary Antibody	Dako	F0205	polyclonal
Rabbit Anti-Mouse Secondary Antibody	Dako	R0270	polyclonal

Table 8. Following primary and secondary antibodies used in Immunofluorescence.

18. Mitochondrial membrane potential measurement

To study the mitochondrial membrane potential (Δψm) alteration during apoptosis, we investigated the variation in Δψm using the BD™ MitoScreen Kit (BD) according to the manufacturer's instruction. The membrane-permeable lipophilic cationic fluorochromes are used as probes of Δψm; they penetrate cells and their fluorescence is a reflection of Δψm. JC-1 is a cationic carbocyanine dye that accumulates in mitochondria. The dye exists as a monomer at low concentrations and emits at 527nm. At higher concentrations, the dye forms J-aggregates that exhibit a broad excitation spectrum and an emission maximum at 590 nm. These characteristics make JC-1 a sensitive marker for mitochondrial membrane potential [143].

For this experiment, $1x10^6$ cells were harvested, washed twice with PBS and incubated with JC-1 solution for 15 minutes at 37 °C. After the staining cells were washed two times and the JC-1 monomers or aggregates were analysed a flow cytometer (BD AccuriTM C6, BD Becton Dickinson) and FCS Express 4 Software (De Novo Software).

19. *In vivo* experiments

Experiments involving animals were approved by the Italian Ministry of Health and have been done in accordance with the applicable Italian laws (D.L.vo 26/14 and following amendments). This are the Institutional Animal Care and Use Committee, and the institutional guidelines at the European Institute of Oncology. *In vivo* studies were carried out in immunodeficient NOD scid gamma (NSG) mice (Charles River, Italy), 6-9-weeks old. The mice were bred and housed under pathogen-free conditions in the animal facilities at the European Institute of Oncology-Italian Foundation for Cancer Research (FIRC) Institute of Molecular Oncology (IEO–IFOM, Milan, Italy)

campus. NSG mice of both sexes were used in our experiments. Twenty-four hours after irradiation (1 Gy), mice were transplanted through the tail vein with 1×10^5 CB-derived $CD34^+$ cells, pre-incubated for 24h with or without 0.5mM DEN. The percentage of human $CD45^+$ cells were evaluated at various intervals (14 days, 1, 2, 3, and 4 months after transplantation) to assess the engraftment. At the time of sacrifice, tibia and femur were collected and cleaned off the flesh by rubbing with a gauze. Once cleaned, bones were put in a 60mm dish containing 5ml of ice-cold PBS supplemented with 1% P/S and 2% of FBS. BM cells were obtained by washing the medullary cavity of the bones with PBS in a 1ml syringe. The cells collected were then centrifuged 1200 rpm at 4°C for 5 minutes. In order to remove erythrocytes, cells were incubated with red cell lysis buffer (155mM NH_4Cl, 12mM $NaHCO_3$, 0.1mM EDTA) for 2 minutes on ice. After incubation, cells were centrifuged again at 1200 rpm at 4°C for five minutes and were passed through a cell 40µm strainer in order to remove clumps and red cellular debris. Leukocytes were used for the described experiments.

20. CompuSyn Report

The Chou-Talalay method for drug combination is based on the median-effect equation, which provides the theoretical basis for the combination index (CI)-isobologram equation. This equation allows quantitative determination of drug interactions, where CI<1, =1, and >1 indicate synergism, additive effect and antagonism, respectively. Based on these algorithms, computer software, Compusyn, is used for determining synergism and antagonism at all doses or effect levels simulated automatically. The effect of the combination between DEN and Ara-C was analysed by this program after 72h treatment.

21. Statistical analysis

Results were expressed as mean ± SEM of at least three separated experiments. Statistical analysis was performed using unpaired two-tailed Student's *t* –test for comparisons between two groups or two-way ANOVA followed by a post-hoc Dunnett's test for comparisons between three or more groups (GraphPad Prism, version 7). P values $p<0.05$ were considered as statistically significant, and indicated as *$p<0.05$, **$p<0.01$, ***$p<0.001$, and ****$p<0.0001$.

Results I

1. AML cells express TAS2Rs

In order to investigate the distribution of TAS2R transcription levels among AML samples, we downloaded the Gene Expression Profile (GEP) CEL files from TCGA AML cohort consisting of 183 AML samples. Based on the $\log_2$ expression levels, we found a strong heterogeneity in the TAS2R expressed transcripts in AML samples. In particular, *TAS2R14*, and *TAS2R43* showed a higher level of TAS2R mRNAs than others (Fig.11).

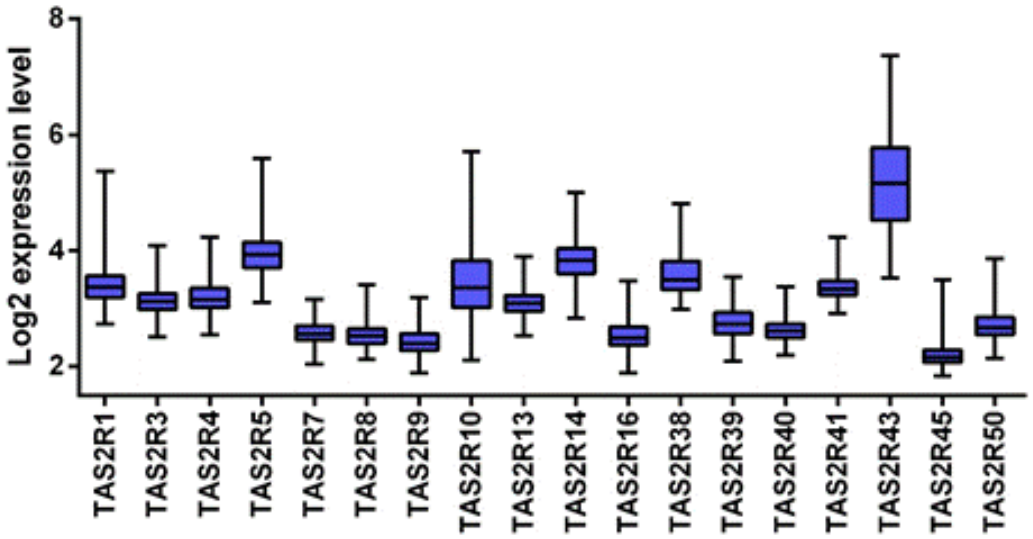

Figure 11. Illustrate relative TAS2R mRNA expression obtained by GEP from the TCGA AML cohort consisting of 183 samples.

To validate these data, we analysed TAS2R expression by GEP in a dataset of 61 samples of AML patients at diagnosis, from our Department. The result confirmed the heterogeneity of TAS2R transcripts. In particular, *TAS2R13*, *TAS2R14*, *TAS2R30*/*47*, *TAS2R31*/*44*, *TAS2R43* showed a higher level of TAS2R mRNAs than others (Fig.12).

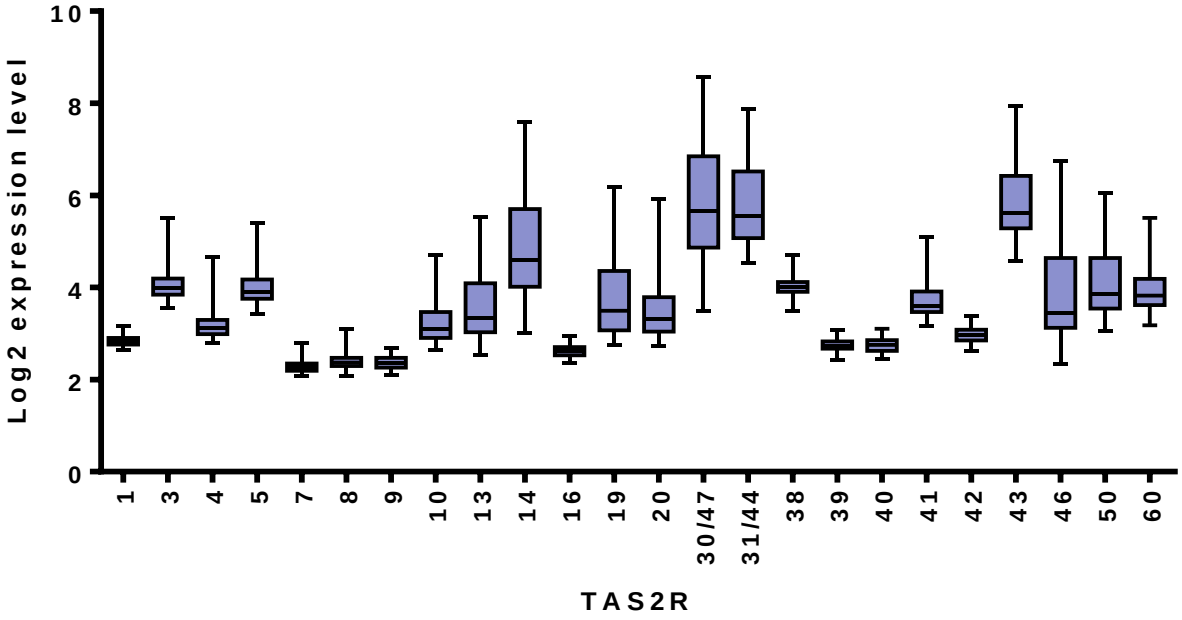

Figure 12. Illustrate relative TAS2R mRNA expression obtained by GEP in a cohort of 61 primary AML samples.

Also, we confirmed the TAS2R mRNA expression levels by qRT-PCR in an independent cohort of 13 AML samples, OCI-AML3 and THP-1 cell lines. Despite the trend of TAS2R expression levels were similar in 61 AML and in the 183 *in silico* AML samples, the qRT-PCR confirmed the trend for only 6 of the 21 TAS2Rs tested but showing the positivity for almost all TAS2Rs (Fig.13).

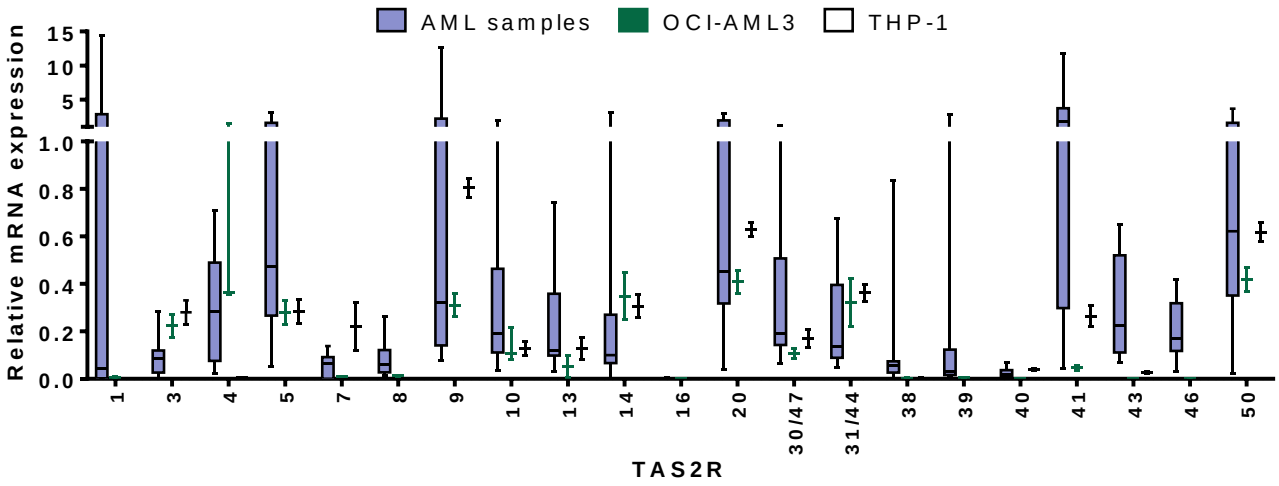

Figure 13. Illustrate TAS2R mRNA expression analysis by qRT-PCR in primary AML samples (n=13) and AML cell lines, THP-1 and OCI-AML3. Error bars refer to THP-1 and OCI-AML3 sample triplicates.

The discrepancy between the dataset from 61 AML, and 183 *in silico* AML samples and the 13 AML samples analysed by qRT-PCR should be due to different size of highly heterogeneous analysed samples.

Taken together, these results demonstrated the heterogeneity of TAS2R gene expression in AML cells.

2. T2Rs are fully functional on AML cells

The T2Rs are G-protein-coupled receptors (GPCRs). After their binding with ligands, the intracellular-cascade signaling goes through the gustducin, a class of receptor-specific G proteins, that stimulate the phospholipase C beta 2 (PLC-ß2) activation, leading to the Ca^{2+} release from intracellular stores.

In order to verify the presence of T2R downstream target in leukemic cells, we analysed ß-gustducin (Gß) and PLC-ß2 mRNA expression by qRT-PCR in primary AML cells, OCI-AML3 and THP-1 cell lines. The result indicated that the factors for canonical

bitter taste signal pathway were present at mRNA levels (Fig.14, panel A), and we confirmed the protein expression of Gß and PLC-ß2 by western blot analysis on five AML samples, OCI-AML3, and THP-1 (Fig.14, panel B).

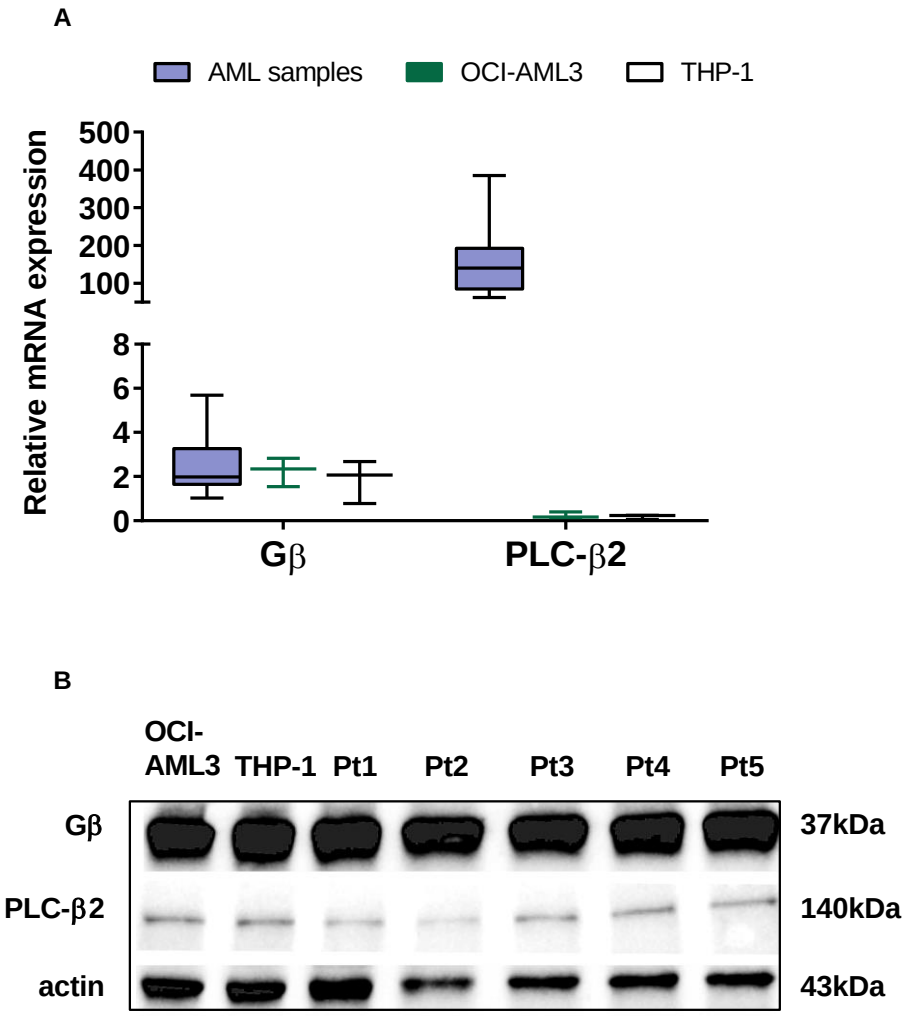

Figure 14. (**A**) qRT-PCR analysis of TAS2R downstream targets in primary AML samples and AML cell lines. (**B**) Western blot analysis of the downstream targets in two AML cell lines and five AML samples (Pt). Actin was shown as the loading control.

We noted that PLC-ß2 mRNA was expressed at lower amounts in AML cell lines as compared to the AML primary cells, while PLC-ß2 protein expression levels seemed to be similar. This result suggested the presence of some mechanism of PLC-ß2 mRNA

upregulation in AML primary samples and/or selective post-transcriptional events modulating PLC-ß2 expression levels.

We next determined the activity of T2Rs by analysing calcium mobilization after stimulation of AML primary cells, OCI-AML3, and THP-1 with three different bitter compounds: Denatonium benzoate (DEN), Quinine (Q), and Chloroquine (CQ). As described, the cytosolic free Ca^{2+} concentrations were measured with the fluorescent indicator fura-2/acetoxymethyl ester (fura-2/AM). A rapid increase in calcium activity was observed in response to DEN (Fig.15, panel A) and Quinine (Fig.15, panel B), while the response to Chloroquine was almost null (data not shown). We ascertained that the measured increase of intracellular calcium was due to store-opened calcium release due to the T2R activation performing the same experiments in the presence of BAPTA-AM or EDTA. The two chelating agents reduced basal intracellular calcium levels, but only BAPTA-AM, which is known to obliterate calcium present in intracellular stores, led to a loss of calcium release into the cytosol following stimulation with DEN and Quinine. However, we observed a slight increase of calcium release also in presence of BAPTA-AM in AML primary samples after stimulation with DEN, suggesting an involvement of other TAS2R-independent pathways as well [144].

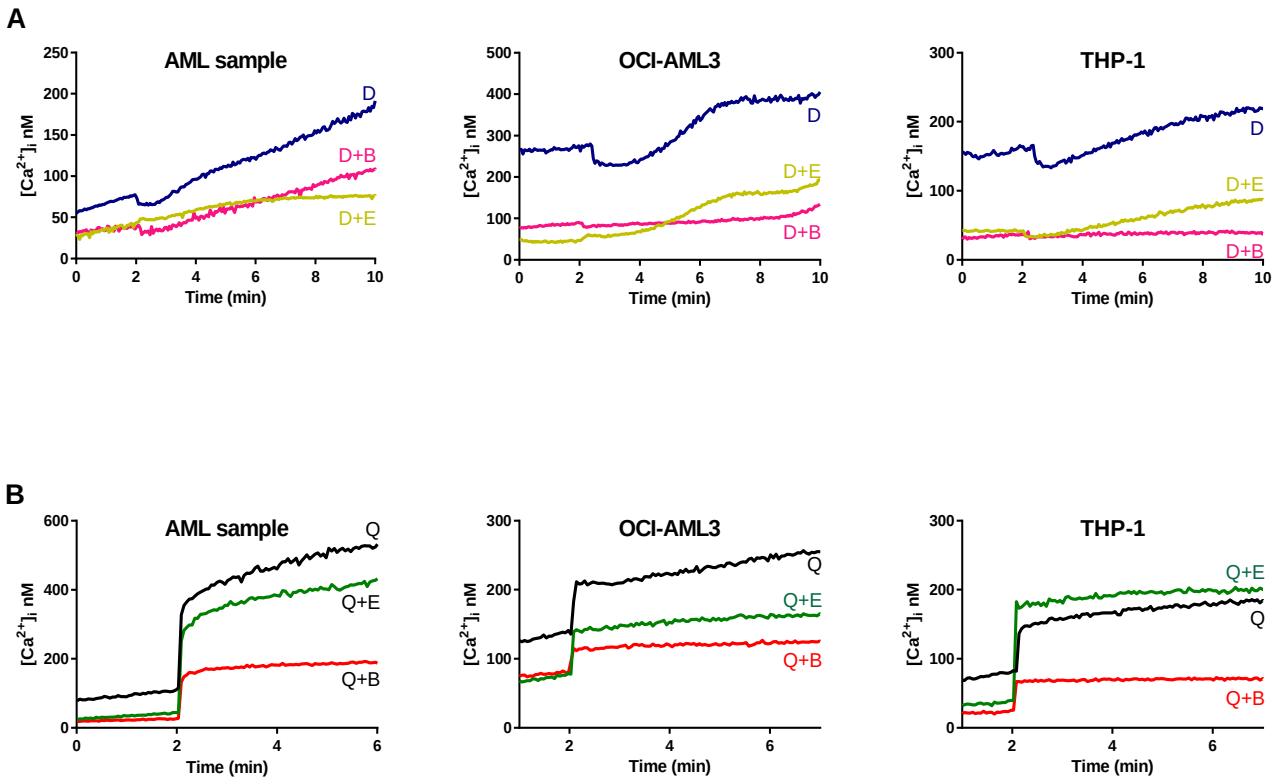

Figure 15. Ca^{2+} release in a representative AML sample and AML cell lines loaded with the Ca^{2+} indicator fura-2/AM and treated with 10mM DEN (indicated as D) (**A**) or 75µM Quinine (indicated as Q) (**B**), in presence of EDTA (indicated as E) or BAPTA-AM (indicated as B) buffer**.**

Taken together, these results demonstrated that AML samples and AML cell lines expressed the canonical factors for T2Rs signal pathway, and that these receptors were activated by bitter compounds.

3. *In silico* analysis reveals a correlation between TAS2R expression levels and AML clinical parameters

To further deepen the significance of TAS2R expression in AML, we investigated the possible relationship between TAS2R transcript levels and clinical parameters in AML patients. For this, we did an association analysis on 183 AML samples from a public database for which clinical data were available. Interestingly, we found a statistically

significant association between some recurrently mutated genes in AML and the TAS2R expression levels. The *TP53* gene, which encodes a tumor suppressor protein containing transcriptional activation, DNA binding, and oligomerization domains, was associated to a lower expression of *TAS2R9* (p-value=0.008) and *TAS2R10* (p-value=0.03) (Fig.16, panel A) when mutated in AML samples. The *TET2* gene, which encodes a protein involved in myelopoiesis, was associated to a lower expression of *TAS2R9* (p-value=0.04) (Fig.16, panel B) when mutated in AML samples.

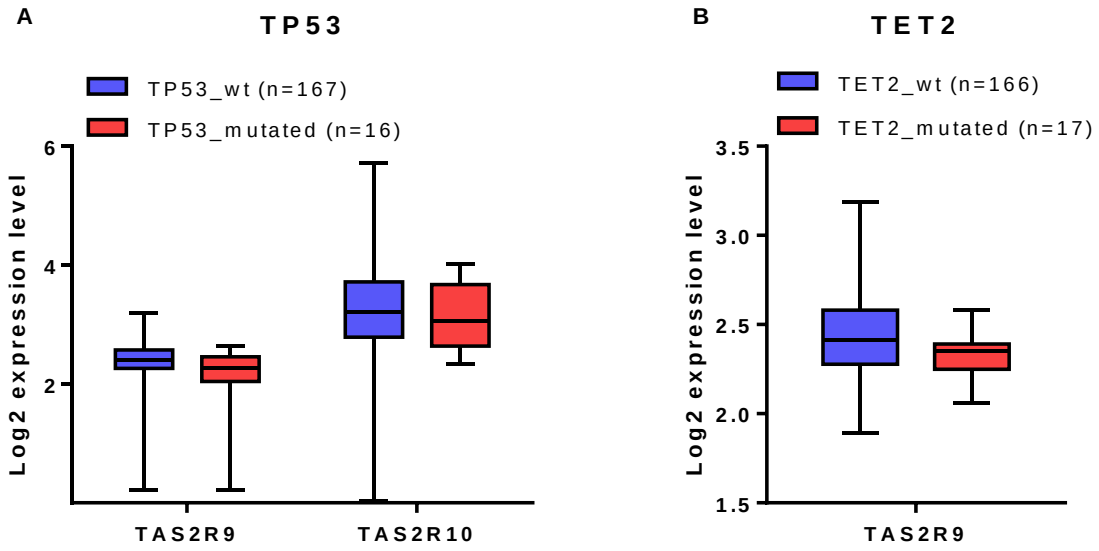

Figure 16. Boxplots of different expression levels of *TAS2R10* and *TAS2R9* in *TP53* (**A**) and *TET2* (**B**) mutated and wild-type (wt) samples. Statistical analysis was performed by Student's *t-test* and Benjamini-Hochberg adjusted *p-value* correction.

On the other hand, analysing the correlation with the cytogenetic and molecular risk, we found that a low expression of *TAS2R9* was significantly associated with both cytogenetics (p-value=0.005) (Fig.17, panel A) and molecular poor risk (p-value=0.02)

and a low expression of *TAS2R14* (p-value=0.02) was associated with a poor molecular risk (Fig.17, panel B).

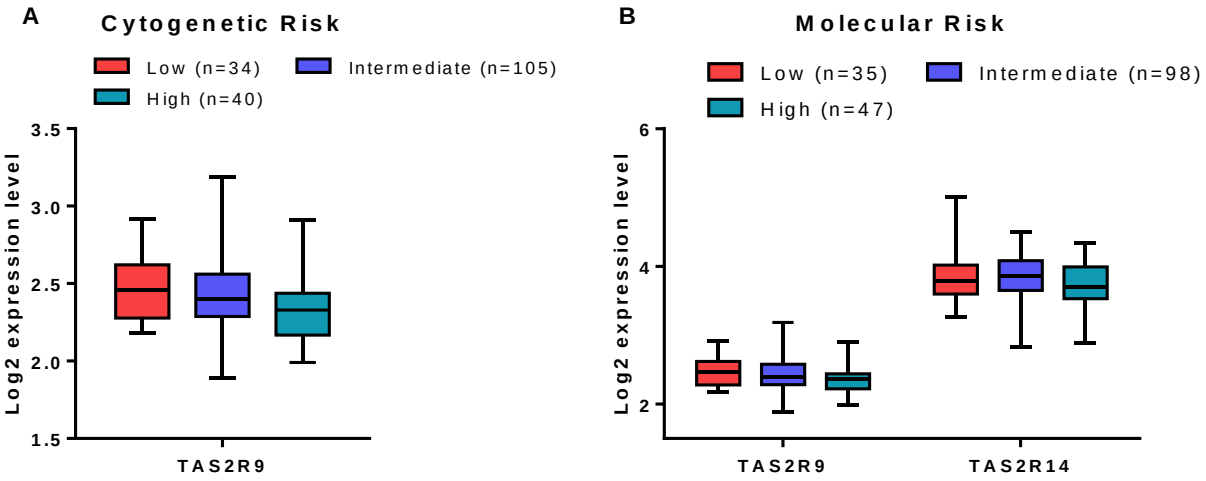

Figure 17. Boxplots of the indicated *TAS2Rs* based on cytogenetic (**A**) and molecular rick (**B**). Statistical analysis was performed by Student's *t-test* and Benjamini-Hochberg adjusted p-*value* correction.

We have also considered the FAB classification, observing a significant association between a reduction in mRNA expression level of *TAS2R10*, *TAS2R5* and *TAS2R14* and a more differentiated status of AML blasts (Fig.18). There were not significant association between *TAS2R* expression levels and other parameters as age, sex or blast percentage in the BM.

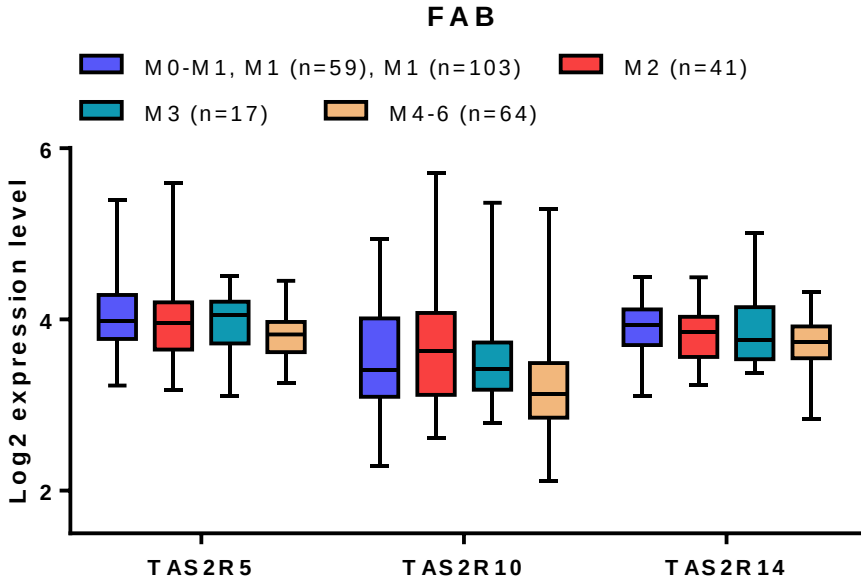

Figure 18. Boxplot of the indicated *TAS2Rs* based on FAB clinical features. Statistical analysis was performed by Student's *t-test* and Benjamini-Hochberg adjusted p-*value* correction.

These data indicated that the expression of some *TAS2Rs* was comparable with some relevant cell-intrinsic alteration of AML cells.

4. The expression of genes involved in AML function are altered by DEN exposure

To assess the effect of T2R activation on leukemic cells, we decided to use the bitter compound DEN as model compound, because, compared to Quinine, it targeted fewer T2Rs that could be downregulated in AML patients. DEN activated 8 of 25 T2Rs [145]: T2R4, T2R8, T2R10, T2R13, T2R30/47, T2R39, T2R43 and T2R46, and we demonstrated that five of these, T2R4, T2R8, T2R10, T2R13, and T2R30/47, were also expressed at protein level both in primary AML samples and in AML cell lines (Fig.19).

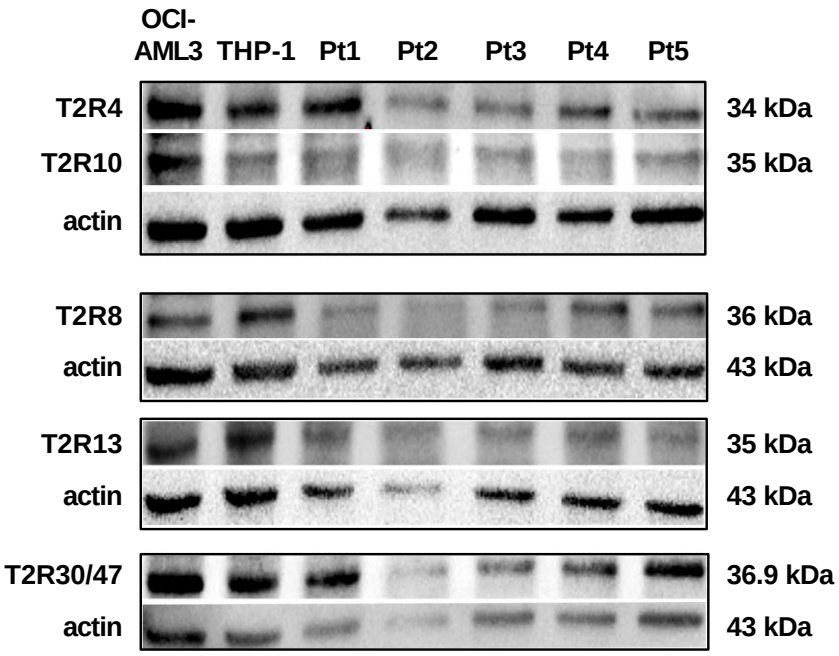

Figure 19. Western blot analysis of the DEN-sensitive T2Rs in two AML cell lines and five AML samples (Pts). Actin was shown as the loading control.

To evaluate the DEN effective/non-toxic doses, we exposed primary AML cells (n=5), OCI-AML3 (n=3), and THP-1 (n=3) to increasing doses of DEN and analysed cell viability (Fig.20).

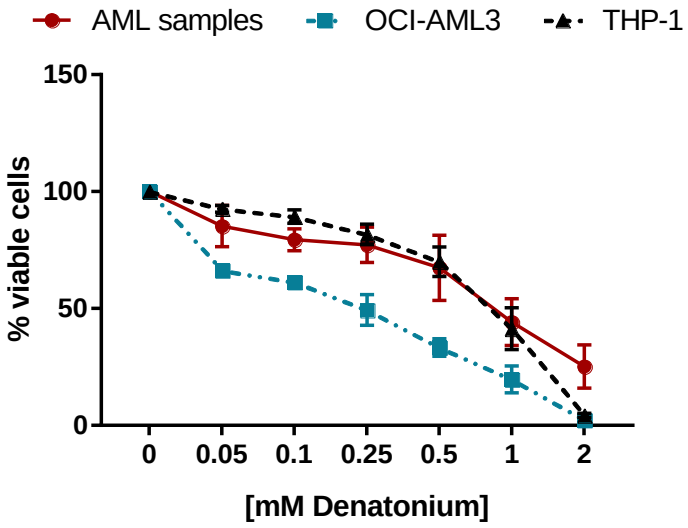

Figure 20. Cell viability detected by CellTiter 96 Aqueous One Solution assay in primary AML samples, OCI-AML3, and THP-1 treated for 48h with increasing doses of DEN.

As shown in the Fig.20, after 48h of exposure to DEN the viability was reduced both in primary AML samples and AML cell lines, in a dose-dependent manner. The viability was significantly reduced to 50% at 1mM in primary AML samples ($p<0.0001$), and in THP-1 ($p<0.0001$), at 0.25mM in OCI-AML3 ($p<0.0001$), indicating a different sensitivity to DEN by the tested cells.

To identify the T2Rs involved in charge of the observed effect, we exposed wt and knockout (KO) THP-1 to increasing doses of DEN and analysed cell viability (Fig.21).

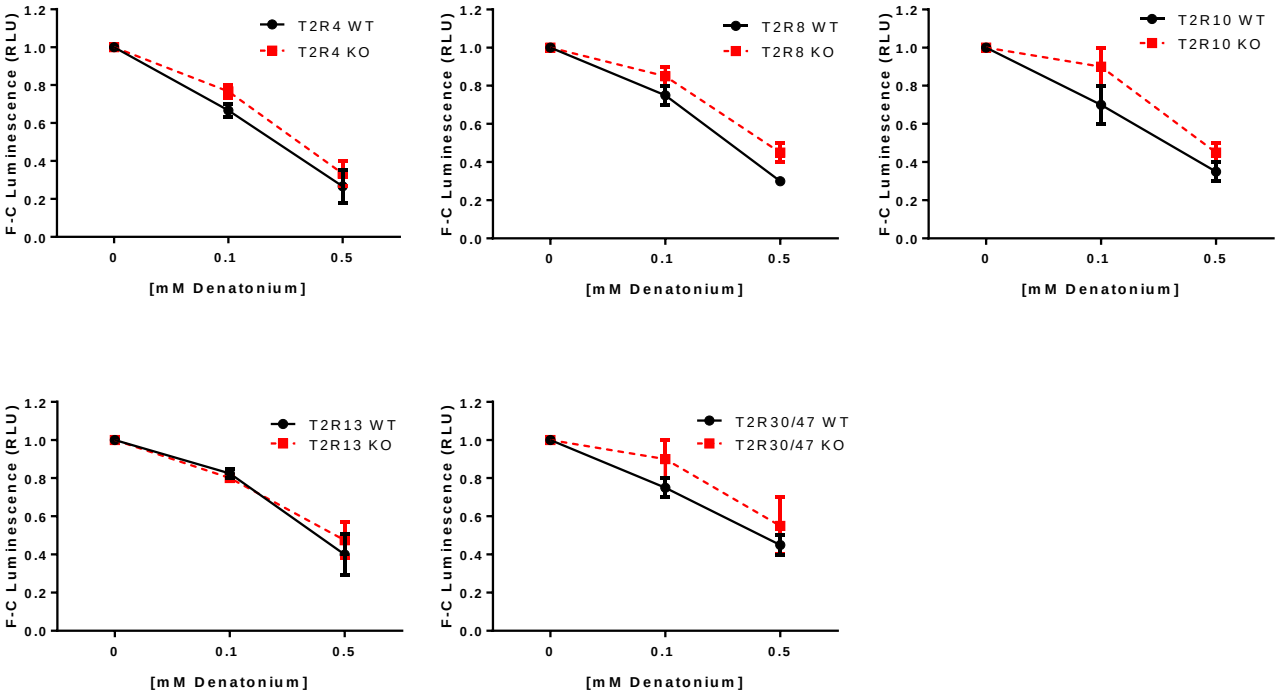

Figure 21. Cell viability detected by CellTiter-Glo assay in wt THP-1 and in T2R4, T2R8, T2R10, T2R13, and T2R30/47 KO THP-1.

As shown in Fig.21, we did not observe significant differences between the wt and KO THP-1 exposed to DEN, and these could be due to the high grade of redundancy in the

expression of DEN-sensitive T2Rs. For this reason, we were not able to identify a unique candidate for our function assays.

Thus, to identify the cellular processes regulated by T2Rs in AML cells, we decided to use non-toxic DEN concentrations for downstream analyses in GEP experiments. Primary AML cells, OCI-AML3, and THP-1 were exposure for 24h at 0.5mM, 0.1mM, and 0.5mM DEN, respectively. Overall, we found that DEN induced the upregulation of 190, 260 and 1109 genes and the downregulation of 325, 570 and 929 genes in primary AML cells, OCI-AML3 and THP-1, respectively. Among the altered genes, we did not find T2Rs or downstream targets. Accordingly, following DEN stimulation at the tested doses any significant modulation was observed in T2R, Gß and PLC-ß2 expression in OCI-AML3 and THP-1 by qRT-PCR analysis. Although a number of genes were uniquely altered in the analysed cell types. Interestingly, a core transcriptional program of 45 upregulated and 87 downregulated genes was shared between OCI-AML3 and THP-1 (Table 9), while 8 genes of them were significantly downregulated also in primary AML cells. Among them, we found *CCNA1*, which controls cell cycle progression, *CDC6* and *RRM2*, that are involved in the early steps of DNA replication and the biosynthesis of deoxyribonucleotides, respectively. In addition, we found *XRCC3*, which plays a role in the homologous recombination repair pathway of double-stranded DNA, *ACOT7*, a member of the acyl coenzyme family hydrolyzing the CoA thioester of long-chain fatty acids and the free fatty acid receptor GPR84 (Table 9).

Pathway	Genes
Apoptosis	TP53, INP1, RNF130, CFLAR, TNFSF10, AIFM2
Cell cycle and DNA damage	FRY, LIG4, AKAP9, ORC1, SPDL1, **CCNA2**, NCAPG2, RAD54B, NCAPG, KIF22, PBK, BTG3, CDC25A, CDC45, PLK1, CDC20, **CDC6**, CDCA3, **XRCC3**, CCNF, CCND1, CENPV, FANCG
Cytoskeleton, cell adhesion and migration	PIK3R5, TUBA8, FSCN1, HMMR, RHOF, EMD
Metabolism	DHCR24, ALDOC, MPI, MSMO1, GYS1, AKR1C2, INSIG1, BCKDK, **ACOT7**, SCD, FADS2, PNP, CPT2, LDHA, GPI, AKR1C1, PFKP, **RRM2**, FAM72A, MGAT4A, ST3GAL6, SPTLC3
Chromatin organization	HIST1H2BB, HIST1H4D, HIST1H3I, HIST1H2BM
Histone Methylation	EZH2
Immune response	TRIM22, DDX58, TLR4, RNASE6, TNFSF13B, GPR18, **C3**
Signaling	GPR3, ITPRIPL1, SDC4, MPZL1, RALGAPA2, DGKD, **GPR84**
Transcription	ETV4, ETV5, BARX1, ZNF394, SFMBT2, ZNF852, ZNF33B, ZNF546,
Translation and post-translational modification	FDFT1, PPME1, **DUSP5**, ATXN3, CTSS, RPS26, **DARS2**
Protein degradation	CLPP, HERC3, FAM63A
Others	NBEAL2, CPXM1, FAM83D, LDLR, SORL1, KCTD7, SLC1A3, FKBP4, NUP205, BORCS7, UCP2, VIT, CLDN15, ADGRL2

Table 9. Core genes altered by DEN treatment at transcriptional level in both OCI-AML3 and THP-1 cells according to functional categories. **Bold genes** are deregulated also in primary AML samples by DEN treatment.

Furthermore, the obtained data showed that the other downregulated transcripts in primary AML cells were significantly enriched for genes involved in cell cycle and DNA damage, cytoskeletal function, cell adhesion, migration, and pyrimidine metabolism (Table 10).

Pathway	p-value	Genes
Cell cycle and DNA damage		
Cell cycle	0,009 0006	CDC7, CCNE2, CDC6, MAD2L1, PCNA, PRKDC, CCNA2, MCM4
G1/S transition of mitotic cell cycle	5,18E-05	CDC7, CCNE2, CDC6, TYMS, RRM2, PCNA, POLA1, USP37, POLA2 , MCM4
Regulation of transcription involved in G1/S transition of mitotic cell cycle	5,22E-04	CDC6, TYMS, RRM2, PCNA, POLA1
DNA replication initiation	1,73E-04	CDC7, CCNE2, CDC6, POLA1, POLA2, MCM4
DNA replication	0,004 543	PCNA, POLA1, POLA2, MCM4, FEN1
DNA strand elongation involved in DNA replication	0,001 7988	GINS3, PCNA, POLA1, POLA2
Cytoskeleton, cell adhesion and migration		
Tight junction	0,118 2671	IGSF5, CLDN18, MRAS, MYH6, JAM2, SRC
Nucleotide biosynthesis		
Pyrimidine metabolism	0,315 4609	TYMS, RRM2, POLA1, POLA2

Table 10. Pathways enrichment analysis for genes downregulated in primary AML cells after DEN exposure.

Moreover, the primary AML cells treated by DEN showed an altered expression of genes involved in apoptosis, carbohydrate, energy, amino acid and lipid (Fig.22).

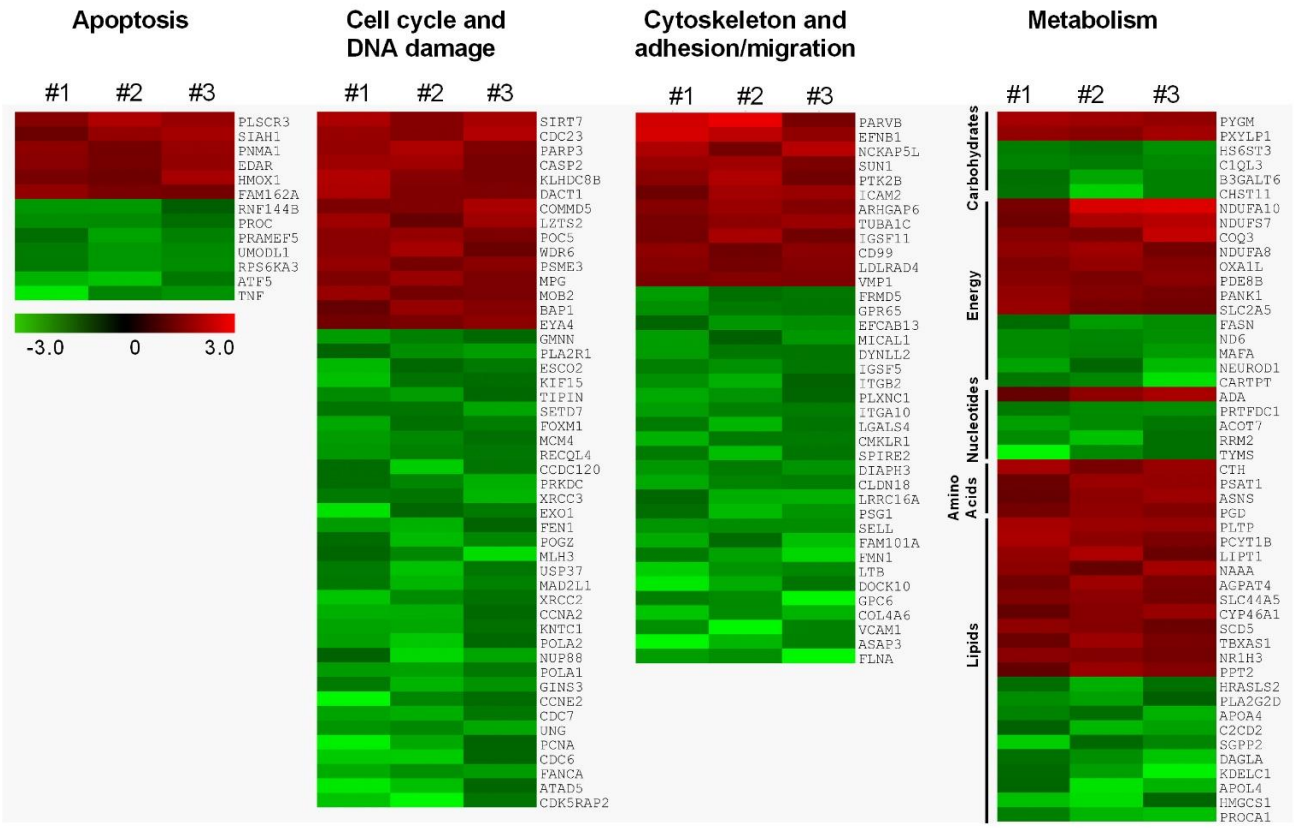

Figure 22. Heatmap of differentially expressed genes involved in apoptosis, cell cycle and DNA damage, cytoskeleton, cell adhesion and migration, and metabolism, following exposure to DEN in three primary AML sample. Columns represent rations between DEN- and vehicle- treated cells for each case. Color changes are quantified by the scale bar.

As regards OCI-AML3 and THP-1 cell-altered genes, we found upregulation of the apoptosis-related genes *TP53, INP1*, *RNF130*, *CFLAR*, *TNFSF10*, and the downregulation of *AIFM2* (Table 9). In addition, the two cell lines shared the deregulation of a core of genes involved in cytoskeletal function, cell adhesion and migration (upregulated: *PIK3R5*; downregulated: *TUBA8*, *FSCN1*, *HMMR*, *RHOF*, *EMD*) and cell cycle/DNA damage (upregulated: *FRY*, *LIG4*, *AKAP9*; downregulated: *ORC1*, *SPDL1*, *NCAPG2*, *RAD54B*, *NCAPG*, *KIF22*, *PBK*, *BTG3*, *CDC25A*, *CDC45*, *PLK1*, *CDC20*, *CDCA3*, *CCNF*, *CCND1*, *CENPV*, *FANCG*). Differentially expressed

transcripts in the tested cell lines were enriched for genes involved in cell cycle, DNA damage and glycolysis. According to the pathway analysis, cytoskeletal function, cell adhesion and migration, biosynthesis of fatty acids and glycolysis were significantly enriched in OCI-AML3, while THP-1 showed a preferential enrichment for transcriptional alterations targeting metabolism-related genes, including bioenergetics pathways (glycolysis and mitochondrial respiration), biosynthetic processes (purine, nucleotides, amino acids) and lipid metabolism (fatty acid, cholesterol).

All these results suggested that the induction of T2R pathway by DEN deregulated relevant cellular processes in AML cells, including cell cycle, survival, migration and metabolism.

5. DEN inhibits AML cell proliferation and clonogenic efficiency

In the previous paragraph, we highlighted the significant inhibition of cell functions due to the treatment by DEN. This was the starting point for the development of functional assays needed to confirm the results observed at the molecular level.

At first, we evaluated the AML cell lines proliferation in presence of increasing doses of DEN, after 48h of treatment. The OCI-AML3 proliferation underwent a significantly decrease up to 40% at the 0.1mM ($p<0.05$), while in THP-1 the significantly reduction was observed up to 30% at 0.5mM ($p<0.05$) (Fig.23).

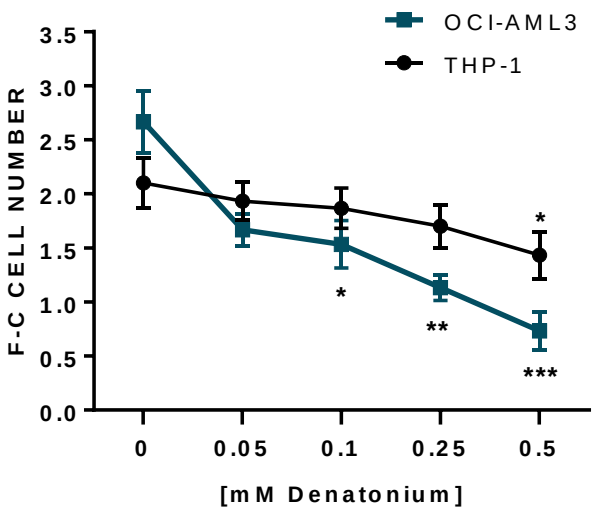

Figure 23. Cell proliferation determined by CellTiter 96 Aqueous One Solution assay and normalized to time 0 in OCI-AML3, and THP-1 cultured for 48h with increasing dosed of DEN.

To confirm this result, we assessed the effect of DEN exposure on cell cycle in AML cell lines. After 48h treatment, the analysis showed that the inhibitory effect of DEN was mainly due to a G0/G1-phase arrest and a concomitant S-phase decrease. In particular, we found a significant arrest in G0/G1-phase ($p<0.05$), and a significant decrease of S-phase ($p<0.01$) in OCI-AML3 (Fig.24, panel A), while a significant result was obtained in the arrest of THP-1 in G0/G1-phase ($p<0.05$) using the highest doses 0.5mM (Fig.24, panel B). Moreover, this result validated the data obtained in microarrays, which showed the alteration of cell cycle-related genes.

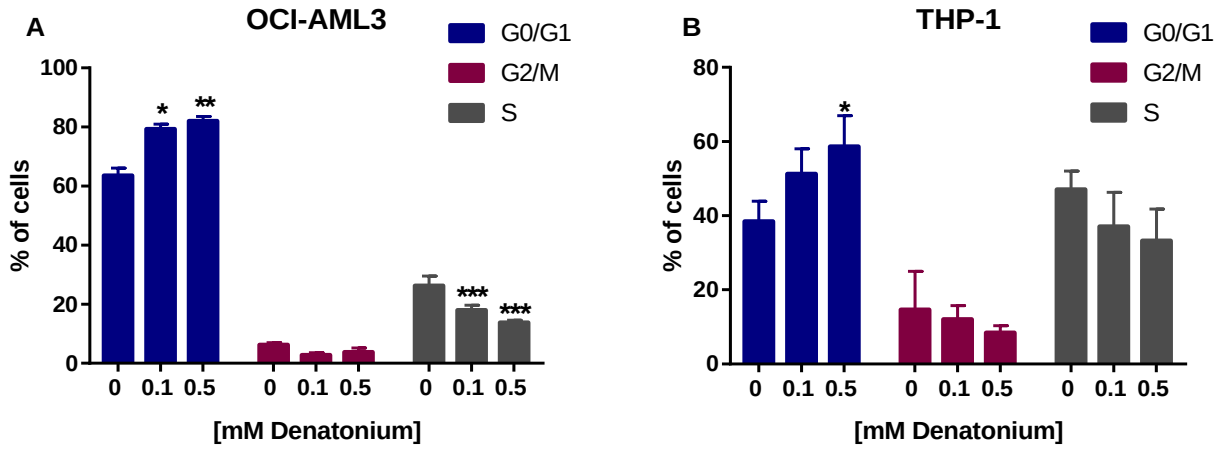

Figure 24. Histograms display cell cycle phase distribution in OCI-AML3 (**A**) and THP-1 (**B**) after 48h of DEN exposure.

To substantiate these data, western blot analysis was used to validate the expression of cell cycle proteins, which GEP analysis indicated as deregulated at the mRNA level. The expression of cyclin D1 [146] and cyclin A2 [147], which normally increase during G1-phase and S-phase progression respectively, was significantly reduced following DEN treatment in both AML cell lines (Fig.25).

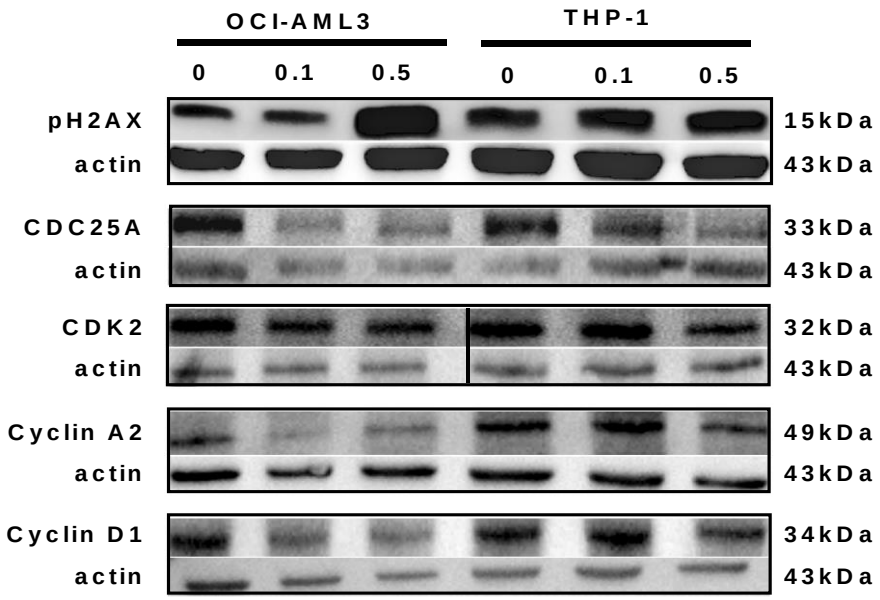

Figure 25. Western blot analysis of the indicated proteins in OCI-AML3 and THP-1 treated with the indicated doses of DEN for 24h. Actin was shown as the loading control.

In parallel, the phosphatase cell division cycle 25 homolog A (CDC25A), able to activate G1/S cyclin-dependent kinase 2 (CDK2) [148], decreased in DEN-treated AML cells. Instead, CDK2 was downregulated to a lesser extent, according to an inactivation mechanism based on cyclin levels oscillation during the cell cycle [149]. Consistently with a cell cycle arrest, the expression of a typical mitotic protein, i.e. polo-like kinase 1 (PLK-1), whose activation relies on cyclin A2-Cdk activity levels [150], was significantly inhibited in DEN-treated AML cell lines (Fig.26).

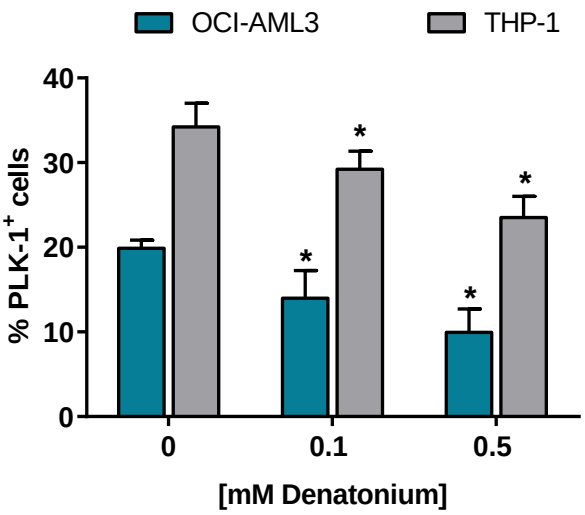

Figure 26. Histograms indicate the percentage of PLK-1⁺ cells analysed by flow cytometry in OCI-AML3 and THP-1 treated with the indicated dosed of DEN for 24h.

Furthermore, we evaluated the effect of non-toxic DEN doses on AML progenitor cells. As showed in the Fig.27, the clonogenic capacity was significantly reduced in a dose-depended manner. This decrease was already evidenced at low doses with an inhibition of 30% at 0.05mM ($p<0.05$) and up to 50% at 0.5mM ($p<0.01$).

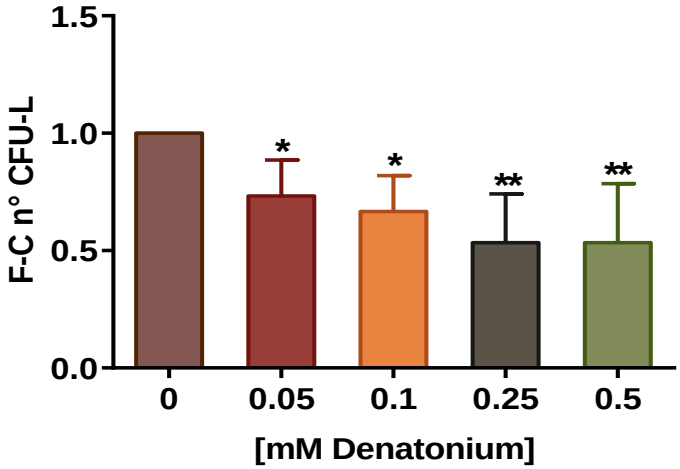

Figure 27. Histograms indicate the fold-change of the CFU-L obtained from primary AML cells cultured in semisolid medium in the presence of cytokines and increasing concentration of DEN.

GEP analysis also highlighted that differentially expressed transcripts were enriched for genes involved in DNA repair (*RAD54B*, *XRCC3*, and *FANCG* showed reduced expression in both cell lines after treatment). Accordingly, protein expression analysis showed an increase in the phosphorylated form of the histone 2AX (pH2AX) following DEN treatment in AML cell lines (Fig.25), indicating an increase in DNA damage, probably due to impaired DNA repair activity.

Overall, these results supported GEP data, suggesting that AML cells responded to T2R activation in the presence of low doses of DEN by accumulating DNA damage and reducing their proliferative and clonogenic potential.

6. Exposure to high doses of DEN induces AML cell apoptosis

Since GEP data showed modulation of apoptosis-related genes and we found a significant reduction of AML cell viability using high doses of DEN, we investigated the potential cytotoxic effect of T2R activation. To this aim, we treated primary AML samples (n=8), OCI-AML3 (n=3), and THP-1 (n=3) with increasing doses up to 2mM DEN and analysed the Annexin-V^+ cells. The DEN exposure increased the percentage of primary AML apoptotic cells up to 60% using the two highest doses of DEN (1mM, and 2mM) (Fig.28, panel A). We obtained the same results both in OCI-AML3 (Fig.28, panel B), and THP-1 (Fig.28, panel C). Instead, it was not observed the necrosis induction, and it was demonstrated by the absence of a PI^{+}/Annexin-V^{-} cell population.

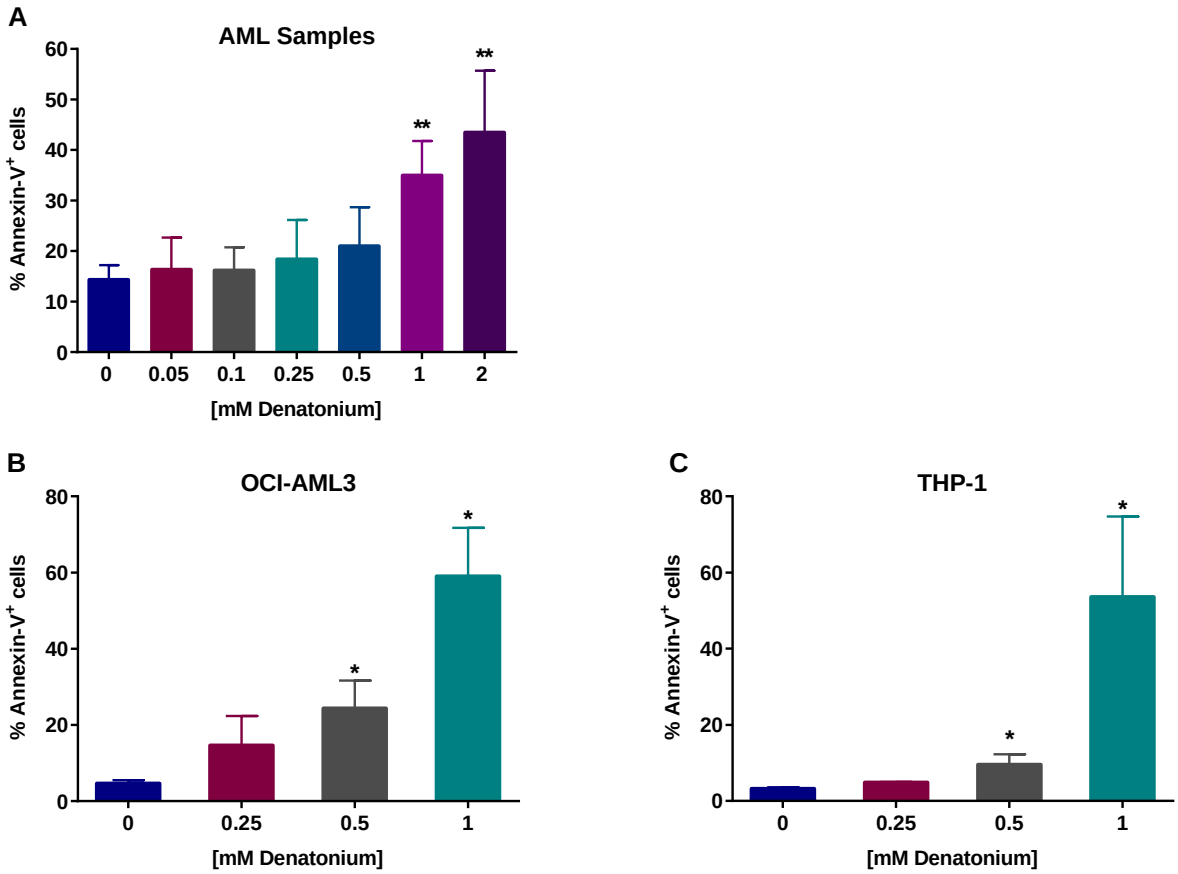

Figure 28. Primary AML cells (**A**), OCI-AML3 (**B**), and THP-1 (**C**) were treated for 48h with increased doses of DEN. Histograms indicate the Annexin V^+ cells, that represent the apoptotic cells.

To better characterize apoptosis after DEN treatment, we firstly evaluated caspase cascade activation by analysing the expression of caspase- 3 active form (Casp-3). This caspase belongs to a family of evolutionally conserved cysteine protease, and plays a key role in regulating programmed cell death, apoptosis, or normal process required for maintenance of tissue homeostasis and the regulation of physiological function [151]. After a treatment of primary AML cells, OCI-AML3, and THP-1 with 1mM DEN for 48h, the flow cytometry analysis revealed a significant increase expression of active

Casp-3 in AML cells after DEN exposure, both in primary AML cells ($p<0.01$) (Fig.29, panel A) and AML cell lines (OCI-AML3, $p<0.05$; THP-1, $p<0.05$) (Fig.29, panel B-C).

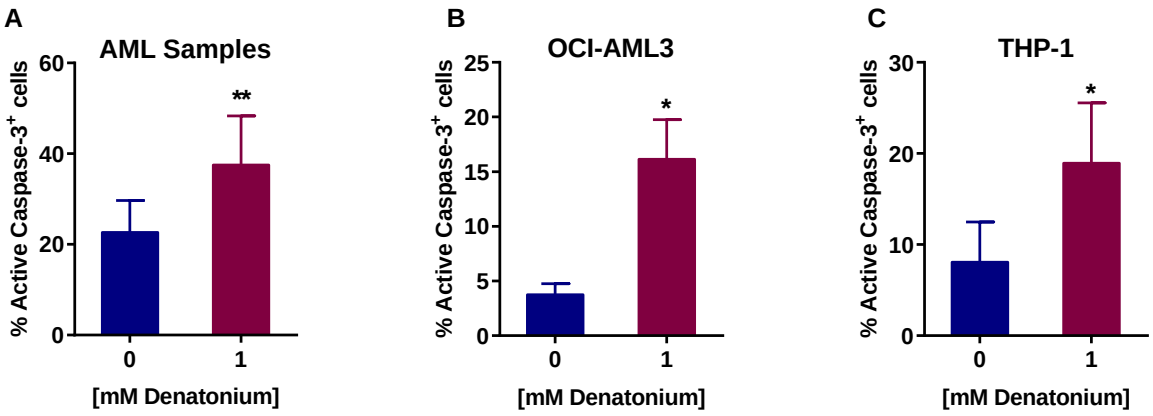

Figure 29. FACS analysis of active Casp-3 expression in primary AML cells (**A**), OCI-AML3 (**B**), and THP-1 (**C**) after treatment with 1mM DEN for 48h.

Activation of Casp-3 was also confirmed by immunofluorescence analysis (Fig.30).

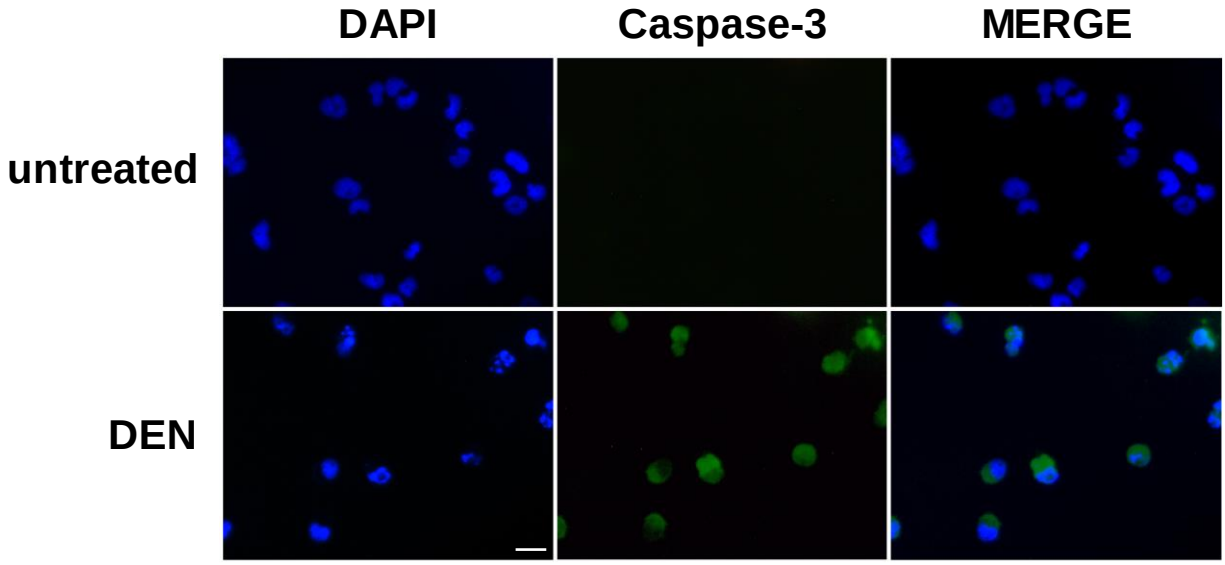

Figure 30. Immunofluorescence analysis of activated Casp-3 (green) after 48h of treatment with 1mM DEN. Nuclei were counterstained with DAPI (blue). 40X magnification, scale bar 20μm.

To evaluate the mitochondrial involvement in apoptosis after DEN treatment, we stained AML cells with JC-1 dye, that can accumulate as aggregates or monomers in healthy or damage mitochondrial, respectively. As shown in the Fig.31, after 48h of DEN exposure the mitochondrial membrane potential ($\Delta\Psi m$) was reduced in treated primary AML cells, compared to control. This was demonstrated by the increase of JC-1 monomers and the concomitant significant decrease of JC-1 aggregation ($p<0.05$) (Fig.31, panel A). The same result was obtained for OCI-AML3 ($p<0.05$) (Fig.31, panel B), and THP-1 ($p<0.05$) (Fig.31, panel C).

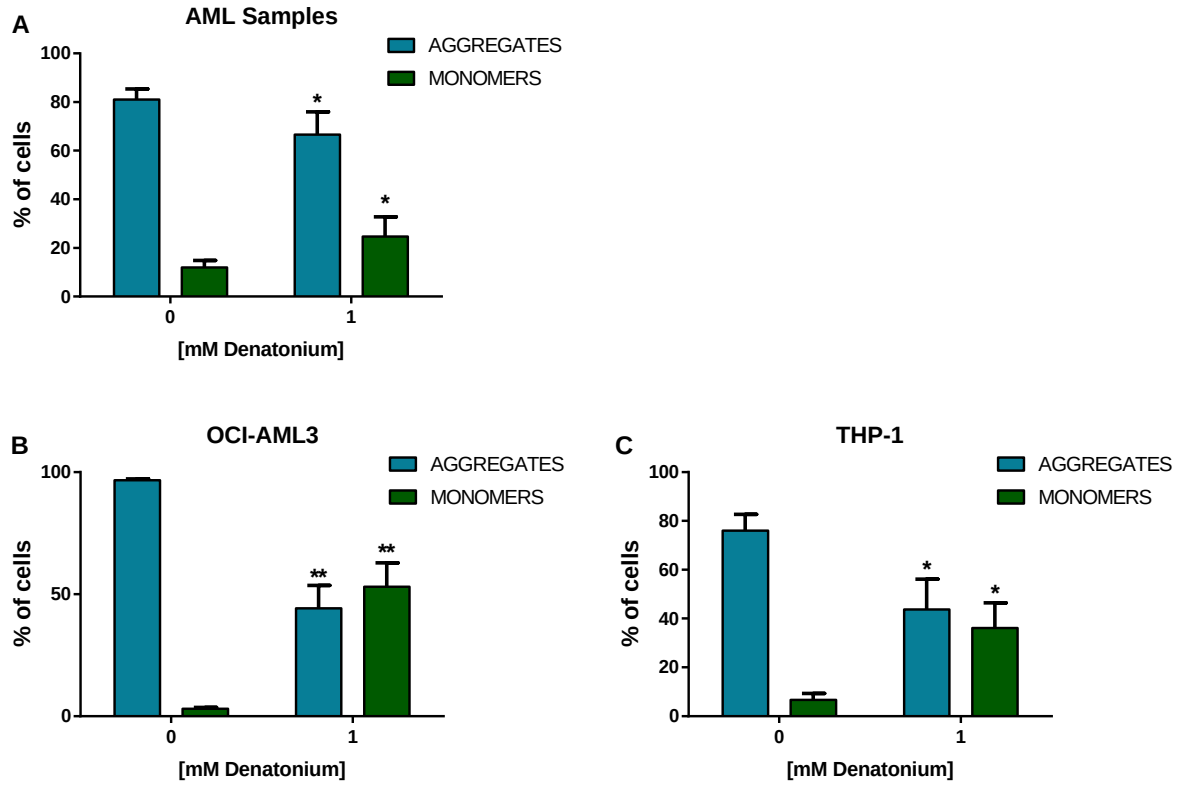

Figure 31. Histograms represent the FACS analysis of mitochondrial membrane potential of primary AML cells (**A**), OCI-AML3 (**B**), and THP-1 (**C**) after 48h of exposure to 1mM DEN.

Overall, these results suggested that the induction of apoptosis was related to the activation of caspase cascade and mitochondrial pathway activation in AML cells exposed to T2R agonist.

7. DEN alters AML cell mitochondrial metabolism

The GEP data suggested an alteration in cellular bioenergetics after T2R activation and GSEA indicated a significant enrichment for gene signature of glycolysis and cycle/oxidative phosphorylation (OXPHOS) in untreated compared to DEN-treated AML cells (Fig.32).

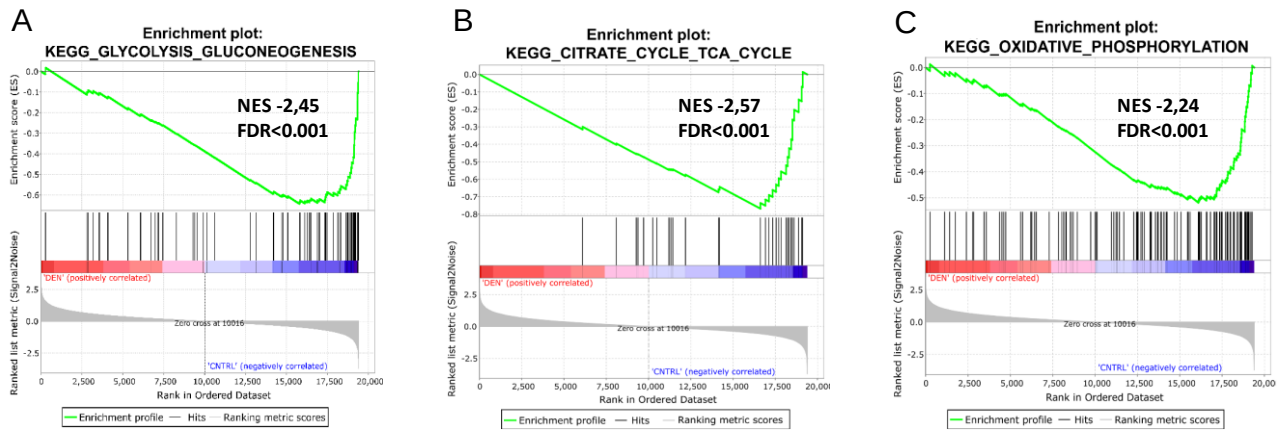

Figure 32. Downregulation of gene signatures of glycolysis (**A**), citrate cycle (**B**) and OXPHOS (**C**) defined by GSEA in THP-1 cells after 24h of exposure to DEN.

To further deepen the alteration that T2R activation induced in AML cell metabolisms, we decided to study the cellular bioenergetics following mitochondrial metabolic stress. To do that, we used the Seahorse XF Mito Stress Test to evaluate the oxygen consumption rate (OCR), the basal respiration, the ATP-linked respiration, and the spare capacity levels in AML cell lines. After 24h of treatment, DEN decreased both basal and maximal mitochondrial respiration in the two AML cell lines (Fig.33, panel

A-B). Specifically, mitochondrial basal respiration was significantly disrupted, as evidenced by the basal respiration drop, of more than 50% in THP-1 at 0.1mM ($p<0.05$) (Fig.33, panel C), while in OCI-AML3 at 0.25mM ($p<0.05$) (Fig.33, panel F). Moreover, there was a significant decrease in ATP-linked respiration in DEN-treated cells, in both THP-1 (Fig.33, panel D) and OCI-AML3 (Fig.33, panel G). Respiratory spare capacity represents the reverse capacity of a cell to generate ATP via OXPHOS following an increased energy demand. This mitochondrial reverse capacity was reduced by more than 50% in both THP-1 (Fig.33, panel E) and OCI-AML3 (Fig.33, panel H) at 0.1mM DEN.

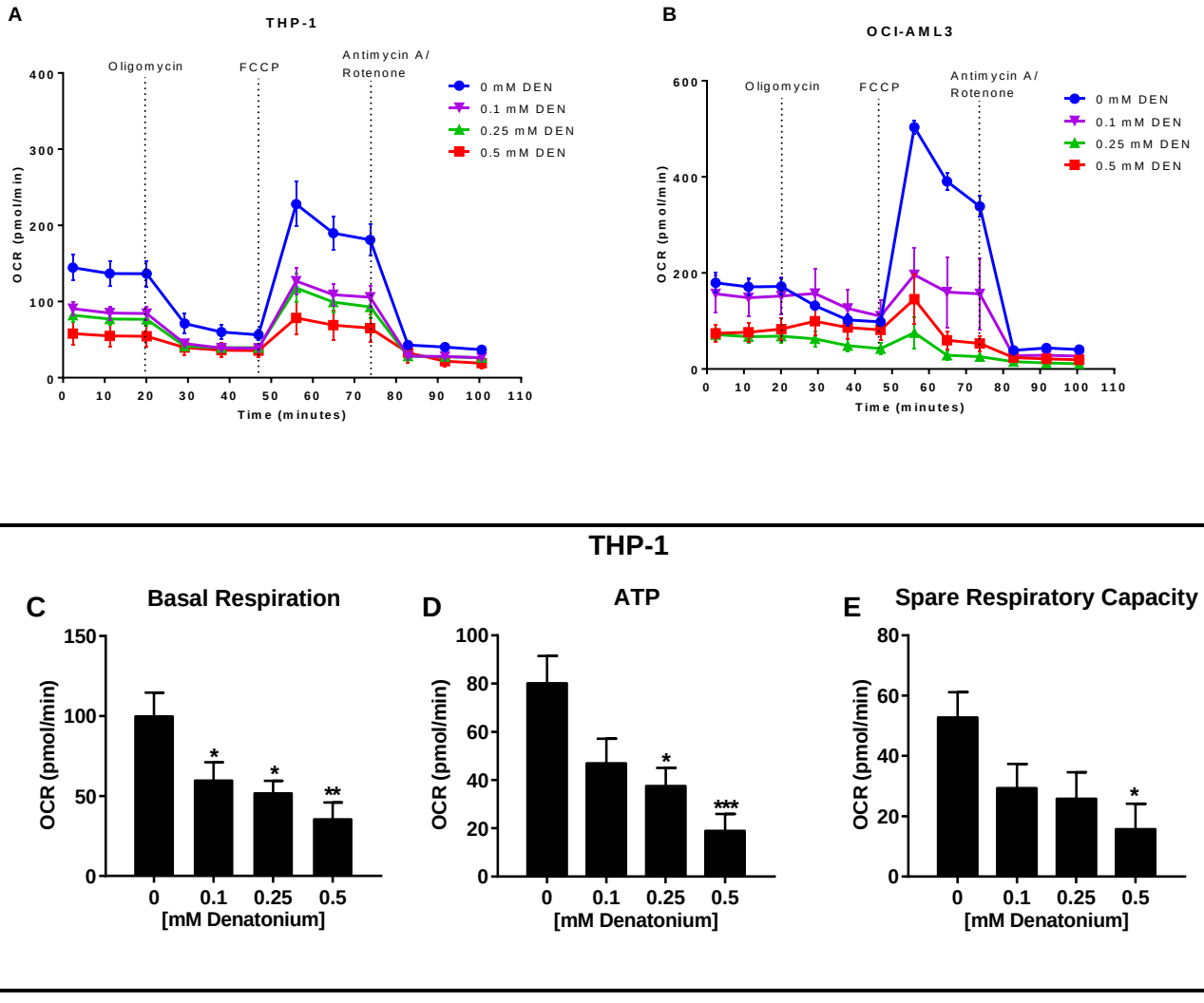

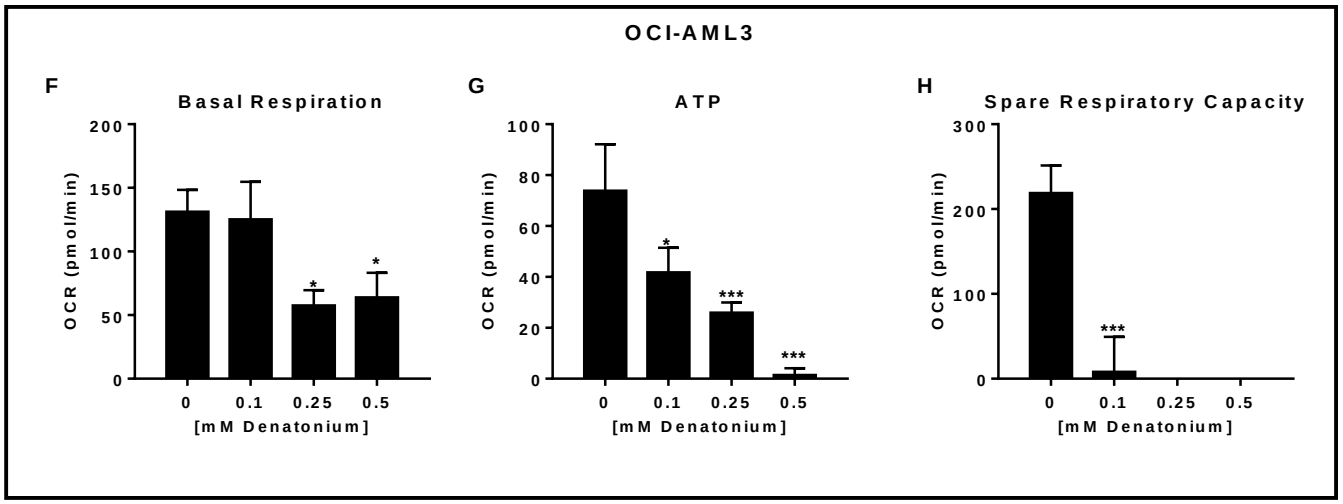

Figure 33. Oxygen consumption (OCR) profile plot obtained by the Seahorse Cell Mito Stress Test in the THP-1 (**A**) and OCI-AML3 (**B**) after 24h of exposure to DEN. (**C, F**) Basal respiration. (**D, G**) ATP-linked respiration. (**E, H**) Spare Respiratory Capacity.

All these results suggested that DEN treatment decreased mitochondrial OXPHOS and made AML cells more prone to oxidative and metabolic stress due to decreased substrate availability or mitochondrial dysfunction.

Moreover, we assessed the relative utilization of glycolysis and OXPHOS after DEN treatment by using the Seahorse XF Glycolytic Rate assay. Measuring the basal glycolysis, there were no differences between the DEN-treated cells and control, both in THP-1 (Fig.34, panel A) and OCI-AML3 (Fig.34, panel C). Instead, the percentage of proton efflux rate (PER) from glycolysis increased in THP-1 treated with 0.5mM DEN (Fig.34, panel B), but this did not seem to be in OCI-AML3 (Fig.34, panel D).

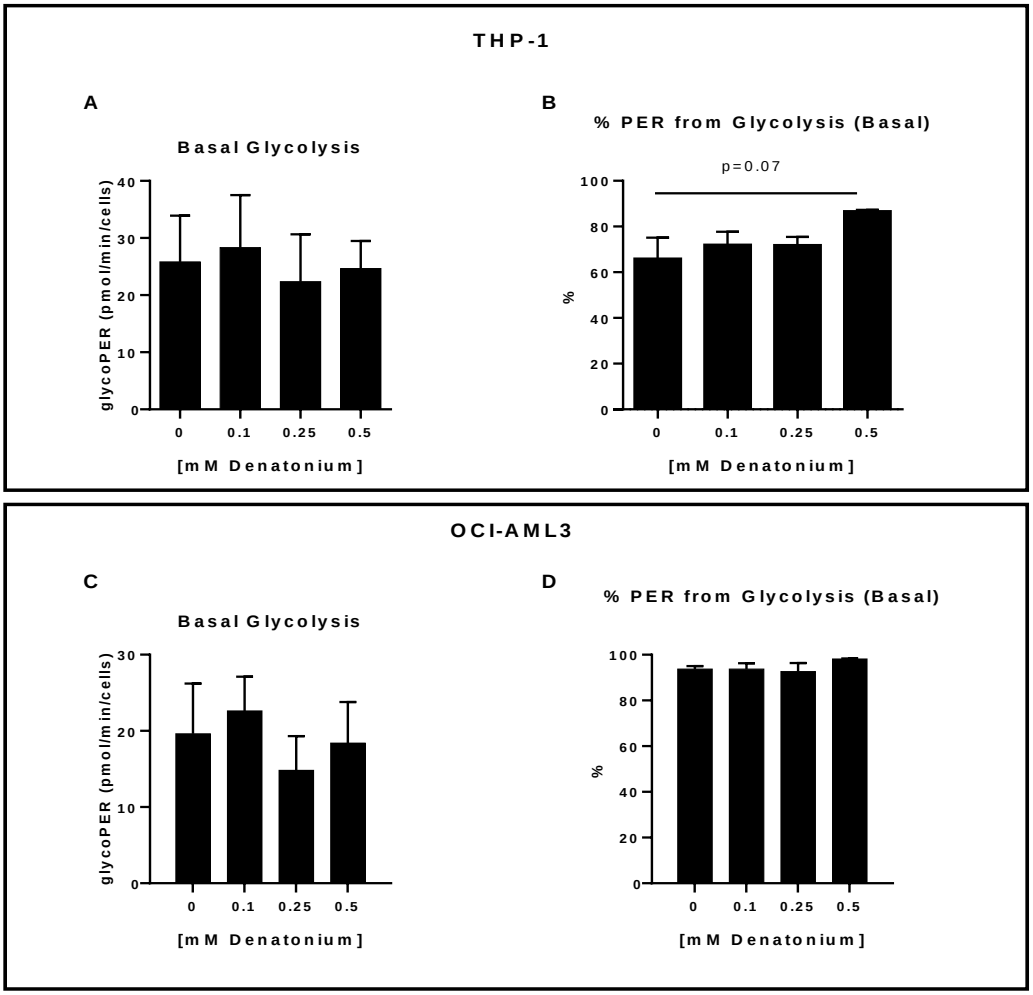

Figure 34. Parameters for basal glycolysis and basal percentage PER from glycolysis in THP-1 (**A-B**) and OCI-AML3 (**C-D**) treated with DEN at different concentration.

Consistent with the dropped level in the basal respiration detected by Mito Stress assay, these data suggested that glycolysis was the main contributor to extracellular acidification and PER.

However, at the same concentration, DEN was able to markedly impair the compensatory glycolysis achieved by the THP-1 after blockage of mitochondrial ATP production (Fig.35, panel A). This mechanism was not present in OCI-AML3 (Fig.35, panel D), that showed a lower impact in terms of glycolytic activity (glycoPER). It was interesting that DEN decreased of 70% the rate of acidification in both THP-1 (Fig.35,

panel B) and OCI-AML3 (Fig.35, panel E) due to mitochondrial metabolism. This indicated that DEN shifted the bioenergetics profile of the cells from OXPHOS toward aerobic glycolysis, likely impaired under stress.

Observing the data about the reduction of both mitochondrial OXPHOS and glycolysis, we hypothesized a potential correlation with a reduction of glucose uptake. The measure of glucose uptake, after 24h treatment, showed a significant decrease both in THP-1 (Fig.35, panel C) and OCI-AML3 (Fig.35, panel F).

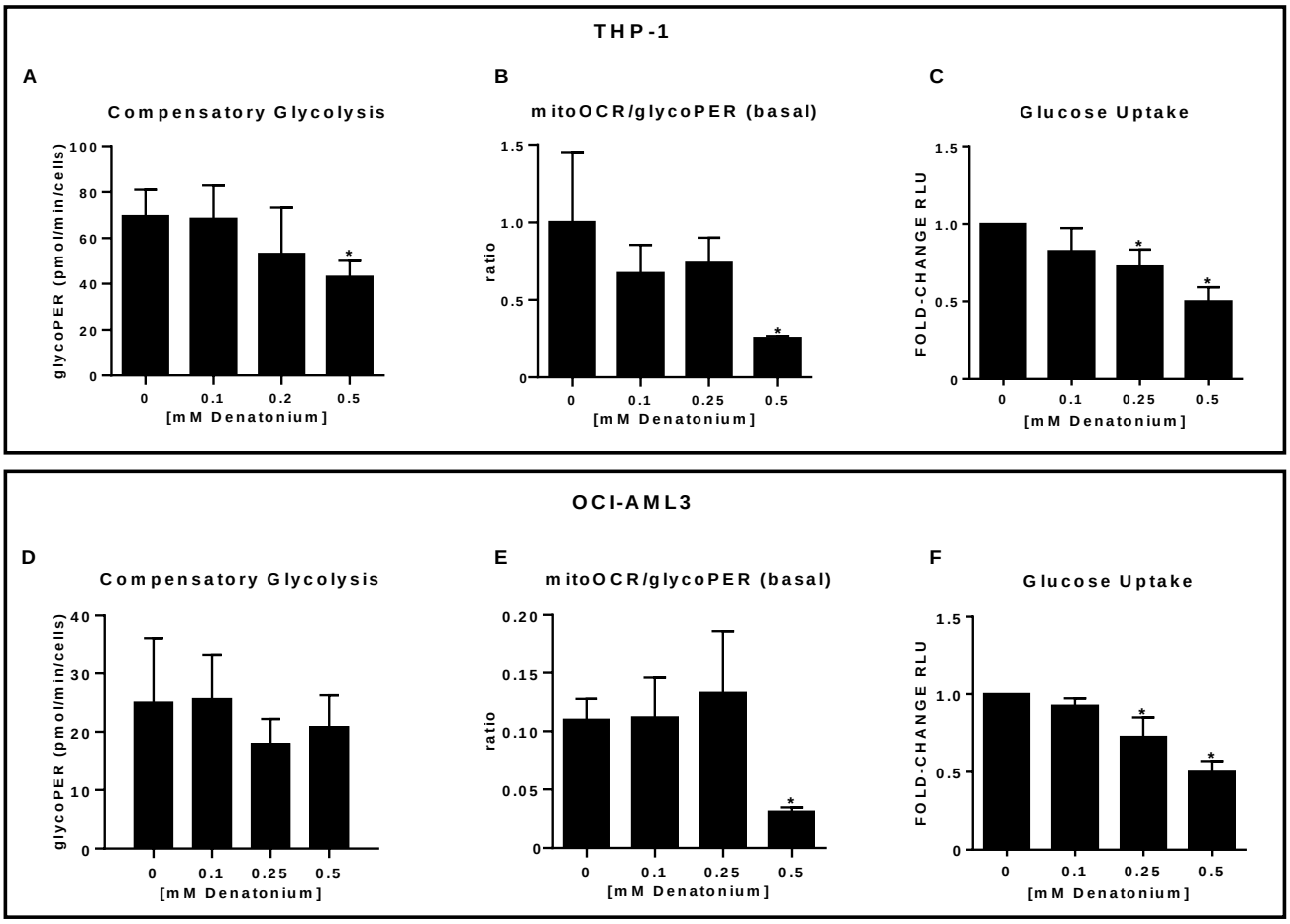

Figure 35. Parameters for quantitative data of compensatory glycolysis and ratios of mitochondrial OCR to glycoPER calculated using Seahorse XF Glycolytic Rate assay in THP-1 (**A-B**) and in OCI-AML3 (**D-E**). Measurement of glucose uptake in THP-1 (**C**) and OCI-AML3 (**F**) after 24h exposure to increasing doses of DEN.

Overall, the results suggested that cells treated with DEN were not able to maintain basic cell function but show a defective phenotype and were not able to use both mitochondrial respiration and glycolysis.

8. DEN inhibits the AML cell motility

Since the GEP data of AML cells exposed to DEN showed an alteration of genes involved in the process of migration, we assessed the functional effect of T2R activation on the migratory capacity of AML cells *in vitro* by using the transwell system. At first, we studied the effect of DEN on primary AML cells, OCI-AML3, and THP-1, directly exposed to the agonist. Thus, increasing doses of DEN were added to the transwell upper chamber. The results showed that the direct exposure to DEN significantly reduced by 50% the spontaneous migration of primary AML cells ($p<0.001$) (Fig.36, panel A), and AML cell lines (OCI-AML3, $p<0.05$; THP-1, $p<0.01$), even at the lower dose of 0.05mM DEN (Fig.36, panel B-C).

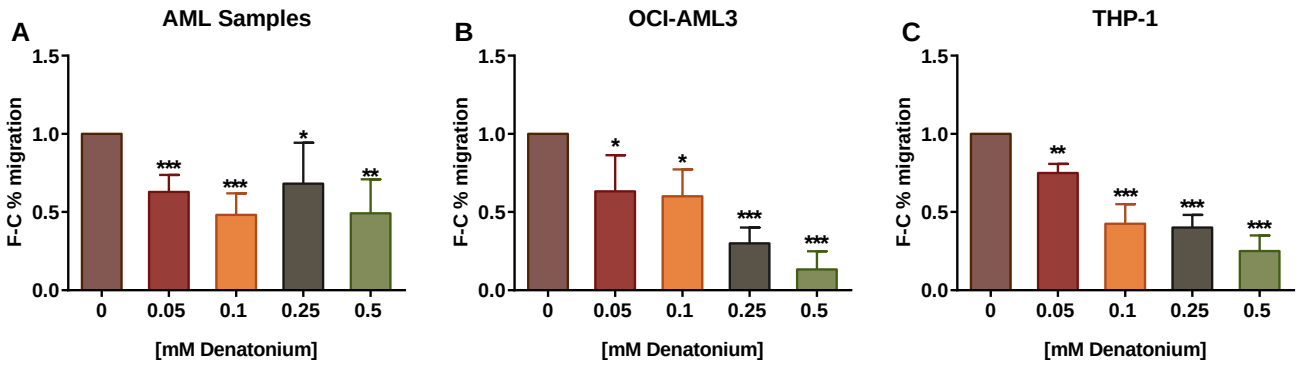

Figure 36. Histograms represent the fold-change percentage of spontaneous migration of primary AML cells (**A**), OCI-AML3 (**B**), and THP-1 (**C**) in presence of increasing doses of DEN in the upper chamber of transwell.

Subsequently, we investigated if this inhibition persisted even if the stimulus was removed from the medium, and we observed that the inhibition of spontaneous migration of both primary AML cells (Fig.37, panel A) and AML cell lines (Fig.37, panel B-C) was noticeable even after a 4 hours' pre-treatment.

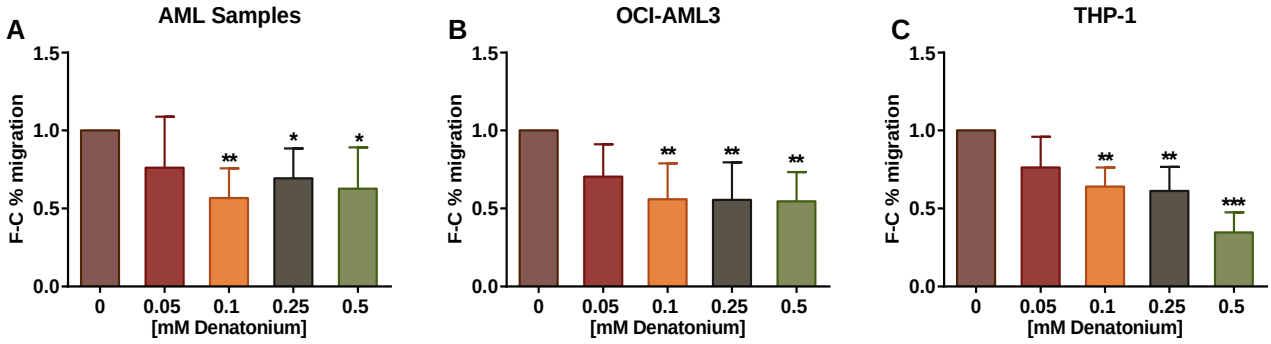

Figure 37. Histograms represent the fold-change percentage of spontaneous migration of primary AML cells (**A**), OCI-AML3 (**B**), and THP-1 (**C**) after a pre-treatment of 4h with increasing dosed of DEN.

Furthermore, we investigated the modulation of AML cell spontaneous migration in presence of DEN gradient. The results showed that the presence of increasing doses of DEN in the lower chamber of the transwell system inhibited spontaneous migration of leukemia cells (Fig.38, panel A-C).

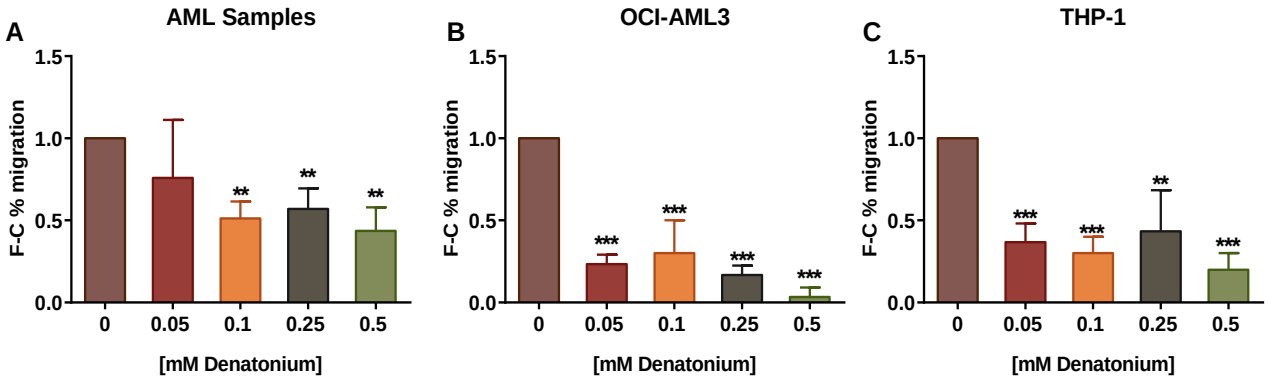

Figure 38. Histograms represent the fold-change percentage of spontaneous migration of primary AML cells (**A**), OCI-AML3 (**B**), and THP-1 (**C**) in presence of increasing doses gradient of DEN in the lower chamber of transwell.

The CXCL12-CXCR4 axis, which is the key mediator in hematopoietic stem cell migration, is also exploited by AML cells. The CXCL12 is produced by the BM microenvironment, binds and activates its cognate receptor CXCR4 on AML cells, facilitates leukemia cell trafficking and homing in the BM microenvironment, and keeps leukemic cells in close contact with the stromal cells and extracellular matrix that constitutively generate growth-promoting and anti-apoptotic signals [152]. Therefore, we investigated if DEN exposure affected the CXCL12-CXCR4 axis. Thus, we decided to use the dose of 0.1mM DEN to assess the DEN effect on AML cells in combination with 150ng/ml of the chemokine CXCL12 (SDF-1) (known concentration to induce hematopoietic cell migration). In presence of DEN, primary AML cells significantly reduced by about 30% ($p<0.01$) (Fig.39, panel A) their migration toward the chemoattractant agent CXCL12, and this result was also confirmed in AML cell lines (Fig.39, panel B-C).

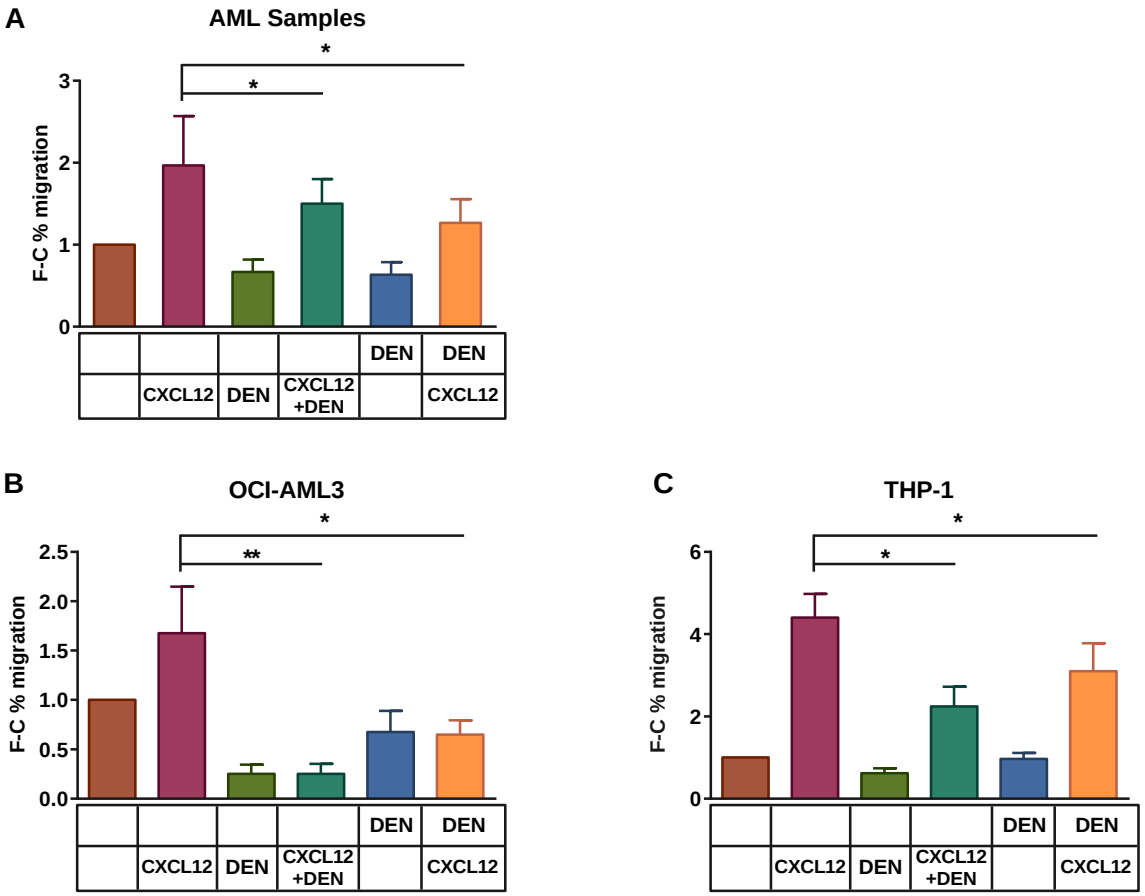

Figure 39. Histograms represent the effect of the presence of 0.1mM DEN in the upper or the lower chamber on the CXCL12 induced chemotaxis in primary AML cells (**A**), OCI-AML3 (**B**), and THP-1 (**C**).

Moreover, we asked if the inhibition of the CXCL12 induced chemotaxis was partially mediated by the modulation of CXCL12 receptor expression. Thus, after overnight exposure to 0.1mM DEN we observed a slight but significant reduction of CXCR4 surface expression in both primary AML cells ($p<0.01$) (Fig.40, panel A) and AML cell lines ($p<0.05$) (Fig.40, panel B-C).

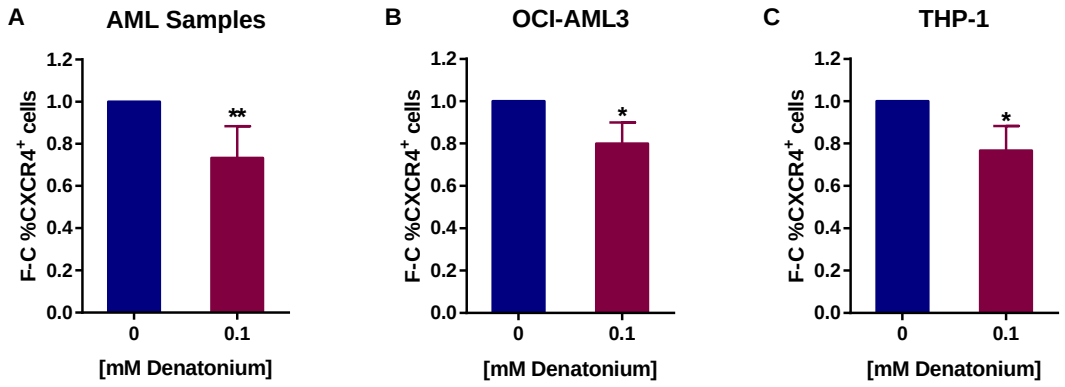

Figure 40. Histograms represent the fold-change of CXCR4 expression analysed by flow cytometer after overnight treatment with DEN in primary AML cells (**A**), OCI-AML3 (**B**), and THP-1 (**C**).

These results suggested that T2R activation attenuated leukemia cell migration likely through the inhibition of the CXCL12-CXCR4 axis.

9. DEN and cytarabine have a synergistic effect on AML cell viability

Considering the anti-proliferative, pro-apoptotic effect of DEN, we hypothesized to potentiate the cytotoxic effect of antineoplastic drugs by using the T2R agonist as adjuvant. We first examined the effect of combining the cytotoxicity of Ara-C with the antineoplastic activity of DEN. To this end, AML cells were treated for 72h with increasing doses of Ara-C with/without DEN. As shown in Fig.41, primary AML cell and AML cell line viability was significantly lower when DEN and Ara-C were combined, compared with their use as single compound. Interestingly, the addition of DEN allowed to reach a high toxicity using lower doses of Ara-C. The drug interaction study demonstrated a synergistic effect of the two compound at the concentration of 0.5mM DEN and 0.25uM Ara-C ($p<0.0001$) in primary AML cells (Fig.41, panel A), and at

0.5uM and 2uM Ara-C with all DEN doses in AML cell lines ($p<0.0001$ both in OCI-AML3, and THP-1) (Fig.41, panel B-C).

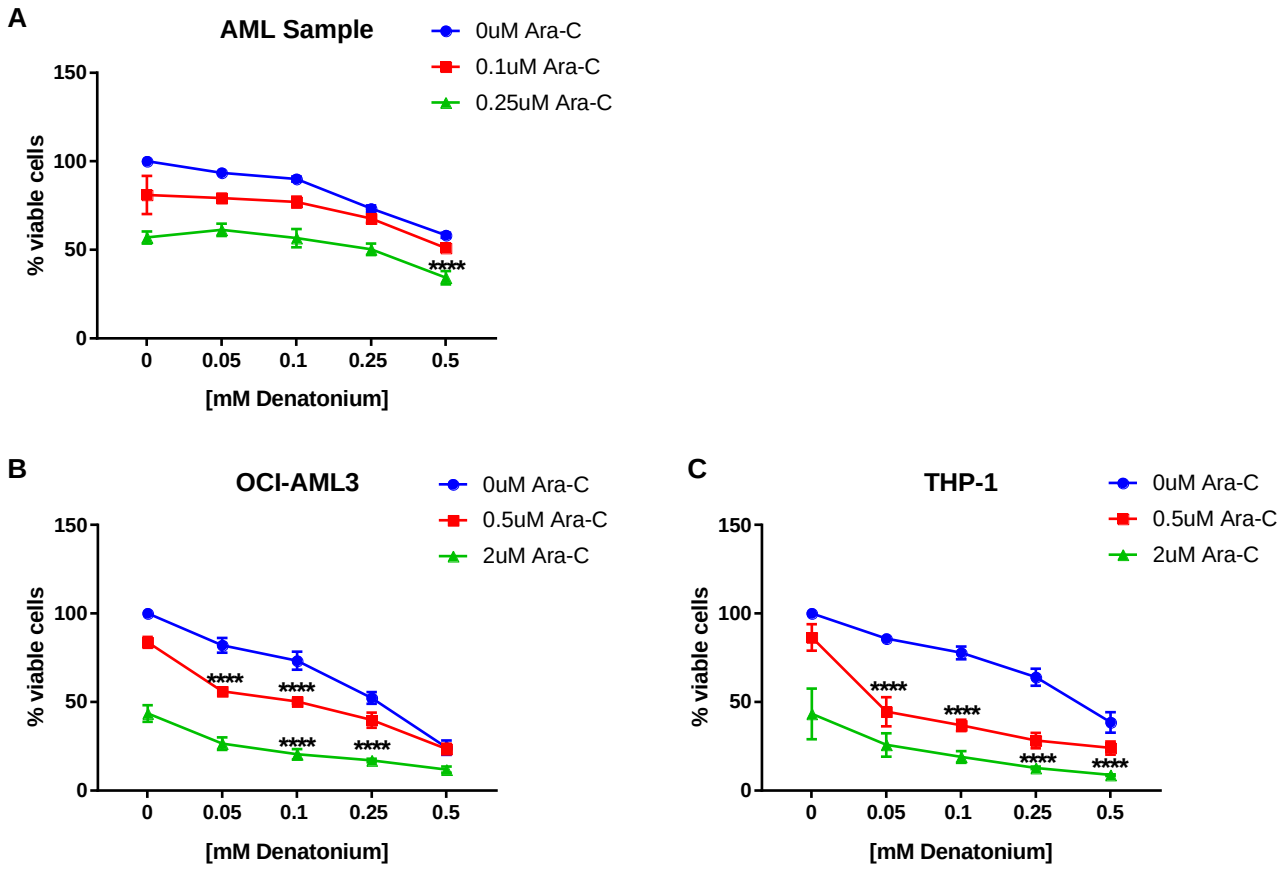

Figure 41. Cell viability detected by CellTiter 96 Aqueous One Solution assay in primary AML samples (**A**), OCI-AML3 (**B**), and THP-1 (**C**) after 72h of treatment with increasing doses of DEN and Ara-C.

Many chemotherapeutic agents have been shown to be substrates of multiple efflux transporters and the T2R triggering has been demonstrated to downregulate ABC transporter expression in pancreatic cancer cells [129]. Thus we analysed the effect of DEN exposure on the expression of the specific ABC transporter for Ara-C, ATP-binding cassette sub-family C member 4 (ABCC4), as possible mechanism responsible for enhancing chemotherapy response. Interestingly, we observed a significant reduction of

the ABCC4 expression in both primary AML samples (Fig.42, panel A), and AML cell lines at higher DEN doses (Fig.42, panel B-C).

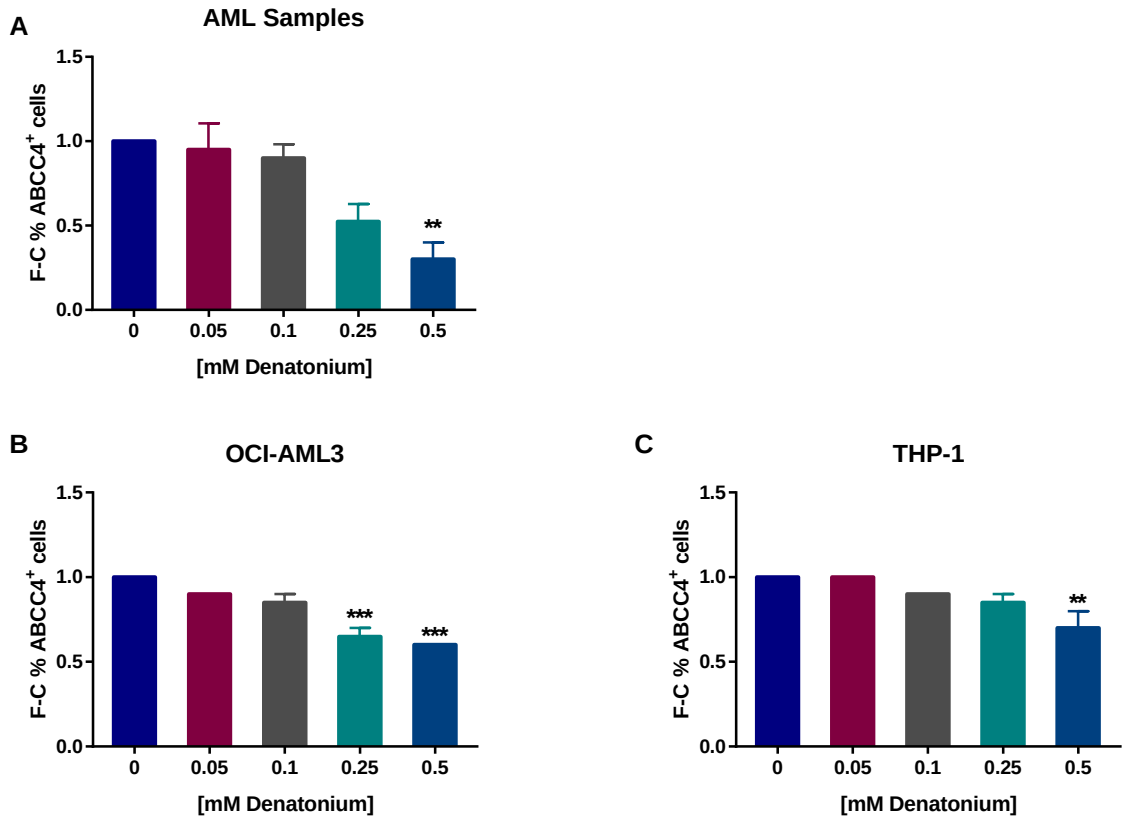

Figure 42. Histograms represent the fold-change of percentage of ABCC4 expression analysed by flow cytometer after 72h treatment with increasing doses of DEN in primary AML samples (**A**), OCI-AML3 (**B**), and THP-1 (**C**).

Overall, there results suggested that T2R activation by DEN had a synergistic effect with Ara-C, reducing leukemia cell viability and allowing to reach a high toxicity using lower doses of chemotherapic agent and this effect may be due to the downregulation of ABCC4, triggering by the T2R agonist.

Results II

1. HSCs express DEN TAS2Rs

Along with the identification of drugs that eradicate leukemia, minimizing the toxicity of antineoplastic agents on the normal HSC compartment represents a major task. In order to test the DEN effect on HSC compartment, normal $CD34^+$ cells were analysed for the TAS2R expression and function under the same culture conditions used for AML cells.

First of all, we downloaded gene expression profiling CEL files from the TCGA CB cohort consisting of 12 samples. We investigated the distribution of TAS2R transcript levels among CB samples, highlighting a strong heterogeneity in the TAS2R expression genes (Fig.43).

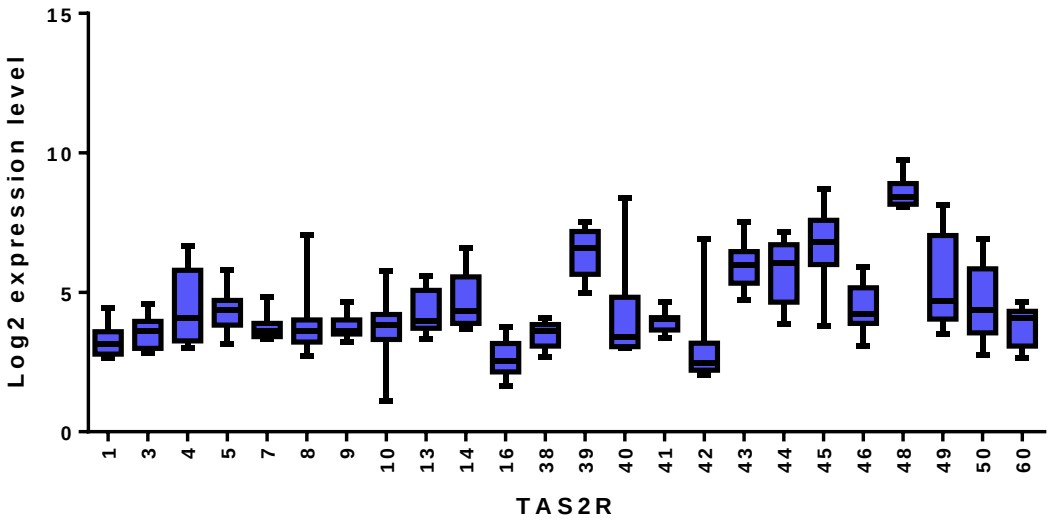

Figure 43. Illustrate relative TAS2R mRNA expression obtained by *in silico* analysis in a cohort of 12 CB-derived $CD34^+$ cells.

Based on the log2 expression levels, we found that CB-derived $CD34^+$ cells express all TAS2Rs with some differences between each receptors.

Thereafter, we confirmed the mRNA expression of DEN-related TAS2Rs by qRT-PCR (Fig.44).

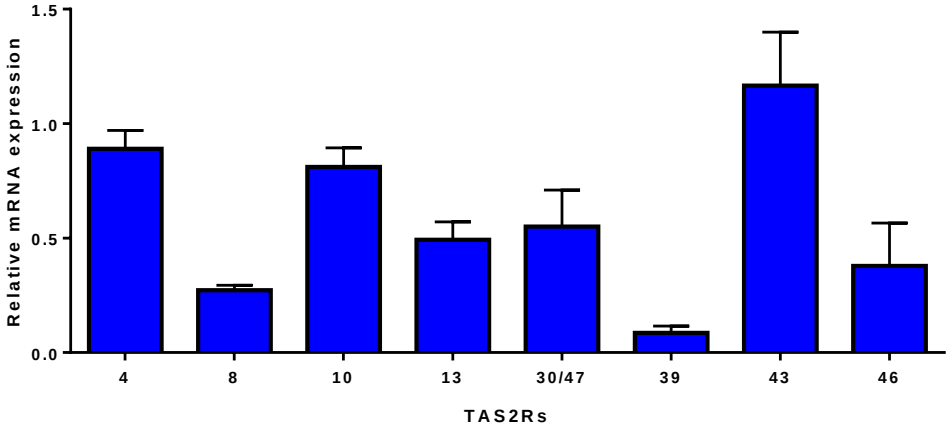

Figure 44. Illustrate TAS2R mRNA expression analysis by qRT-PCR in a pool of CB-derived $CD34^+$ cells (n=14).

In our pool of 14 CB-derived $CD34^+$ cells, we observed that HSCs expressed all the eight TAS2Rs activated by DEN and showed a higher expression of *TAS2R4*, *TAS2R8*, and *TAS2R43*.

The expression of T2R4 was also confirmed at protein level (Fig.45).

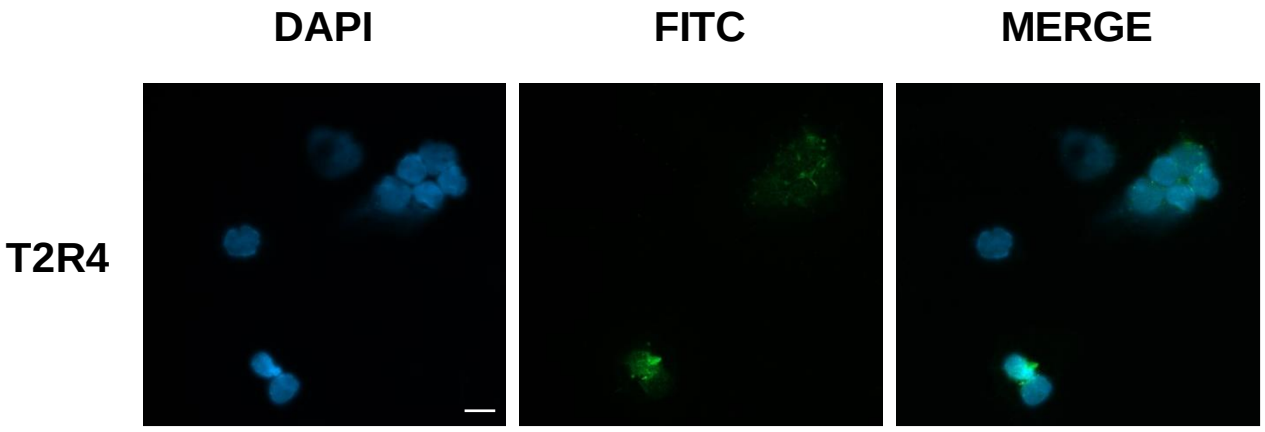

Figure 45. Immunofluorescence analysis of T2R4 expression. Nuclei were counterstained with DAPI (blue). 40X magnification, scale bar 20µm.

Overall, these results showed for the first time that HSCs expressed TAS2Rs.

2. T2Rs are fully functional on HSCs

We next verified the presence of T2R downstream targets in HSCs. Thus, we analysed Gß and PLC-ß2 mRNA expression levels by qRT-PCR in a pool of 14 CB-derived $CD34^+$ cells.

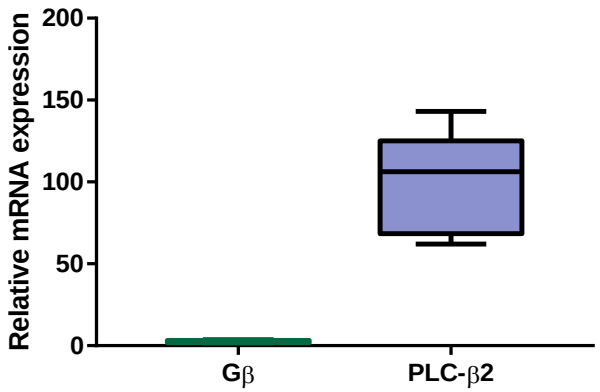

Figure 46. qRT-PCR analysis of TAS2R downstream targets in a pool of CB-derived $CD34^+$ cells (n=14).

The result indicated that the factors for the canonical bitter taste signal pathway were expressed both at mRNA (Fig.46) and protein (Fig.47) level.

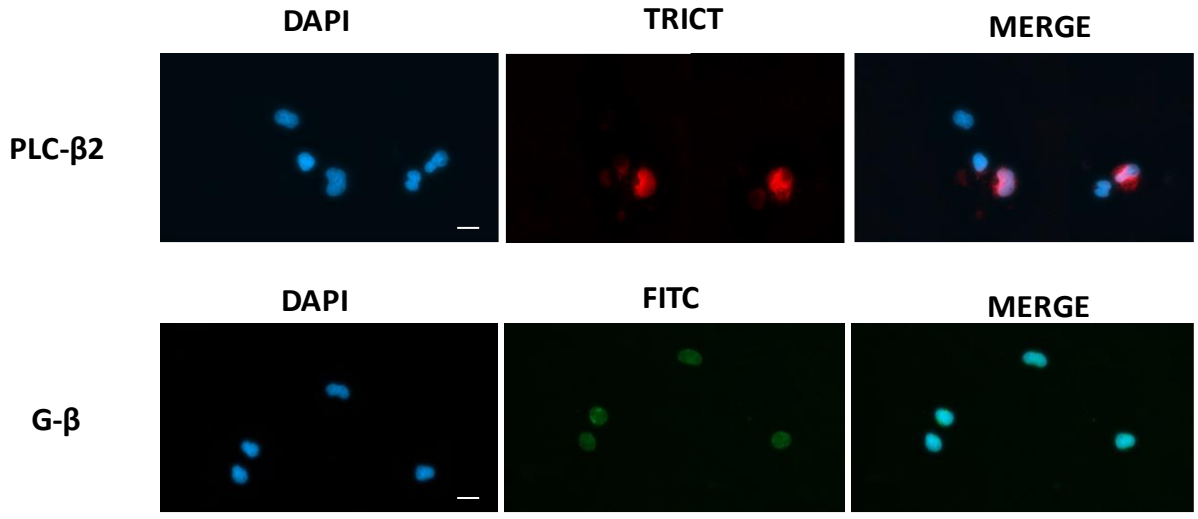

Figure 47. Immunofluorescence analysis of PLC-ß2, and Gß expression. Nuclei were counterstained with DAPI (blue). 40X magnification, scale bar 20µm.

After observing the presence of signal transduction cascade of GPCRs, we demonstrated the T2R activity by analysing the Ca^{2+} mobilization after stimulation of HSCs with DEN (Fig.48).

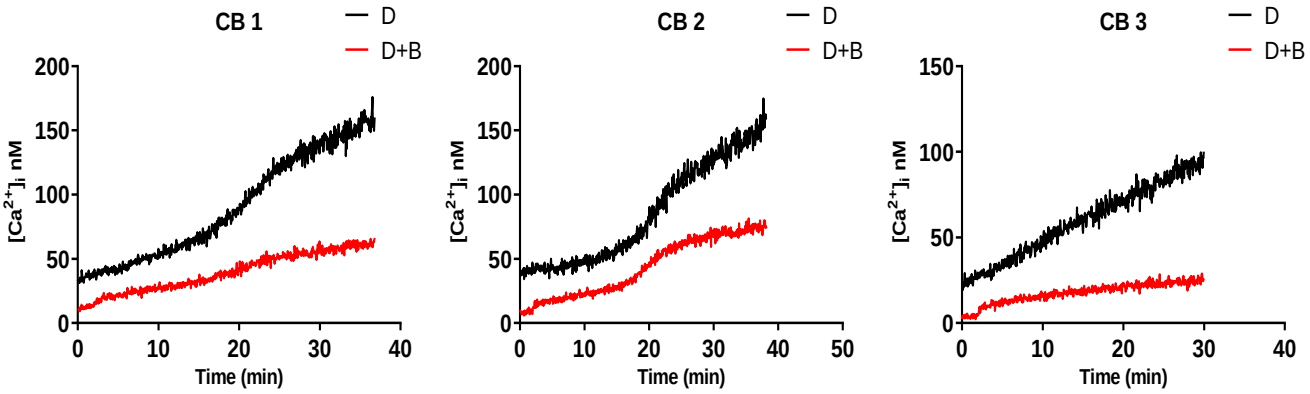

Figure 48. Ca^{2+} release in three CB-derived $CD34^{+}$ cells loaded with the Ca^{2+} indicator fura-2/AM and treated with 10mM DEN (indicated as D) in presence of BAPTA-AM (indicated as B) buffer**.**

The graphs showed a rapid increase in Ca^{2+} release in response to DEN, while that did not append in presence of BAPTA-AM in which the reduction of Ca^{2+} release was evident.

Taken together, these results demonstrated that HSCs expressed functional T2Rs.

3. Effects of T2R activation on HSC viability and apoptosis

To evaluate the DEN effect on HSC viability, we exposed HSCs for 48h to increasing doses of DEN. After treatment, we analysed viability, cytotoxicity and apoptosis induction (Fig.49, panel A-D).

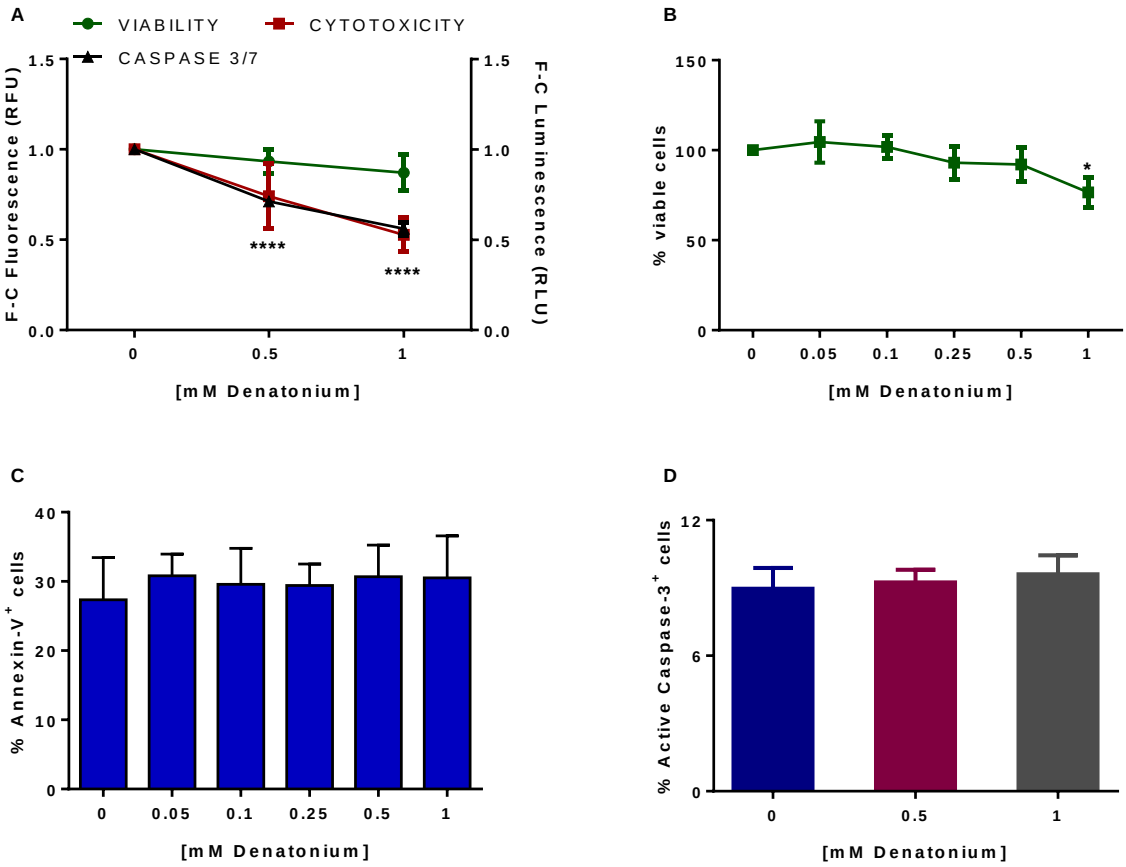

Figure 49. HSCs were treated for 48h with increasing doses of DEN. The measures of viability (green line), cytotoxicity (red line), and caspase 3/7 activity (black line) was detected by ApoTox-Glo™ Triplex Assay (**A**). Cell viability was detected by CellTiter 96 Aqueous One Solution assay (B). Histograms represent the percentage of Annexin-V$^+$ cells (**C**), and Activate Caspase-3$^+$ cells (**D**).

The results showed that DEN treatment did not exert a cytotoxic effect on HSCs (Fig.49, panel A) and did not affect HSC viability (Fig.49, panel A-B). In support of this, we observed neither necrosis nor apoptosis induction (Fig.49, panel C), as well as the activation of Casp-3 (Fig.49, panel D). On the other hand, there was a significant decrease in caspase 3/7 activity, both at 0.5mM, and 1mM ($p<0.0001$) (Fig.49, panel A). Taken together, these results showed that DEN did not impair the HSC viability and apoptosis.

4. T2R activation modulates HSC subsets and clonogenic capacity

Seeing the important HSC function in BM niche, we investigated how T2R activation may influence the HSC compartment. Thus, we analysed whether DEN exposure modulated the HSC subsets.

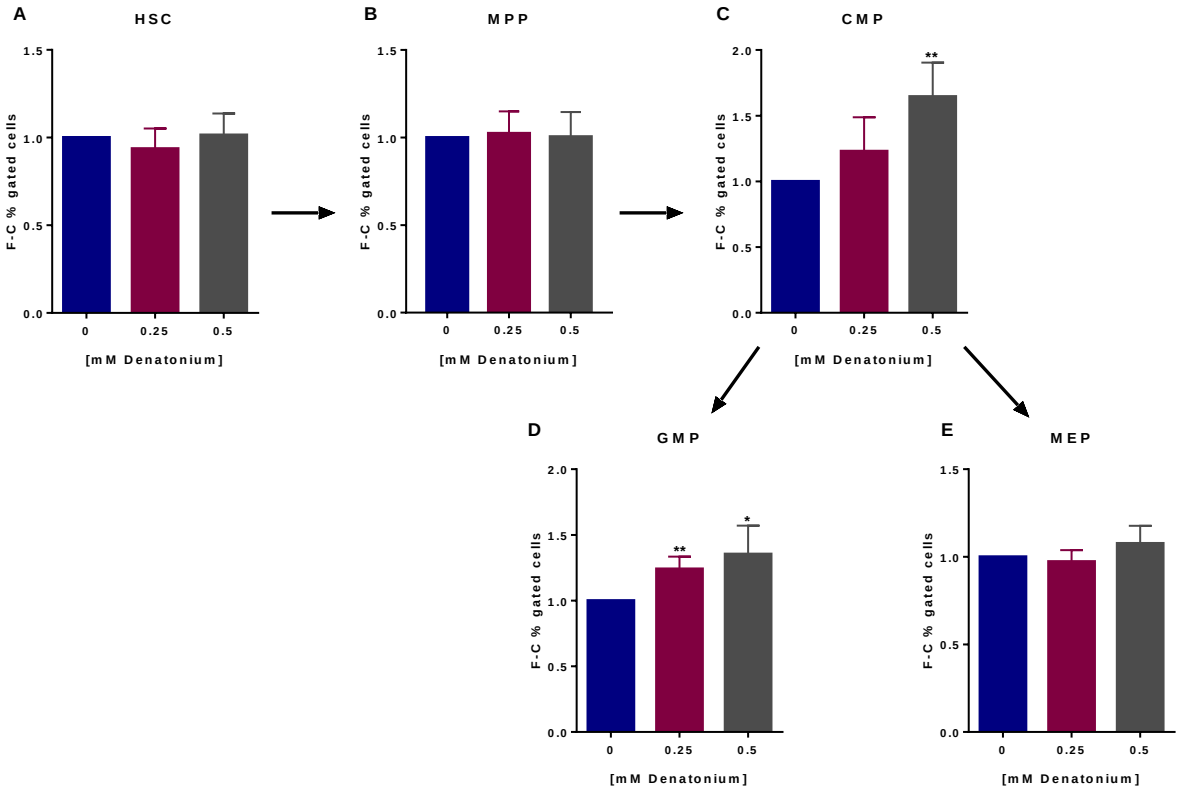

Figure 50. Histograms indicate the fold-change of different progenitor subsets obtained from CB-derived $CD34^+$ cells (n=7) cultured for 48h with increasing doses of DEN.

The data showed that DEN exposure affected the frequency of the progenitor subsets. In particular, after 48h DEN exposure, we observed an expansion of more differentiated progenitors, as indicated by the significant increase of CMPs ($p<0.01$) (Fig.50, panel C), GMPs ($p<0.05$) (Fig.50, panel D), and the slight increase in MEPs (Fig.50, panel E). However, if the stimulus was prolonged up to six days, we observed a gradual depletion

of more primitive compartment, as suggested by the significant reduction of the HSC ($p<0.001$) (Fig.51, panel A), and MPP ($p<0.0001$) (Fig.51, panel B) frequency.

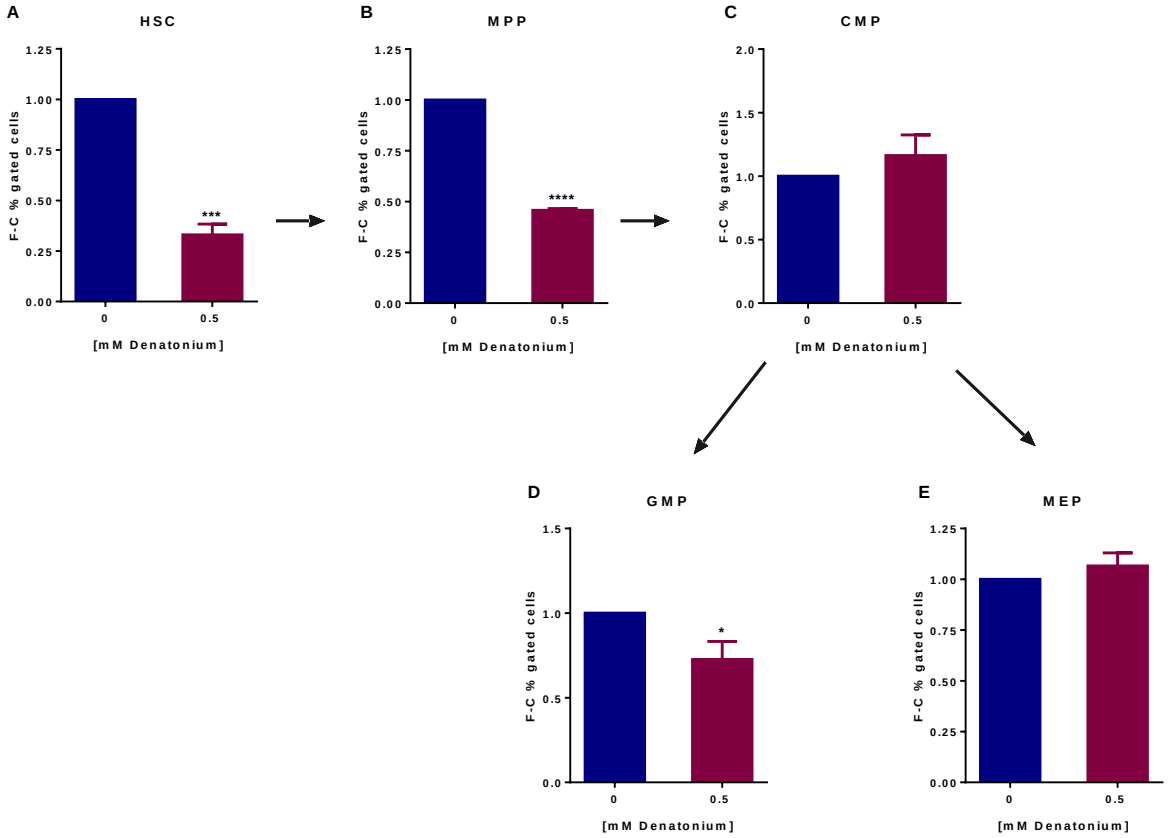

Figure 51. Histograms indicate the fold-change of different progenitor subsets obtained from CB-derived $CD34^+$ cells (n=5) cultured for 6 days with DEN.

Furthermore, we evaluated the effect of DEN on the HSC clonogenic capacity. As showed in the Fig.52, DEN promoted the growth of CB-derived $CD34^+$ cell colonies ($p<0.05$), supporting the observation that DEN exposure expanded the differentiated progenitors.

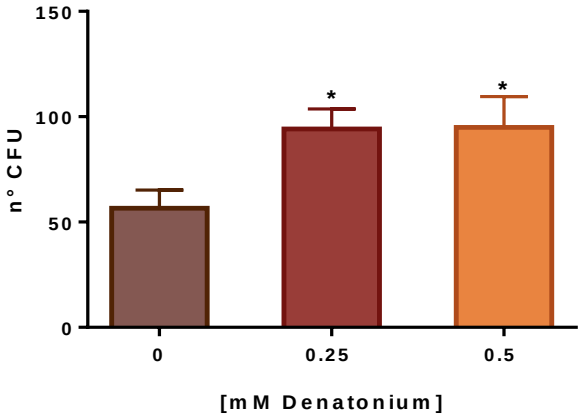

Figure 52. Histograms indicate the number of total CFU obtained from CB-derived $CD34^+$ cells (n=6) cultured for 6 days in liquid cultures with cytokines and DEN, and then in semisolid medium.

On the other hand, we observed a significant decrease in long-term culture initiating cells (LTC-IC), the most primitive hematopoietic progenitors. In particular, cells were cultured on fibroblast feeder layers and received repeated doses of DEN, up to a period of 5 weeks. LTC-IC quantification showed that DEN stimulation negatively affected the overall LTC-IC output compared with untreated cells ($p<0.05$) (Fig.53), suggesting the exhaustion of more primitive progenitors.

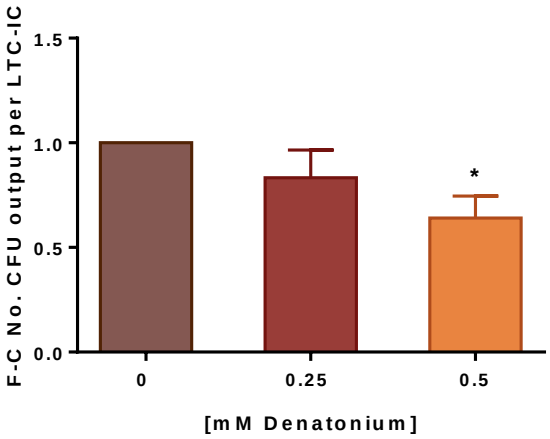

Figure 53. Histograms indicate the fold-change number of CFU output per LTC-IC of CB-derived $CD34^+$ cells (n=4) cultured with increasing doses of DEN.

Overall, these results showed that DEN exposure modulated the stem cell compartment, promoting HSC differentiation and reducing the frequency of more undifferentiated progenitors.

5. DEN exposure enhances HSC engraftment in mice

In order to confirm *in vivo* the DEN effect observed *in vitro* on HSC compartment, we analysed the engraftment potential of DEN pre-treated CB-derived $CD34^+$ cells injected into NSG-immunodeficient mice, and we evaluated the frequency of human HSC subsets in the BM at the mice sacrifice. As shown in Fig.54, NSG mice transplanted with DEN-treated $CD34^+$ cells showed a significantly increased engraftment in BM matched by an increased frequency of MEPs (Fig.55, panel E) ($p<0.05$), and the slight increase in GMPs (Fig.55, panel D).

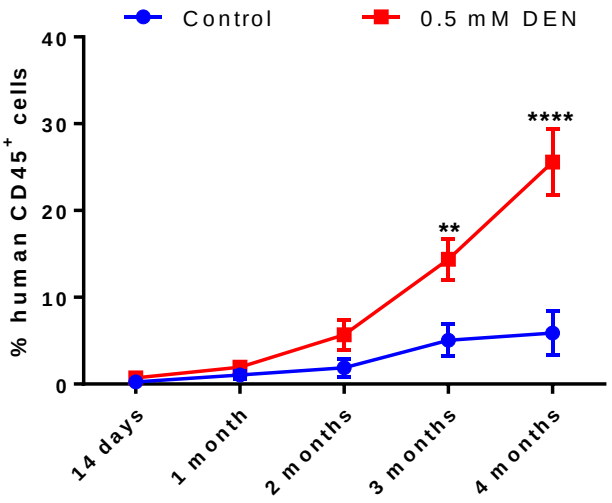

Figure 54. Graph represents the percentage of human $CD45^+$ cells in mice PB after 14 days, 1, 2, 3, and 4 months of recovery after transplantation.

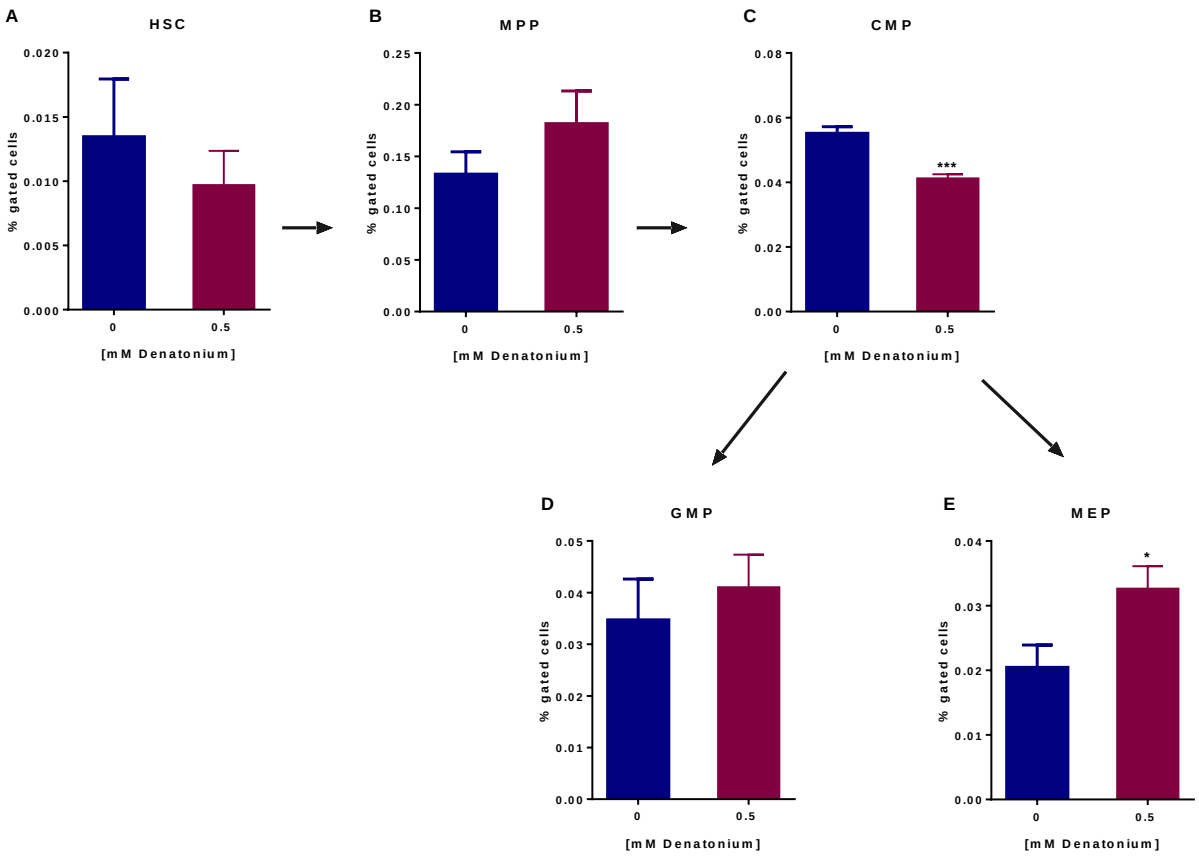

Figure 55. Histograms indicate the percentage of human different progenitor subsets in BM at the mice sacrifice (n=6).

Overall, these results suggested that DEN exposure induced an expansion of short-term progenitors and increased frequency of more differentiated progenitors, and this was in line with *in vitro* results.

The analysis of transplantation into secondary recipient mice will help us to confirm DEN impact on HSC compartment and is ongoing at the time of this thesis.

Discussion

The TAS2Rs are normally found on the surface of the tongue. They are known for the primary role as a central warning signal to induce aversion toward noxious or harmful substances. Recent studies have shown that TAS2Rs are widely expressed in various parts of human anatomy and are involved in the physiology of the respiratory system, the gastrointestinal tract, the endocrine system and also in the cancer settings, suggesting a wider function in "sensing microenvironment".

The present work extends our knowledge about the expression of TAS2Rs to the field of hematological malignancies. For the first time, we demonstrated that TAS2Rs are involved in the regulation of leukemia cell functions (the reported results have been recently published [153]) and their activation also affects the normal hematopoiesis. We demonstrated that AML cells express TAS2Rs, coupled with the downstream targets of the bitter taste signaling pathway (Gß and PLC-ß2). In the bitter taste signal transduction, Gß of G-proteins are known to initiate the dominant signaling of the pathway, via PLC-ß2 activation and Ca^{2+} release [77]. To demonstrate the T2R functionality, we used DEN and Quinine, two common bitter taste compounds known to activate T2Rs [94, 144, 154], and we observed that both mobilized the intracellular Ca^{2+}. This was the evidence that T2Rs were fully functional because their activation is known to increase the intracellular Ca^{2+} due to the open of Ca^{2+} stores [125]. Supporting a potential functional role of T2Rs in AML cells, their expression has been significantly correlated in a large cohort of AML patients with some relevant biological features, commonly used for diagnosis and risk stratification. In particular, we observed the modulation of some TAS2Rs in *TP53*- and *TET2*-mutated patients, within the poor-prognosis AML groups, in line with the observed TAS2R level decrease in breast cancer cells with a more aggressive phenotype [131].

To assess the function of T2R activation in AML cells, we decided to use DEN because it targeted more T2Rs in AML cells, compared to Quinine. In the downstream pathway analysis by GEP, we found that the DEN exposure downregulated transcripts enriched for genes involved in the cell cycle, DNA damage, cytoskeletal function, cell adhesion, and migration. Moreover, we found alterations of genes involved in apoptosis, and bioenergetics pathways in AML cells.

Consistent with GEP results, we found that *in vitro* DEN exposure exerted an anti-proliferative effect on AML cells, correlated to a G0/G1-phase arrest, and to the inhibition of leukemic progenitor cells. These results were in line with the evidence that T2R activation by DEN provides an anti-proliferative signal in ovarian, prostate, and breast cancer cells [130, 155]. Unfortunately, the high grade of redundancy in T2R expression in AML cells did not help to identify a unique candidate accounting for the T2R-mediated phenotype, also by using knockdown cells.

Studies have shown that DEN might induce apoptosis in different cell types, through the mitochondrial signaling pathway [156]. For this reason, we investigated the possible death mechanism in AML cells. Our data confirmed that DEN exposure induced AML cell apoptosis and that this acted through the mitochondrial, and caspase-3 pathway activation. Overall, these results suggest that in AML cells, as in breast, ovarian, and prostate cancer cells, the T2R activation is correlated with the anti-proliferative effect and induction of apoptosis [130, 155]. These data highlight the possibility that the AML cells might downregulate some T2Rs to evade these anti-proliferative effects, as demonstrated in breast cancer [131], and this hypothesis is supported by low expression levels of some TAS2Rs in *TP53*- and *TET2*-mutated AML patients.

Furthermore, we found that T2R activation is able to alter the AML mitochondrial metabolism. It is known that a highly diverse and flexible metabolism contributes to the aggressiveness of the disease, which is still difficult to treat. By using different sources of nutrients for energy and biomass supply, AML cells gain metabolic plasticity and rapidly outcompete normal hematopoietic cells. Moreover, it is known that AML cells greatly depend on OXPHOS to satisfy the heightened energy demand [157]. Interestingly, our data showed that T2R activation limited the mitochondrial activity with a shift of bioenergetics profile from OXPHOS to aerobic glycolysis. Maybe it was due to the metabolic reprogramming that AML cells exerted to offset the mitochondrial metabolic pathway.

Cell migration is an important capacity in HSC, but also in AML cells. In fact, the persistence of leukemic cells outside the BM microenvironment and, in particular, their infiltration into extramedullary organs are considered unfavorable prognostic factors [158]. Our results showed that T2R activation reduced both the spontaneous migration and migration due to the presence of CXCL12. Moreover, we demonstrated that this reduction might be related to the decrease of CXCR4 expression levels in treated AML cells. However, *in vivo* experiments did not show a reduction of leukemia cell homing to the BM after *ex-vivo* T2R activation by DEN, and this could be due to an *in vivo* upregulation of CXCR4 in hypoxic conditions [159]. In this context, mitochondrial has been emerging as a novel regulator of cell motility [160], so the reduction obtained in AML cells might be in line with the mitochondrial damage observed in T2R-activated AML cells. Moreover, the observed inhibition of migration is possibly correlated with cell cycle arrest and CyclinD1 and Cyclin A2 decrease. Indeed, these cell cycle proteins are also involved in cellular structure organization and motility regulation [150, 161].

The T2R activation showed also to sensitize AML cells to the main common chemotherapeutic agent used in this hematological disease, the Ara-C. Our results showed that DEN allowed reaching high toxicity using low doses of Ara-C and that the two compounds had a synergistic effect. Moreover, the enhanced response to chemotherapy was partially due to the decrease of ABCC4 transporter, and our results were in line with the previously reported role of T2R10 in downregulating the ABC transporter expression in pancreatic cancer cells [129].

Several natural bitter compounds have been displayed anti-cancer effects against various cancer types [162-165] similar to DEN, and many of these are recognized as T2R agonists [166, 167], but it is unclear if the anticancer effects evoked by them are mediated by T2Rs or other indirect and unknown mechanisms. Indeed, Quinine was used in a phase 3 multi-centric randomized study as MDR inhibitor in AML cells [168] and it was also reported the use of other bitter compounds in combination with chemotherapic drugs to enhance the anticancer activity [141, 169, 170].

The observed antitumor activity of DEN in AML cells suggested TAS2Rs as potential therapeutic targets. For this reason, it was important to assess the effect of DEN treatment on the normal stem cell compartment. There are no published data about the DEN effect on stem cells and only one report about T2R activity and regulation of stem cell function. In this paper, the authors show the suppressive T2R activity on the cancer stemness characteristic and cell invasion in the cancer stem cells of neuroblastoma [128].

For the first time, we demonstrated that CB-derived $CD34^+$ cells express fully functional TAS2Rs and their downstream signaling targets. Interestingly, DEN treatment did not induce a cytotoxic effect on HSCs, and did not affect cell viability, conversely to AML

cells. However, we observed that DEN exhausted the most primitive hematopoietic progenitors and stimulated the HSC differentiation, as supported by *in vivo* experiments. These results highlight the need to identify the off-target effects of endogenous bitter taste compounds present in the HSC niche. For example, a better knowledge of HSC niche can improve the hematopoietic stem-cell transplantation, because the graft failure is still a serious complication.

In conclusion, we could speculate that TAS2Rs may represent a novel receptor-based pathway by which blood cells "taste" their microenvironment and respond to it accordingly. In humans, there are 25 TAS2Rs that could be activated by many common drugs, such as antibiotics, chloroquine, haloperidol, erythromycin, procainamide, and ofloxacin known to be bitter tasting [171]. Although, the mechanism and the specific TAS2R involved in each process remains to be elucidated, and our data suggested that "bitter" molecules present endogenously in the BM microenvironment, such as amino acids [172, 173], or extrinsic factors, such as drugs [145], might interact with TAS2Rs and affect leukemia cell functions, or regulate the normal hematopoiesis. The different response to TAS2R activation suggests this pathway as a potential target for the development of the new therapeutic strategy.

Bibliography

1. Blank, U. and S. Karlsson, *TGF-β signaling in the control of hematopoietic stem cells.* Blood, 2015. **125**(23): p. 3542-50.

2. Gordon, M.Y., J.L. Lewis, and S.B. Marley, *Of mice and men...and elephants.* Blood, 2002. **100**(13): p. 4679-80.

3. Orkin, S.H. and L.I. Zon, *Hematopoiesis: an evolving paradigm for stem cell biology.* Cell, 2008. **132**(4): p. 631-44.

4. Seita, J. and I.L. Weissman, *Hematopoietic stem cell: self-renewal versus differentiation.* Wiley Interdiscip Rev Syst Biol Med, 2010. **2**(6): p. 640-53.

5. Weissman, I.L. and J.A. Shizuru, *The origins of the identification and isolation of hematopoietic stem cells, and their capability to induce donor-specific transplantation tolerance and treat autoimmune diseases.* Blood, 2008. **112**(9): p. 3543-53.

6. Akashi, K., et al., *Lymphoid development from stem cells and the common lymphocyte progenitors.* Cold Spring Harb Symp Quant Biol, 1999. **64**: p. 1-12.

7. Akashi, K., et al., *A clonogenic common myeloid progenitor that gives rise to all myeloid lineages.* Nature, 2000. **404**(6774): p. 193-7.

8. Drissen, R., et al., *Identification of two distinct pathways of human myelopoiesis.* Sci Immunol, 2019. **4**(35).

9. Drissen, R., et al., *Distinct myeloid progenitor-differentiation pathways identified through single-cell RNA sequencing.* Nat Immunol, 2016. **17**(6): p. 666-676.

10. McDermott, S.P., et al., *Comparison of human cord blood engraftment between immunocompromised mouse strains.* Blood, 2010. **116**(2): p. 193-200.

11. de Haan, G. and G. Van Zant, *Intrinsic and extrinsic control of hemopoietic stem cell numbers: mapping of a stem cell gene.* J Exp Med, 1997. **186**(4): p. 529-36.

12. BECKER, A.J., E.A. McCULLOCH, and J.E. TILL, *Cytological demonstration of the clonal nature of spleen colonies derived from transplanted mouse marrow cells.* Nature, 1963. **197**: p. 452-4.

13. SIMINOVITCH, L., E.A. MCCULLOCH, and J.E. TILL, *THE DISTRIBUTION OF COLONY-FORMING CELLS AMONG SPLEEN COLONIES.* J Cell Comp Physiol, 1963. **62**: p. 327-36.

14. Bryder, D., D.J. Rossi, and I.L. Weissman, *Hematopoietic stem cells: the paradigmatic tissue-specific stem cell.* Am J Pathol, 2006. **169**(2): p. 338-46.

15. Kondo, M., et al., *Biology of hematopoietic stem cells and progenitors: implications for clinical application.* Annu Rev Immunol, 2003. **21**: p. 759-806.

16. Baum, C.M., et al., *Isolation of a candidate human hematopoietic stem-cell population.* Proc Natl Acad Sci U S A, 1992. **89**(7): p. 2804-8.

17. Notta, F., et al., *Isolation of single human hematopoietic stem cells capable of long-term multilineage engraftment.* Science, 2011. **333**(6039): p. 218-21.

18. Lemischka, I.R., D.H. Raulet, and R.C. Mulligan, *Developmental potential and dynamic behavior of hematopoietic stem cells.* Cell, 1986. **45**(6): p. 917-27.

19. Wilkinson, A.C., K.J. Igarashi, and H. Nakauchi, *Haematopoietic stem cell self-renewal in vivo and ex vivo.* Nat Rev Genet, 2020.

20. Hordyjewska, A., Ł. Popiołek, and A. Horecka, *Characteristics of hematopoietic stem cells of umbilical cord blood.* Cytotechnology, 2015. **67**(3): p. 387-96.

21. Laurenti, E., et al., *The transcriptional architecture of early human hematopoiesis identifies multilevel control of lymphoid commitment.* Nat Immunol, 2013. **14**(7): p. 756-63.

22. Cabezas-Wallscheid, N., et al., *Identification of regulatory networks in HSCs and their immediate progeny via integrated proteome, transcriptome, and DNA methylome analysis.* Cell Stem Cell, 2014. **15**(4): p. 507-522.

23. Mendelson, A. and P.S. Frenette, *Hematopoietic stem cell niche maintenance during homeostasis and regeneration.* Nat Med, 2014. **20**(8): p. 833-46.

24. Tajer, P., et al., *Ex Vivo Expansion of Hematopoietic Stem Cells for Therapeutic Purposes: Lessons from Development and the Niche.* Cells, 2019. **8**(2).

25. Zhang, P., et al., *The physical microenvironment of hematopoietic stem cells and its emerging roles in engineering applications.* Stem Cell Res Ther, 2019. **10**(1): p. 327.

26. Ho, Y.H. and S. Méndez-Ferrer, *Microenvironmental contributions to hematopoietic stem cell aging.* Haematologica, 2020. **105**(1): p. 38-46.

27. Tamma, R. and D. Ribatti, *Bone Niches, Hematopoietic Stem Cells, and Vessel Formation.* Int J Mol Sci, 2017. **18**(1).

28. Nakamura, Y., et al., *Isolation and characterization of endosteal niche cell populations that regulate hematopoietic stem cells.* Blood, 2010. **116**(9): p. 1422-32.

29. Crane, G.M., E. Jeffery, and S.J. Morrison, *Adult haematopoietic stem cell niches.* Nat Rev Immunol, 2017. **17**(9): p. 573-590.

30. Pinho, S. and P.S. Frenette, *Haematopoietic stem cell activity and interactions with the niche.* Nat Rev Mol Cell Biol, 2019. **20**(5): p. 303-320.

31. Kunisaki, Y., et al., *Arteriolar niches maintain haematopoietic stem cell quiescence.* Nature, 2013. **502**(7473): p. 637-43.

32. Zhao, X., et al., *Interactions of Hematopoietic Stem Cells with Bone Marrow Niche.* Methods Mol Biol, 2020.

33. Pinho, S., et al., *Lineage-Biased Hematopoietic Stem Cells Are Regulated by Distinct Niches.* Dev Cell, 2018. **44**(5): p. 634-641.e4.

34. Christodoulou, C., et al., *Live-animal imaging of native haematopoietic stem and progenitor cells.* Nature, 2020. **578**(7794): p. 278-283.

35. Crippa, S. and M.E. Bernardo, *Mesenchymal Stromal Cells: Role in the BM Niche and in the Support of Hematopoietic Stem Cell Transplantation.* Hemasphere, 2018. **2**(6): p. e151.

36. Galán-Díez, M. and S. Kousteni, *The osteoblastic niche in hematopoiesis and hematological myeloid malignancies.* Curr Mol Biol Rep, 2017. **3**(2): p. 53-62.

37. Ramalingam, P., M.G. Poulos, and J.M. Butler, *Regulation of the hematopoietic stem cell lifecycle by the endothelial niche.* Curr Opin Hematol, 2017. **24**(4): p. 289-299.

38. Ferrara, F. and C.A. Schiffer, *Acute myeloid leukaemia in adults.* Lancet, 2013. **381**(9865): p. 484-95.

39. Löwenberg, B., J.R. Downing, and A. Burnett, *Acute myeloid leukemia.* N Engl J Med, 1999. **341**(14): p. 1051-62.

40. Cornell, R.F. and J. Palmer, *Adult acute leukemia.* Dis Mon, 2012. **58**(4): p. 219-38.

41. Estey, E. and H. Döhner, *Acute myeloid leukaemia.* Lancet, 2006. **368**(9550): p. 1894-907.

42. Shipley, J.L. and J.N. Butera, *Acute myelogenous leukemia.* Exp Hematol, 2009. **37**(6): p. 649-58.

43. Arber, D.A., et al., *The 2016 revision to the World Health Organization classification of myeloid neoplasms and acute leukemia.* Blood, 2016. **127**(20): p. 2391-405.

44. Rashidi, A. and J.F. DiPersio, *Targeting the leukemia-stroma interaction in acute myeloid leukemia: rationale and latest evidence.* Ther Adv Hematol, 2016. **7**(1): p. 40-51.

45. Isidori, A., et al., *The role of the immunosuppressive microenvironment in acute myeloid leukemia development and treatment.* Expert Rev Hematol, 2014. **7**(6): p. 807-18.

46. Di Virgilio, F., *Purines, purinergic receptors, and cancer.* Cancer Res, 2012. **72**(21): p. 5441-7.

47. Lapidot, T. and O. Kollet, *The essential roles of the chemokine SDF-1 and its receptor CXCR4 in human stem cell homing and repopulation of transplanted immune-deficient NOD/SCID and NOD/SCID/B2m(null) mice.* Leukemia, 2002. **16**(10): p. 1992-2003.

48. Forte, D., et al., *The tissue inhibitor of metalloproteinases-1 (TIMP-1) promotes survival and migration of acute myeloid leukemia cells through CD63/PI3K/Akt/p21 signaling.* Oncotarget, 2017. **8**(2): p. 2261-2274.

49. Reya, T., et al., *A role for Wnt signalling in self-renewal of haematopoietic stem cells.* Nature, 2003. **423**(6938): p. 409-14.

50. Zhao, C., et al., *Loss of beta-catenin impairs the renewal of normal and CML stem cells in vivo.* Cancer Cell, 2007. **12**(6): p. 528-41.

51. Hanahan, D. and L.M. Coussens, *Accessories to the crime: functions of cells recruited to the tumor microenvironment.* Cancer Cell, 2012. **21**(3): p. 309-22.

52. Salvestrini, V., et al., *Extracellular ATP induces apoptosis through P2X7R activation in acute myeloid leukemia cells but not in normal hematopoietic stem cells.* Oncotarget, 2017. **8**(4): p. 5895-5908.

53. Witkowski, M.T., S. Kousteni, and I. Aifantis, *Mapping and targeting of the leukemic microenvironment.* J Exp Med, 2020. **217**(2).

54. Tabe, Y. and M. Konopleva, *Role of Microenvironment in Resistance to Therapy in AML.* Curr Hematol Malig Rep, 2015. **10**(2): p. 96-103.

55. Baryawno, N., et al., *A Cellular Taxonomy of the Bone Marrow Stroma in Homeostasis and Leukemia.* Cell, 2019. **177**(7): p. 1915-1932.e16.

56. Duarte, D., et al., *Inhibition of Endosteal Vascular Niche Remodeling Rescues Hematopoietic Stem Cell Loss in AML.* Cell Stem Cell, 2018. **22**(1): p. 64-77.e6.

57. Hanoun, M., et al., *Acute myelogenous leukemia-induced sympathetic neuropathy promotes malignancy in an altered hematopoietic stem cell niche.* Cell Stem Cell, 2014. **15**(3): p. 365-375.

58. Medyouf, H., et al., *Myelodysplastic cells in patients reprogram mesenchymal stromal cells to establish a transplantable stem cell niche disease unit.* Cell Stem Cell, 2014. **14**(6): p. 824-37.

59. Platten, M., W. Wick, and B.J. Van den Eynde, *Tryptophan catabolism in cancer: beyond IDO and tryptophan depletion.* Cancer Res, 2012. **72**(21): p. 5435-40.

60. Godin-Ethier, J., et al., *Indoleamine 2,3-dioxygenase expression in human cancers: clinical and immunologic perspectives.* Clin Cancer Res, 2011. **17**(22): p. 6985-91.

61. Hussong, J.W., G.M. Rodgers, and P.J. Shami, *Evidence of increased angiogenesis in patients with acute myeloid leukemia.* Blood, 2000. **95**(1): p. 309-13.

62. Benito, J., et al., *Pronounced hypoxia in models of murine and human leukemia: high efficacy of hypoxia-activated prodrug PR-104.* PLoS One, 2011. **6**(8): p. e23108.

63. Passaro, D., et al., *Increased Vascular Permeability in the Bone Marrow Microenvironment Contributes to Disease Progression and Drug Response in Acute Myeloid Leukemia.* Cancer Cell, 2017. **32**(3): p. 324-341.e6.

64. Wellmann, S., et al., *Activation of the HIF pathway in childhood ALL, prognostic implications of VEGF.* Leukemia, 2004. **18**(5): p. 926-33.

65. Frisch, B.J., et al., *Functional inhibition of osteoblastic cells in an in vivo mouse model of myeloid leukemia.* Blood, 2012. **119**(2): p. 540-50.

66. Ho, Y.H., et al., *Remodeling of Bone Marrow Hematopoietic Stem Cell Niches Promotes Myeloid Cell Expansion during Premature or Physiological Aging.* Cell Stem Cell, 2019. **25**(3): p. 407-418.e6.

67. Scheiermann, C., et al., *Adrenergic nerves govern circadian leukocyte recruitment to tissues.* Immunity, 2012. **37**(2): p. 290-301.

68. Naveiras, O., et al., *Bone-marrow adipocytes as negative regulators of the haematopoietic microenvironment.* Nature, 2009. **460**(7252): p. 259-63.

69. Tikhonova, A.N., et al., *The bone marrow microenvironment at single-cell resolution.* Nature, 2019. **569**(7755): p. 222-228.

70. Castillo, J.J., et al., *Relationship between obesity and clinical outcome in adults with acute myeloid leukemia: A pooled analysis from four CALGB (alliance) clinical trials.* Am J Hematol, 2016. **91**(2): p. 199-204.

71. Shafat, M.S., et al., *Leukemic blasts program bone marrow adipocytes to generate a protumoral microenvironment.* Blood, 2017. **129**(10): p. 1320-1332.

72. Max, M., et al., *Tas1r3, encoding a new candidate taste receptor, is allelic to the sweet responsiveness locus Sac.* Nat Genet, 2001. **28**(1): p. 58-63.

73. Montmayeur, J.P., et al., *A candidate taste receptor gene near a sweet taste locus.* Nat Neurosci, 2001. **4**(5): p. 492-8.

74. Nelson, G., et al., *An amino-acid taste receptor.* Nature, 2002. **416**(6877): p. 199-202.

75. Nelson, G., et al., *Mammalian sweet taste receptors.* Cell, 2001. **106**(3): p. 381-90.

76. Sainz, E., et al., *Identification of a novel member of the T1R family of putative taste receptors.* J Neurochem, 2001. **77**(3): p. 896-903.

77. Kinnamon, S.C., *Taste receptor signalling - from tongues to lungs.* Acta Physiol (Oxf), 2012. **204**(2): p. 158-68.

78. Adler, E., et al., *A novel family of mammalian taste receptors.* Cell, 2000. **100**(6): p. 693-702.

79. Chandrashekar, J., et al., *T2Rs function as bitter taste receptors.* Cell, 2000. **100**(6): p. 703-11.

80. Behrens, M. and W. Meyerhof, *Bitter taste receptor research comes of age: from characterization to modulation of TAS2Rs.* Semin Cell Dev Biol, 2013. **24**(3): p. 215-21.

81. Kuhn, C., et al., *Oligomerization of TAS2R bitter taste receptors.* Chem Senses, 2010. **35**(5): p. 395-406.

82. Giovannucci, D.R., et al., *Targeted phosphorylation of inositol 1,4,5-trisphosphate receptors selectively inhibits localized Ca2+ release and shapes oscillatory Ca2+ signals.* J Biol Chem, 2000. **275**(43): p. 33704-11.

83. Taruno, A., et al., *How do taste cells lacking synapses mediate neurotransmission? CALHM1, a voltage-gated ATP channel.* Bioessays, 2013. **35**(12): p. 1111-8.

84. Zhang, Z., et al., *The transduction channel TRPM5 is gated by intracellular calcium in taste cells.* J Neurosci, 2007. **27**(21): p. 5777-86.

85. Behrens, M. and W. Meyerhof, *Gustatory and extragustatory functions of mammalian taste receptors.* Physiol Behav, 2011. **105**(1): p. 4-13.

86. Laffitte, A., F. Neiers, and L. Briand, *Functional roles of the sweet taste receptor in oral and extraoral tissues.* Curr Opin Clin Nutr Metab Care, 2014. **17**(4): p. 379-85.

87. Lee, R.J., et al., *Bitter and sweet taste receptors regulate human upper respiratory innate immunity.* J Clin Invest, 2014. **124**(3): p. 1393-405.

88. Cohen, N.A., *The genetics of the bitter taste receptor T2R38 in upper airway innate immunity and implications for chronic rhinosinusitis.* Laryngoscope, 2017. **127**(1): p. 44-51.

89. Li, F. and M. Zhou, *Depletion of bitter taste transduction leads to massive spermatid loss in transgenic mice.* Mol Hum Reprod, 2012. **18**(6): p. 289-97.

90. Clark, A.A., et al., *TAS2R bitter taste receptors regulate thyroid function.* FASEB J, 2015. **29**(1): p. 164-72.

91. Wu, S.V., et al., *Expression of bitter taste receptors of the T2R family in the gastrointestinal tract and enteroendocrine STC-1 cells.* Proc Natl Acad Sci U S A, 2002. **99**(4): p. 2392-7.

92. Tizzano, M., et al., *Nasal chemosensory cells use bitter taste signaling to detect irritants and bacterial signals.* Proc Natl Acad Sci U S A, 2010. **107**(7): p. 3210-5.

93. Shah, A.S., et al., *Motile cilia of human airway epithelia are chemosensory.* Science, 2009. **325**(5944): p. 1131-4.

94. Deshpande, D.A., et al., *Bitter taste receptors on airway smooth muscle bronchodilate by localized calcium signaling and reverse obstruction.* Nat Med, 2010. **16**(11): p. 1299-304.

95. Upadhyaya, J.D., et al., *Dextromethorphan mediated bitter taste receptor activation in the pulmonary circuit causes vasoconstriction.* PLoS One, 2014. **9**(10): p. e110373.

96. Foster, S.R., et al., *Expression, regulation and putative nutrient-sensing function of taste GPCRs in the heart.* PLoS One, 2013. **8**(5): p. e64579.

97. Maurer, S., et al., *Tasting Pseudomonas aeruginosa Biofilms: Human Neutrophils Express the Bitter Receptor T2R38 as Sensor for the Quorum Sensing Molecule N-(3-Oxododecanoyl)-l-Homoserine Lactone.* Front Immunol, 2015. **6**: p. 369.

98. Wölfle, U., et al., *Expression and functional activity of the bitter taste receptors TAS2R1 and TAS2R38 in human keratinocytes.* Skin Pharmacol Physiol, 2015. **28**(3): p. 137-46.

99. Jeon, T.I., Y.K. Seo, and T.F. Osborne, *Gut bitter taste receptor signalling induces ABCB1 through a mechanism involving CCK.* Biochem J, 2011. **438**(1): p. 33-7.

100. Cummings, D.E. and J. Overduin, *Gastrointestinal regulation of food intake.* J Clin Invest, 2007. **117**(1): p. 13-23.

101. Kok, B.P., et al., *Intestinal bitter taste receptor activation alters hormone secretion and imparts metabolic benefits.* Mol Metab, 2018.

102. Wang, Y., et al., *Metal Ions Activate the Human Taste Receptor TAS2R7.* Chem Senses, 2019. **44**(5): p. 339-347.

103. Singh, N., et al., *Functional bitter taste receptors are expressed in brain cells.* Biochem Biophys Res Commun, 2011. **406**(1): p. 146-51.

104. Dehkordi, O., et al., *Neuronal expression of bitter taste receptors and downstream signaling molecules in the rat brainstem.* Brain Res, 2012. **1475**: p. 1-10.

105. Lee, R.J., et al., *T2R38 taste receptor polymorphisms underlie susceptibility to upper respiratory infection.* J Clin Invest, 2012. **122**(11): p. 4145-59.

106. Lee, R.J., et al., *Mouse nasal epithelial innate immune responses to Pseudomonas aeruginosa quorum-sensing molecules require taste signaling components.* Innate Immun, 2014. **20**(6): p. 606-17.

107. Barham, H.P., et al., *Solitary chemosensory cells and bitter taste receptor signaling in human sinonasal mucosa.* Int Forum Allergy Rhinol, 2013. **3**(6): p. 450-7.

108. Lu, P., et al., *Extraoral bitter taste receptors in health and disease.* J Gen Physiol, 2017. **149**(2): p. 181-197.

109. Gerbe, F., et al., *Intestinal epithelial tuft cells initiate type 2 mucosal immunity to helminth parasites.* Nature, 2016. **529**(7585): p. 226-30.

110. Howitt, M.R., et al., *Tuft cells, taste-chemosensory cells, orchestrate parasite type 2 immunity in the gut.* Science, 2016. **351**(6279): p. 1329-33.

111. von Moltke, J., et al., *Tuft-cell-derived IL-25 regulates an intestinal ILC2-epithelial response circuit.* Nature, 2016. **529**(7585): p. 221-5.

112. Malki, A., et al., *Class I odorant receptors, TAS1R and TAS2R taste receptors, are markers for subpopulations of circulating leukocytes.* J Leukoc Biol, 2015. **97**(3): p. 533-45.

113. Shaw, L., et al., *Personalized expression of bitter 'taste' receptors in human skin.* PLoS One, 2018. **13**(10): p. e0205322.

114. Shiffman, D., et al., *Association of gene variants with incident myocardial infarction in the Cardiovascular Health Study.* Arterioscler Thromb Vasc Biol, 2008. **28**(1): p. 173-9.

115. Carrai, M., et al., *Association between TAS2R38 gene polymorphisms and colorectal cancer risk: a case-control study in two independent populations of Caucasian origin.* PLoS One, 2011. **6**(6): p. e20464.

116. Dotson, C.D., et al., *Bitter taste receptors influence glucose homeostasis.* PLoS One, 2008. **3**(12): p. e3974.

117. Orsmark-Pietras, C., et al., *Transcriptome analysis reveals upregulation of bitter taste receptors in severe asthmatics.* Eur Respir J, 2013. **42**(1): p. 65-78.

118. Robinett, K.S., et al., *Bitter taste receptor function in asthmatic and nonasthmatic human airway smooth muscle cells.* Am J Respir Cell Mol Biol, 2014. **50**(4): p. 678-83.

119. An, S.S., et al., *TAS2R activation promotes airway smooth muscle relaxation despite β(2)-adrenergic receptor tachyphylaxis.* Am J Physiol Lung Cell Mol Physiol, 2012. **303**(4): p. L304-11.

120. Latorre, R., et al., *Expression of the Bitter Taste Receptor, T2R38, in Enteroendocrine Cells of the Colonic Mucosa of Overweight/Obese vs. Lean Subjects.* PLoS One, 2016. **11**(2): p. e0147468.

121. Garcia-Esparcia, P., et al., *Functional genomics reveals dysregulation of cortical olfactory receptors in Parkinson disease: novel putative chemoreceptors in the human brain.* J Neuropathol Exp Neurol, 2013. **72**(6): p. 524-39.

122. Ansoleaga, B., et al., *Decrease in olfactory and taste receptor expression in the dorsolateral prefrontal cortex in chronic schizophrenia.* J Psychiatr Res, 2015. **60**: p. 109-16.

123. Velázquez-Fernández, D., et al., *Differential RNA expression profile by cDNA microarray in sporadic primary hyperparathyroidism (pHPT): primary parathyroid hyperplasia versus adenoma.* World J Surg, 2006. **30**(5): p. 705-13.

124. Adappa, N.D., et al., *T2R38 genotype is correlated with sinonasal quality of life in homozygous ΔF508 cystic fibrosis patients.* Int Forum Allergy Rhinol, 2016. **6**(4): p. 356-61.

125. Shaik, F.A., et al., *Bitter taste receptors: Extraoral roles in pathophysiology.* Int J Biochem Cell Biol, 2016. **77**(Pt B): p. 197-204.

126. Pydi, S.P., et al., *Recent advances in structure and function studies on human bitter taste receptors.* Curr Protein Pept Sci, 2012. **13**(6): p. 501-8.

127. Johnson, T.S. and D.H. Munn, *Host indoleamine 2,3-dioxygenase: contribution to systemic acquired tumor tolerance.* Immunol Invest, 2012. **41**(6-7): p. 765-97.

128. Seo, Y., et al., *Anti-cancer stemness and anti-invasive activity of bitter taste receptors, TAS2R8 and TAS2R10, in human neuroblastoma cells.* PLoS One, 2017. **12**(5): p. e0176851.

129. Stern, L., et al., *Overcoming chemoresistance in pancreatic cancer cells: role of the bitter taste receptor T2R10.* J Cancer, 2018. **9**(4): p. 711-725.

130. Martin, L.T.P., et al., *Bitter taste receptors are expressed in human epithelial ovarian and prostate cancers cells and noscapine stimulation impacts cell survival.* Mol Cell Biochem, 2018.

131. Singh, N., et al., *Differential expression of bitter taste receptors in non-cancerous breast epithelial and breast cancer cells.* Biochem Biophys Res Commun, 2014. **446**(2): p. 499-503.

132. Simonetti, G., et al., *Aneuploid acute myeloid leukemia exhibits a signature of genomic alterations in the cell cycle and protein degradation machinery.* Cancer, 2019. **125**(5): p. 712-725.

133. Gaida, M.M., et al., *Expression of the bitter receptor T2R38 in pancreatic cancer: localization in lipid droplets and activation by a bacteria-derived quorum-sensing molecule.* Oncotarget, 2016. **7**(11): p. 12623-32.

134. Ley, T.J., et al., *Genomic and epigenomic landscapes of adult de novo acute myeloid leukemia.* N Engl J Med, 2013. **368**(22): p. 2059-74.

135. Livak, K.J. and T.D. Schmittgen, *Analysis of relative gene expression data using real-time quantitative PCR and the 2(-Delta Delta C(T)) Method.* Methods, 2001. **25**(4): p. 402-8.

136. Corradi, G., et al., *Mesenchymal stromal cells from myelodysplastic and acute myeloid leukemia patients display in vitro reduced proliferative potential and similar capacity to support leukemia cell survival.* Stem Cell Res Ther, 2018. **9**(1): p. 271.

137. Giuliani, A.L., et al., *Trophic activity of human P2X7 receptor isoforms A and B in osteosarcoma.* PLoS One, 2014. **9**(9): p. e107224.

138. Nicholls, D.G., et al., *Bioenergetic profile experiment using C2C12 myoblast cells.* J Vis Exp, 2010(46).

139. Salvestrini, V., et al., *Purinergic signaling inhibits human acute myeloblastic leukemia cell proliferation, migration, and engraftment in immunodeficient mice.* Blood, 2012. **119**(1): p. 217-26.

140. Ritchie, M.E., et al., *limma powers differential expression analyses for RNA-sequencing and microarray studies.* Nucleic Acids Res, 2015. **43**(7): p. e47.

141. Solary, E., et al., *Feasibility of using quinine, a potential multidrug resistance-reversing agent, in combination with mitoxantrone and cytarabine for the treatment of acute leukemia.* J Clin Oncol, 1992. **10**(11): p. 1730-6.

142. Lemoli, R.M., et al., *Cycling status of CD34+ cells mobilized into peripheral blood of healthy donors by recombinant human granulocyte colony-stimulating factor.* Blood, 1997. **89**(4): p. 1189-96.

143. Cossarizza, A., et al., *A new method for the cytofluorimetric analysis of mitochondrial membrane potential using the J-aggregate forming lipophilic cation 5,5',6,6'-tetrachloro-1,1',3,3'-tetraethylbenzimidazolcarbocyanine iodide (JC-1).* Biochem Biophys Res Commun, 1993. **197**(1): p. 40-5.

144. Sawano, S., et al., *G-protein-dependent and -independent pathways in denatonium signal transduction.* Biosci Biotechnol Biochem, 2005. **69**(9): p. 1643-51.

145. Meyerhof, W., et al., *The molecular receptive ranges of human TAS2R bitter taste receptors.* Chem Senses, 2010. **35**(2): p. 157-70.

146. Preisler, H.D., et al., *Parallel studies of clonogenic leukaemia cells and the leukaemia cell population as a whole in acute myelogenous leukaemia.* Eur J Cancer, 1994. **30A**(10): p. 1511-6.

147. McDonnell, T.J., *Cell division versus cell death: a functional model of multistep neoplasia.* Mol Carcinog, 1993. **8**(4): p. 209-13.

148. Liu, S., et al., *Measures of cell turnover (proliferation and apoptosis) and their association with survival in breast cancer.* Clin Cancer Res, 2001. **7**(6): p. 1716-23.

149. Salazar-Roa, M. and M. Malumbres, *Fueling the Cell Division Cycle.* Trends Cell Biol, 2017. **27**(1): p. 69-81.

150. Chi, Y., et al., *Identification of CDK2 substrates in human cell lysates.* Genome Biol, 2008. **9**(10): p. R149.

151. Shalini, S., et al., *Old, new and emerging functions of caspases.* Cell Death Differ, 2015. **22**(4): p. 526-39.

152. Cho, B.S., H.J. Kim, and M. Konopleva, *Targeting the CXCL12/CXCR4 axis in acute myeloid leukemia: from bench to bedside.* Korean J Intern Med, 2017. **32**(2): p. 248-257.

153. Salvestrini, V., et al., *Denatonium as a Bitter Taste Receptor Agonist Modifies Transcriptomic Profile and Functions of Acute Myeloid Leukemia Cells.* Front Oncol, 2020. **10**: p. 1225.

154. Pulkkinen, V., et al., *The bitter taste receptor (TAS2R) agonists denatonium and chloroquine display distinct patterns of relaxation of the guinea pig trachea.* Am J Physiol Lung Cell Mol Physiol, 2012. **303**(11): p. L956-66.

155. Singh, N., et al., *Chemosensory bitter taste receptors T2R4 and T2R14 activation attenuates proliferation and migration of breast cancer cells.* Mol Cell Biochem, 2020. **465**(1-2): p. 199-214.

156. Wen, X., et al., *Denatonium inhibits growth and induces apoptosis of airway epithelial cells through mitochondrial signaling pathways.* Respir Res, 2015. **16**: p. 13.

157. Molina, J.R., et al., *An inhibitor of oxidative phosphorylation exploits cancer vulnerability.* Nat Med, 2018. **24**(7): p. 1036-1046.

158. Dusenbery, K.E., et al., *Extramedullary leukemia in children with newly diagnosed acute myeloid leukemia: a report from the Children's Cancer Group.* J Pediatr Hematol Oncol, 2003. **25**(10): p. 760-8.

159. Fiegl, M., et al., *CXCR4 expression and biologic activity in acute myeloid leukemia are dependent on oxygen partial pressure.* Blood, 2009. **113**(7): p. 1504-12.

160. Cunniff, B., et al., *AMPK activity regulates trafficking of mitochondria to the leading edge during cell migration and matrix invasion.* Mol Biol Cell, 2016. **27**(17): p. 2662-74.

161. Neumeister, P., et al., *Cyclin D1 governs adhesion and motility of macrophages.* Mol Biol Cell, 2003. **14**(5): p. 2005-15.

162. Ray, R.B., et al., *Bitter melon (Momordica charantia) extract inhibits breast cancer cell proliferation by modulating cell cycle regulatory genes and promotes apoptosis.* Cancer Res, 2010. **70**(5): p. 1925-31.

163. Barken, I., J. Geller, and M. Rogosnitzky, *Noscapine inhibits human prostate cancer progression and metastasis in a mouse model.* Anticancer Res, 2008. **28**(6A): p. 3701-4.

164. Muhammad, N., et al., *Bitter melon extract inhibits breast cancer growth in preclinical model by inducing autophagic cell death.* Oncotarget, 2017. **8**(39): p. 66226-66236.

165. Jeong, J.H., et al., *Effects of low dose quercetin: cancer cell-specific inhibition of cell cycle progression.* J Cell Biochem, 2009. **106**(1): p. 73-82.

166. Roland, W.S., et al., *Bitter taste receptor activation by flavonoids and isoflavonoids: modeled structural requirements for activation of hTAS2R14 and hTAS2R39.* J Agric Food Chem, 2013. **61**(44): p. 10454-66.

167. Hariri, B.M., et al., *Flavones modulate respiratory epithelial innate immunity: Anti-inflammatory effects and activation of the T2R14 receptor.* J Biol Chem, 2017. **292**(20): p. 8484-8497.

168. Solary, E., et al., *Quinine as a multidrug resistance inhibitor: a phase 3 multicentric randomized study in adult de novo acute myelogenous leukemia.* Blood, 2003. **102**(4): p. 1202-10.

169. Chougule, M.B., et al., *Antitumor activity of Noscapine in combination with Doxorubicin in triple negative breast cancer.* PLoS One, 2011. **6**(3): p. e17733.

170. Sasaki, K., et al., *Chloroquine potentiates the anti-cancer effect of 5-fluorouracil on colon cancer cells.* BMC Cancer, 2010. **10**: p. 370.

171. Clark, A.A., S.B. Liggett, and S.D. Munger, *Extraoral bitter taste receptors as mediators of off-target drug effects.* FASEB J, 2012. **26**(12): p. 4827-31.

172. Bassoli, A., et al., *The taste of D- and L-amino acids: In vitro binding assays with cloned human bitter (TAS2Rs) and sweet (TAS1R2/TAS1R3) receptors.* Food Chem, 2014. **150**: p. 27-33.

173. Kohl, S., et al., *Amino acids and peptides activate at least five members of the human bitter taste receptor family.* J Agric Food Chem, 2013. **61**(1): p. 53-60.